Robert E. Smith 260-5559

FINAL REPORT
October 15, 1993 - October 14, 1995

EPA GRANT NO. CR822015-01-0

Coupled Reaction-Transport Modeling of Deep Well Waste Injection

Prepared for

EPA Office of Groundwater and Drinking Water
Robert E. Smith, Project Officer

by

Peter Ortoleva and Xinghui Liu

Laboratory for Computational Geodynamics
Department of Chemistry
Indiana University
Bloomington IN 47405
(812) 855-2717 (office)
(812) 855-8300 (fax)
ortoleva@indiana.edu (email)

Abstract

The use of geochemical reaction-transport codes for No-Migration Petitions, setting overall policy, and ongoing reservoir assessment and management in the context of deep well waste injection is evaluated. The study is based on CIRF.A (Chemical Interaction of Rock and Fluid) model, a fully coupled groundwater flow, contaminant transport, and fluid and mineral reaction simulator. Although the Sandia Waste Isolation Flow and Transport Model (SWIFT) is commonly used for No-Migration Petition modeling, it can not account for chemical reactions involving rock, wastes, and formation fluids and their effects on contaminant transport, rock permeability and porosity, and the integrity of the reservoir and confining units. CIRF.A can model all these processes.

The CIRF.A simulator is shown to be invaluable in analyzing near borehole and reservoir-scale effects during waste injection and predicting the 10,000 years fate of the waste plume. Conclusions are based on numerical simulations of all aspects of the waste injection problems using CIRF.A. Recommendations are given for future model development, calibration and verification, parameter sensitivity analysis, the benefit of underpressured compartments as waste repositories, and use of optimization theory to design the strategies of waste injection and damage remediation.

Disclaimer

The author's conclusions and opinions are based on their expertise and experience and do not necessarily reflect the official policies of the US EPA.

Table of Contents

I Introduction and Overview

Injection of waste fluids into a reservoir can activate a host of complex chemical reactions and material or energy transport phenomena that make setting regulations and granting operation licenses a challenging endeavor. No-Migration Petition modeling is currently performed to calculate the configuration of the injected waste plume during the operation period and predicting its 10,000 year fate. Although models currently used in support of No-Migration Petition applications include the effects of groundwater flow and contaminant transport, they do not account for the coupling of reaction and transport and its impact on the waste plume composition, geometry and extent nor do they account for the possible destruction of confining units due to waste fluid-rock interactions. The goal of this project is to investigate the use of the coupled reaction-transport code CIRF.A to address these and other critical issues related to waste injection and storage.

Injection of a fluid into a rock and the resulting evolution in time of the spatial distribution of fluid composition and rock mineralization and properties are at the heart of the regulatory challenge. In principle, the implaced fluid could lose or diminish its toxicity and could remain sequestered on the 10,000 year time scale and beyond. As *in situ* experiments are usually not feasible or even desirable (as the experiments could themselves cause problems), a reliable predictive model is essential. A predictive model can be used in a number of ways:

- evaluate the effects of the waste injectate fluid/solid matrix interactions on contaminant transport and reservoir confining unit integrity;
- delineate ideal reservoir mineralization and type for a given class of waste chemistry;
- determine effects associated with waste detoxification, long-time sequestration, waste escape and migration, and destruction or enhancement of reservoir quality (porosity and permeability);
- prediction of reservoir capacity in view of potential for waste escape and reservoir damage;
- to set forth regulations; and
- to formulate or review No-Migration Petitions.

In this study, these issues are addressed using the CIRF.A reaction-transport simulator.

One goal of this study is to identify the features a fluid waste repository simulator should have to be reliable and robust. By using CIRF.A to carry out simulations of a number of types of situations, we have identified many of these characteristics. Furthermore, we believe that our study demonstrates that it is well within the capabilities of contemporary modeling techniques to develop such a model. Finally, CIRF.A is found to have many of the required features and characteristics.

This study also addresses two related issues in waste repository predictive modeling. CIRF.A was used to make a preliminary investigation of the intriguing possibility of using deep, underpressured compartments as waste repositories. It is found that they have a number of highly desirable characteristics and, when correctly managed, will be very valued repositories. The second issue is that of optimization operation procedures. Here we suggest the use of optimal control theory to determine the ideal waste fluid composition and injection scenario to make best use of a given repository or to set forth best reservoir characteristics (notably mineralogy) for a given waste chemistry.

In Chapter II, geochemical modeling is reviewed to assess and understand the current "state of the art", and to place this project in the proper context. The CIRF.A reaction-transport simulator is presented in detail so that the assumptions underlying it and its features can be appreciated. The verification of CIRF.A with other simulators and analytical solutions as well as other theoretical checks on code validity are noted.

In Chapter III, CIRF.A simulator testing and calibration by laboratory core flood data are discussed. Near-borehole simulations are carried out to predict precipitation-induced formation damage and reaction-front fingering during injection.

In Chapter IV we present field scale simulations including operation and 10,000 year fate analysis. Site specific data of waste injection are simulated by CIRF.A for a carbonate reservoir and a sandstone reservoir. In the carbonate reservoir, the waste fluid caused significant increase in porosity and permeability near the wellbore. Simulation results from CIRF.A are quantitatively consistent with field data. In the sandstone reservoir, field evidence indicates that formation damage problems occurred during waste injection. Simulation studies using CIRF.A also indicate the existence of formation damage and provide a detailed explanation of it in terms of the waste fluid, reservoir aqueous and mineral chemistry. Our simulations were also extended to include a 10,000 year post operational period. The major focus in that part of our study was to predict the extent of the waste plume in the reservoir and waste transformations due to chemical reactions over time.

In Chapter V we present concepts and advantages of waste injection into underpressured compartments. Simulation results indicated that injected waste could escape from a normally pressured reservoir (compartment) but not from one which is similar except that it is underpressured.

A key implication of a reaction-transport analysis of waste injection is the possibility of determining the optimal emplacement strategy. This is discussed in Chapter VI in the framework of optimal control theory.

Our study not only serves to identify some of the phenomena important to waste injection but also serves to clarify the characteristics that a waste injection simulator must have to be an effective regulatory and repository assessment and management vehicle. Conclusions and recommendations on reaction-transport modeling of deep-well waste injection using CIRF.A or other models are presented in Chapter VII.

II
The CIRF.A Reaction-Transport Simulator

A . General Description

The CIRF.A simulator was designed to analyze the effects of the injection of a fluid into a rock that arise out of the reaction and transport processes. It was originally designed to analyze problems in diagenesis and petroleum engineering.

The key achievement of CIRF.A is its capacity to account for the strong coupling between the operating processes. For example, the infiltrating fluid can dissolve certain minerals and thereby affect permeability. The latter affects the flow of the infiltrating reactive fluid. One cannot, therefore, analyze fluid flow and mineral reaction separately. These processes are strongly coupled and must be co-evolved.

The effects of strong coupling can be dramatic. In Fig. II-1 the flow self-focusing phenomenon is illustrated (Chadam et al., 1986, 1988, 1990; Chen and Ortoleva, 1990a, 1992; Ortoleva 1994a). The infiltration of a reactive fluid is seen to cause a mineral alteration front and associated permeability change. If permeability in the altered (upstream) side is greater than in the unaltered zone (downstream side), then a feedback can occur whereby flow is focused through a protrusion in the front, extending the protrusion downstream and thereby allowing for the growth of such protrusions.

Thus, a reaction front can be unstable to such protrusions. In the context of waste injection, the waste plume can extend much further than could have been predicted by the average movement of a planar or spherical alteration front.

The co-evolution of all processes is achieved in CIRF.A via a finite time difference approximation to the partial differential equations of fluid mass conservation and grain growth/dissolution. At each time advancement step all these equations are solved iteratively before advancing the system one time step. The general approach is as suggested in Fig. II-2.

Our reaction-transport code CIRF.A has been applied to analyze a variety of problems (Liu et al, 1996; Ortoleva, 1994a; Potdevin et al., 1992; Chen et al., 1990). CIRF.A simulates the fluid and fluid-rock reactions and single or multi-phase transport phenomena that take place when a fluid of given chemistry is injected into a formation. It contains large built-in kinetic and thermodynamic data bases and has great chemical generality. It can be run in one dimensional, radial, fully two dimensional and quasi-three dimensional modes. The latter accounts for bed thickness variations. In the two dimensional and quasi-three dimensional modes, fluids may enter or leave any boundary or through user-sited wells. CIRF.A accounts for the following processes:

- finite rate mineral dissolution/precipitation reactions
- aqueous pore fluid reaction equilibria
- Darcy or Brinkman flow with a permeability that reflects changes in grain size and shape due to precipitation/dissolution reactions and relative permeability and capillarity effects for two fluid phase flow
- nucleation threshholds for precipitating new phases
- conservation of pore fluid solute mass due to flow, dispersion/diffusion and aqueous phase and mineral reactions
- temperature calculated via the conservation of energy equation
- solute species activities corrected for temperature, pressure and ionic strength

- evolution in one or fully two dimensions or special symmetric configurations in three dimensions
- single or multiple injection or production wells in a reservoir.

The program comes with a built-in data base for the thermodynamic and kinetic parameters. Graphical and other model-building and -analysis tools are included so that the reaction-transport simulator can conveniently be used in research or applied environments.

The input to CIRF.A is the spatial distribution of the original grain size and number of grains per rock volume within the reservoir for each mineral in the domain to be simulated and the time-course of the injection fluid composition, temperature and flow rate. The output is the time-course of the spatial distribution of porosity, permeability, mineral grain size and volume fraction, and pore fluid composition within the reservoir.

B. Comparison with Other Models

In the report entitled "Assessing the Geochemical Fate of Deep-Well-Injected Hazardous Waste: Summaries of Recent Research" (U.S. EPA, 1990), a number of equilibrium geochemical and contaminant transport models were reviewed. None of these models has the capabilities of CIRF.A which can simulate flow coupled with chemical equilibrium and nonequilibrium reactions.

In this study, geochemical and transport models, such as DYNAMIX, FASTCHEM, MINTEQ/PRODEF and SWIFT are reviewed. The most significant difference between CIRF.A and these three programs is that CIRF.A is the only code which couples all the following processes:

- Reaction kinetics;
- Reaction transport equations for pore fluid solutes;
- Darcy and Brinkman flow with permeability depending on reaction-mediated textural changes;

- The temperature distribution is calculated by an energy balance equation;
- All equations are solved self-consistently with each other.

CIRF.A is the only one among these programs which preserves the dynamic feedback of flow and water-rock interactions. A brief comparison with each program is as follows.

1. MINTEQ/PRODEF

MINTEQ is a speciation program with extensive database and surface adsorption capabilities (Felmy et. al., 1986). It has no flow and mass transport capabilities, nor kinetically controlled water-rock interaction options. PRODEF is a user-friendly interface for the MINTEQ speciation code.

2. FASTCHEM

FASTCHEM (Fly Ash and Scrubber sludge Transport and Chemistry) is an EPRI (Electrical Power Research Institute) proprietary code (McIntosh, 1991). It is constructed from two pre-existing programs, SATURN, a hydrologic flow model (a proprietary code of Geo Trans, Inc.), and the MINTEQ speciation code.

The module based on SATURN solves the Darcy flow problem through a Markov Chain method. Theoretically, the method can be used for one- to three-dimensional flow, however, the computational methods do not appear to be efficient. This is especially true since the Markov Chain method leaves unaddressed the question of residual noise due to insufficient statistics associated with a limited number of individual trajectories.

An evaluation of the program on an example application (Bohac, et. al., 1991) indicates the program requires significant computational time and data analysis. Because FASTCHEM uses the MINTEQ speciation code, the program does not account for kinetics, nor does it account for permeability modification due to water-rock interaction.

3. DYNAMIX

A special feature of the DYNAMIX model is its redox reaction capability (Liu and Narasimhan, 1989a). The program is constructed from pre-existing programs TRUMP and PHREEQE. TRUMP is a flow and mass transport model and PHREEQE is a chemical speciation code based on the reaction-path methods. Liu and Narasimhan (1989b) indicate that substantial revision to both programs were made to integrate them.

The chemical speciation and kinetics methods used by DYNAMIX has many similarities to CIRF.A. While DYNAMIX models redox phenomena using Eh explicitly, CIRF.A models redox reactions by using aqueous species of different oxidation states--thereby making the CIRF.A approach more natural for the analysis of kinetic problems. The kinetic rate law of DYNAMIX is also very similar to that used in CIRF.A, however, the rate law used in CIRF.A accounts for a more general class of processes. For example, CIRF.A expresses the dependence of both dissolution and precipitation rate on water chemistry while DYNAMIX only expresses the water chemistry dependence of the dissolution rate. Furthermore, CIRF.A allows the use of multiple reactions per mineral and thereby permits the user to account for the pH-dependence of rates.

Using the integrated finite difference method, one- to three-dimensional simulations can be carried out by DYNAMIX (Narasimhan et. al., 1986), while CIRF.A simulates 1- and 2-dimensional systems. As of 1989 (Liu and Narasimhan) DYNAMIX did not account for pressure correction on thermodynamic properties, and it was limited to isothermal systems. CIRF.A accounts for pressure-corrections on thermodynamic properties, and solves for the temperature distribution through the energy balance equation.

4. SWIFT

SWIFT is a three-dimensional finite difference code that can be used to simulate ground water flow, contaminant transport, and heat transport in single or dual porosity media (Reeves et al., 1986). SWIFT has been extensively documented and verified (Finley and Reeves, 1982; Ward et al., 1984). The code has been used extensively to model deep

well disposal including the effects of variable density injection (Larkin et al., 1994). In SWIFT, the equations governing groundwater flow and solute transport are coupled through: 1) the pore fluid velocity; 2) the dependence of the fluid density on pressure, solute mass fraction and temperature; and 3) the dependence of fluid viscosity on solute mass fraction and temperature.

C. Basic Model Equations

The model on which our simulator is based consists of a set of mass and momentum conservation equations. The mass conservation equations are supplemented with reaction rates and sink/source terms representing injection/production wells. Grain texture-porosity-permeability relations are also included to complete the model formulation.

1. Mass Conservation of Solutes

The equation of conservation of mass for the concentration of aqueous species α is taken in the form:

$$\frac{\partial}{\partial t}(\phi s_w c_\alpha) = -\vec{\nabla}\cdot(-\phi s_w D_\alpha \vec{\nabla} c_\alpha + \vec{u}_w c_\alpha) + \sum_{j=1}^{N_f} v_{\alpha j}^f W_j^f + \sum_{j=1}^{N_s} v_{\alpha j}^s W_j^s + q_\alpha \quad \alpha = 1, 2, ..., N. \qquad \text{(II.1)}$$

Here c_α is the molar concentration of aqueous species α; ϕ is porosity; s_w is the saturation of the water (aqueous solvent) phase; D_α is the dispersion coefficient of species α and $\vec{u}_w$ is the filtration or flow velocity of the aqueous phase; Nf is the number of aqueous reactions (equilibrium reactions) and N_s is the number of mineral reactions (kinetic reactions); W_j^f and W_j^s are reaction rates of the *j-th* aqueous and *j-th* mineral reaction; q_α stands for the source/sink term for species α arising from injection/production well effects; N is the number of aqueous species.

2. Reactions and Rate Laws

In this model, all reactions are grouped into two categories: aqueous and mineral reactions. An aqueous reaction only involves aqueous species while a mineral reaction involves both mineral and aqueous species. Acid dissociation is an aqueous reaction. Mineral dissolution and precipitation are mineral reactions.

An aqueous reaction can be written in the following form:

$$\sum_{\alpha=1}^{N} v_{\alpha j}^{f} S_{\alpha} = 0. \qquad \text{(II.2)}$$

Here $v_{\alpha j}^{f}$ is the stoichiometric coefficient for aqueous species S_{α} in aqueous reaction j. The aqueous reactions are often fast relative to the mineral reactions. In the model, they are taken to be fast and hence are maintained at equilibrium. Because the aqueous reactions are fast it is necessary for computational reasons to take a matrix transformation of Equation (II.1) so as to eliminate the aqueous reaction rates, W_j^f.

In order to solve all aqueous species concentrations, the matrix-transformed equations must be supplemented with the following independent equilibrium relations:

$$K_j^f = \prod_{\alpha=1}^{N} a_{\alpha}^{n_{\alpha j}^{f}} \quad j = 1, 2, \ldots, N_f. \qquad \text{(II.3)}$$

Here K_j^f is the equilibrium constant of aqueous reaction j and a_{α} is the activity of aqueous species α.

Consider mineral reaction j leading to the dissolution of mineral i of the form

$$M_{i(j)} + \sum_{\alpha=1}^{N} v_{\alpha j}^{\lambda} S_{\alpha} = 0. \qquad \text{(II.4)}$$

The notation $i(j)$ indicates the mineral (denoted i) that is affected by the j *th* reaction. Also $v_{\alpha j}^{\lambda}$ is the stoichiometric coefficient for aqueous species α in mineral reaction j that affects mineral $M_{i(j)}$ ($v_{\alpha j}^{\lambda} < 0$ for reactants, while for products $v_{\alpha j}^{\lambda} > 0$). With this we have

$$G_j = k_j \left(\prod_{\alpha=1}^{N} a_{\alpha}^{v_{\alpha j}^{\lambda}} - \prod_{\alpha=1}^{N} a_{\alpha}^{v_{\alpha j}^{\lambda}} / K_j \right). \qquad \text{(II.5)}$$

Here k_j and K_j^s are the dissolution rate and equilibrium constant of mineral reaction j, respectively.

The reaction rate associated with the *j-th* mineral reaction as it contributes to the conservation of mass in Equation (II.1) for the solutes, W_j^s takes the form

$$W_j^s = n_i \rho_{i(j)} 4\pi R_{i(j)}^2 G_j. \tag{II.6}$$

Here n_i is the number of grains of mineral i per rock volume; ρ_i is the molar density of mineral i (number of moles of mineral i per grain volume). It is assumed that $4\pi R_i^2$ is the reactive surface area for a grain of mineral i.

3. Grain Growth/Dissolution and Texture Dynamics

Mineral reactions can lead to grain growth or dissolution. There can be several reactions for each mineral, Equation (II.5) being one of them. Therefore, the radial grain growth rate for mineral i is given by

$$\frac{\partial R_i}{\partial t} = \sum_{j=1}^{N_s} G_j. \tag{II.7}$$

The restriction of j on the sum is for only those reactions (of the N_s in total) affecting mineral i. According to Equation (II.5), a positive value of G_j stands for mineral dissolution while a negative value means mineral growth.

In the model, porosity is expressed in terms of the grain texture by

$$\phi + \sum_{i=1}^{N_m} n_i V_i = 1. \tag{II.8}$$

Here N_m is the number of minerals; V_i is the volume of a grain of mineral i. All the grains of a given mineral are assumed to be of the same size. Under a further assumption that all mineral grains are spherical, the volume of a grain of mineral i with radius R_i is given by

$$V_i = (\tfrac{4}{3})\pi R_i^3. \qquad \text{(II.9)}$$

As grains grow and dissolve, grain volumes and porosity vary.

4. Mass Conservation of Fluids

A general mass conservation equation for the two-phase flow of water (w) and oil (o) is given by

$$\frac{\partial}{\partial t}(\phi s_\ell \rho_\ell) = -\vec{\nabla}\cdot(\rho_\ell \vec{u}_\ell) + Q_\ell \quad \ell = w \text{ and } o. \qquad \text{(II.10)}$$

Here ρ_ℓ and Q_ℓ account for the mass density and the source/sink term of the fluid ℓ. This equation also applies to the single-phase flow (s_ℓ=1) and flow in free space (ϕ=1). By definition, the sum of the saturations is one:

$$s_w + s_o = 1. \qquad \text{(II.11)}$$

5. Fluid Motion

The Darcy law is typically used as the momentum equation to describe fluid motion through porous media. For two-phase, porous medium flow, Darcy's law is assumed to generalize to the form:

$$\vec{u}_\ell = -\frac{k k_{r\ell}}{\mu_\ell}(\vec{\nabla} p_\ell + \rho_\ell g \vec{z}) \quad \ell = w \text{ and } o. \qquad \text{(II.12)}$$

Here k is rock permeability, $k_{r\ell}$ and μ_ℓ are the relative permeability and the viscosity respectively of the fluid ℓ, g is the gravitational acceleration, and $\vec{z}$ is a unit upward pointing vector. The relationship between the pressures of the water and oil phases is conventionally assumed in petroleum engineering to be given by

$$p_o - p_w = p_c. \qquad \text{(II.13)}$$

Here p_c is the capillary pressure in the porous medium.

Reactive infiltration coupling can lead to the development of dissolution fingers and the creation of flow channels or wormholes in the case of complete matrix dissolution. These phenomena are commonly observed in the case of the injection of acid into a carbonate mineral-bearing formation, but also occur for sandstones injected with highly concentrated HF or NaOH solution. In this case the Darcy equation cannot account for the transport of fluid in the zone where the matrix is completely dissolved. An equation proposed by Brinkman (1946) allows one to describe the single-phase fluid motion in both porous media and free fluid domains:

$$(\mu_\ell / k)\vec{u}_\ell - \mu_\ell \nabla^2 u_\ell = -\vec{\nabla} p_\ell, \quad \ell = w \text{ or } o. \tag{II.14}$$

For fluid flow in a porous medium, the Laplacian term is relatively small and Brinkman's law reverts to the Darcy equation. For fluid flow in a channel, the Darcy term is negligible and this law becomes the Stokes equation. Experiments (Arquis, 1990) show that even in the boundary layer between the porous medium and the channel, the velocity field can be adequately described by the Brinkman equation.

D. Additional Model Equations

There are a number of options for the dependence of the thermodynamic, kinetic and transport coefficients that have been suggested in the literature. The following are those which have implemented in CIRF.A. The laws may be relatively easily changed to accommodate the user's need.

1. Thermodynamic and Rate Law Phenomenology

The phenomenology in CIRF.A is based on activity corrected thermodynamics and mass action rate laws. There are corrections for salinity and pressure. Equilibrium constants and rate coefficients are also corrected for temperature. The explicit formulae used are as follows.

a. Salinity corrections

In this version of CIRF.A the extended Debye-Huckel (EDH) corrections to the aqueous species activities are implemented. A review of the Pitzer (1973a,b) and Helgeson (1969, 1974) approaches can be found in Sverjensky (1989) and Weare (1989), respectively; more extensive treatments of thermodynamics can be found in Pitzer (1987), Harvie et al. (1984) and Moeller (1988) for the Pitzer model, and Helgeson et al. (1981), Shock and Helgeson (1988), Tanger and Helgeson (1988), and Oelkers and Helgeson (1988) for the Helgeson model. Higher order corrections for the ionic and neutral molecules and for water, using the Pitzer model, will be implemented in future versions of CIRF.A.

For less concentrated solutions, the phenomenology assumed in the current CIRF.A is adequate. The following approach is adapted: if a_α is the activity of solute α, then $a_\alpha = c_\alpha \gamma_\alpha$ where

$$\log_{10} \gamma_\alpha = -\frac{z_\alpha^2 A I^{1/2}}{1 + a_\alpha^0 B I^{1/2}} + bI,$$

$$I \equiv \frac{1}{2}\sum_{\alpha=1}^{N} z_\alpha^2 m_\alpha, \qquad \text{(II.15)}$$

$$A = \frac{1.8246 \times 10^6 \rho_w^{1/2}}{(\varepsilon_w T)^{3/2}}$$

$$B = \frac{50.29 \times 10^8 \rho_w^{1/2}}{(\varepsilon_w T)^{1/2}}.$$

Rather than using these expressions explicitly, CIRF.A uses equivalent data for A, B, and b provided by EQ3NR (Wolery, 1983). By least-square fitting of EQ3NR data of A, B and b, we get

$$A = 0.49754 + 7.8488 \times 10^{-3} T - 2.2085 \times 10^{-5} T^2 + 2.3926 \times 10^{-8} T^3$$

$$B = 0.31164 + 4.21 \times 10^{-5} T + 3.3026 \times 10^{-7} T^2$$

$$b = 1.1808 + 1.2711 \times 10^{-2} T - 4.9492 \times 10^{-5} T^2 + 8.5601 \times 10^{-8} T^3$$

$-5.5352\times10^{-11}T^4$

The values of the ionic size parameters, a_α^o, are contained in the CIRF.A database. Further discussions and data on the a_α^o are given in Helgeson et al. (1981) and Oelkers and Helgeson (1988). Note that in the above equations the concentration unit should be in molality, but in the formulation of CIRF.A, molarity is used for mass balance bookkeeping. To use the above formulation for salinity corrections but retain the convenience of molarity, those coefficients A, B and b will yield small errors in γ_α. For dilute solutions ($I < 0.4$) where the Debye-Huckle limit law is still valid, this error can be ignored and the equation and the values of those coefficients fitted for molality units can be used for molarity concentration c_α.

b. Temperature effects on equilibrium and rate parameters

Thermal transport and variations of rate and equilibrium constants with temperature are accounted for. Thermal effects contribute to:

- reaction rate coefficients,
- equilibrium constants,
- energy transport,
- temperature dependence of activities of solutes and solids,
- thermal expansion of fluids and minerals,
- temperature dependence of transport coefficients (diffusion coefficients, fluid viscosity) and rock rheology,
- temperature dependence of surface free energies.

Only the first five effects are included to date.

The temperature dependence of an equilibrium constant is accounted for by using the following polynomials:

$$\log_{10} K = \sum_{i=1}^{N_T} A_i T^{a_i} \qquad \text{(II.16)}$$

where

N_T = number of terms in the expansion

A_i = coefficient for i-*th* term

a_i = exponent for i-*th* term

A rate constant is taken to have the Arrheneous dependence on absolute temperature

$$k = k_O \exp(-E_a/RT) \tag{II.17}$$

where

k_o = high temperature limit of the rate coefficient,

E_a = activation energy,

R = gas constant,

T = absolute temperature.

2. Permeability Correlation

The permeability of the porous medium is a function of texture. There are several empirical equations describing this dependence. The Fair-Hatch equation (Bear, 1972, pp. 134) is used in the modified form:

$$k = \frac{\phi^3}{J(1-\phi)^2} \cdot \frac{1}{[\sum_{i=1}^{N_m} \theta_i n_i V_i / R_i]^2}. \tag{II.18}$$

Here J is a packing factor (≈ 5); θ_i is a geometric factor ($= 6$ for spherical grains).

3. Diffusion and Dispersion

The diffusion/dispersion law for porous media involves an effective dispersion coefficient that is a sum of the diffusion contribution and the dispersion term D^*, i.e.:

$$D = D_0 \phi^d + D^* \tag{II.19}$$

where

$$D^* = \langle L \rangle |v| \tag{II.20}$$

$$\langle L \rangle \equiv \sum_{i=1}^{M} \phi_i L_i / (1-\phi) \qquad \text{(II.21)}$$

Here D_0 is the molecular diffusion, a ranges from 1 to 2 (the default value assumed is 2), L_i is the size of grain i ($L_i^3 = 4\pi R_i^3/3$) and $\vec{v}$ is fluid velocity.

4. Relative Permeability and Capillary Pressure

The relative permeabilities and capillary pressure depend on rock and fluid properties. For a given rock system, they are expressed as functions of fluid saturations. Their saturation dependence has been determined experimentally for a number of systems. If data is not available, published correlations are often used.

The following correlation for relative permeabilities is used in CIRF.A for the oil/water system (Lake, 1988):

$$k_{rl} = k_{rl}^{o}\left(\frac{s_l - s_{lr}}{1 - s_{or} - s_{wr}}\right)^{n_l}. \qquad \text{(II.22)}$$

Here n_l, s_{lr}, and k_{rl}^{o} are the exponential constant, residual saturation and end-point relative permeability for fluid phase l, respectively. The capillary pressure is represented by a three-parameter, hyperbolic function (Donaldson et al., 1991):

$$p_c = \frac{c_1 + c_2 s_w}{1 + c_3 s_w}. \qquad \text{(II.23)}$$

Here c_1, c_2 and c_3 are constants determined by fitting experimental capillary pressure data to the correlation. This correlation fits experimental data very well, and is readily differentiated, integrated, or extrapolated for mathematical calculations.

5. Fluid Density

The density of the fluid phase l is calculated by the following equation:

$$\rho_l = \rho_{0l}\left[1 + c_l(p_l - p_{0l}) - c_{Tl}(T - T_o) + c_c \sum_{\alpha=1}^{N} c_\alpha\right]. \qquad \text{(II.24)}$$

Here ρ_{0l}, c_l, p_{0l}, and c_{Tl} are the pure substance density, isothermal compressibility, initial pressure, and thermal expansion factor for fluid phase l, respectively. The term c_c is an assumed constant proportionality factor that accounts for the solute dependence of the aqueous fluid density. The value of this term is zero for the oil phase.

E. Geometrical Features

CIRF.A allows for the simulation of systems of a variety of geometries. A number of these features are useful for waste repository analysis as follows.

1. 1-D Cartesian

Here, flow is along one spatial dimension. This feature is useful for the analysis of core flood experiments, particularly in the context of developing the network of key reactions and the list of fluid phase species. The user must specify the initial formation mineralogy and texture as well as the initial formation fluid composition.

2. 1-D Radial

Here the system is assumed to have cylindrical symmetry — i.e., rotational invariance with respect to the angle of rotation around the borehole, as well as invariance along the borehole. Thus, the only spatial variable is the distance from the borehole. The user needs to specify the injection rate and composition and the initial formation fluid composition and initial formation mineralogy and the mineral abundances.

3. 2-D Cartesian

Here the system is rectangular. Fluid may enter from one boundary at user-specified

rate and composition. This mode is useful for identifying flow self-focusing and formation damage or enhancement and, in particular, some of their geometric aspects related to original reservoir heterogeneity or flow self-focusing instabilities.

4. 2-D Radial

This mode of CIRF.A simulation is useful for analyzing phenomena in cross-sections when the problem has cylindrical (rotational) symmetry about the borehole. Examples are for near-borehole damage analysis.

5. Other Geometric Features

The CIRF.A simulation domain can be chosen to have a number of other features. One may simulate in map view, placing injection or withdrawal (production) wells at user-specified positions. The scenario of injection or production at each well can be specified individually.

The simulations may be run in a pseudo-three dimensional mode by specifying the formation thickness at each grid node in map view.

System boundaries need not be rectangular. Rather, one can specify system boundary shape. An auxiliary program can be used to fit a quadrilateral grid within and tailored to a user-specified domain. At all points on the domain, one may specify fluid pressure or in-flux or outflux rate. In the case of the influx, the scenario of injection rate and composition must be specified.

F. Verification

1. Flow and Transport

Simulation results of flow and transport for two generic cases using CIRF.A were compared with SWIFT simulation results and analytical solutions. Input parameters for the

sand and carbonate cases are given in Tables II.1 and II.2 respectively. Identical simulations were performed using SWIFT and CIRF.A to compare with the analytical solutions. A single well was specified in the center of a cylindrical region which was initially homogenous and isotropic within a single layer of constant thickness. The injection was for a total of 20 years at a rate of 100 gallons per minute (gpm). A total of 100 grid nodes were logarithmically spaced in the simulations. The radial extent of the reservoir is 25,529 feet. At the outer boundary, a no flow condition was specified. The analytical solution of Ramey and Cobb (1971) as presented in Earlougher (1977; p. 197) was used to calculate the pressure increase in a closed circular reservoir for comparison with the numerical results.

Calculated pressures and velocities for the generic cases are presented in Figs. II-3, 4, 5, and 6. Excellent agreement was obtained for pressures at the wellbore and at distance for all times. Some very small differences can be discerned mainly because CIRF.A is a grid centered finite difference code while SWIFT is a block centered code. This resulted in values being calculated at slightly different radii in some cases. Fig. II-6 shows the model calculated velocity versus distance at 100 days. Furthermore, excellent agreement between the two simulation results was obtained at all times.

Relative concentrations of brine in the formation after injecting for 1,000 days were calculated from both the SWIFT and CIRF.A models for the generic sand case. These results, as shown in Fig. II-7, compare favorably with the analytic solution. It should be noted that the analytic solution is an approximate solution and also subject to errors (Bear, 1972, pp. 637).

The verification modeling results clearly demonstrate that flow and transport calculations are accurate and in agreement between CIRF.A and SWIFT. This gives us confidence in the ability of CIRF.A to accurately model fluid flow and contaminant transport in a No-Migration Petition context.

2. Chemical Aspects

Thermodynamic calculations in CIRF.A are based on the data from our database. These are essentially those of EQ3/6 (1992). The data of EQ3/6 have been verified by its developer and other users. When formation fluids are specified in equilibrium with formation minerals, species concentrations obtained from CIRF.A do not change during simulations. Another type of verification involves placing a reactive fluid in a closed reservoir. Once CIRF.A simulation is started, the fluid will eventually become in equilibrium with all the formation minerals. These two examples demonstrate the validation of our numerical algorithms for both thermodynamics and kinetics. More complex verification of our codes with laboratory core flood data is presented in Chapter III.

Table II.1 CIRF.A and SWIFT simulation input data for waste injection into a typical Gulf Coast sandstone reservoir (with no chemical reactions).

Input Parameter	Value	Comments
Hydraulic Conductivity	2.043 ft/day	Representative for Gulf Coast sand
Intrinsic Permeability	450 md (at 140°F)	
Formation Fluid Density	68.4 lb/ft^3 at 140°F	16% NaCl solution (Perry et al., 1984)
Injectate Fluid Density	68.4 lb/ft^3 at 140°F	Same as formation brine
Porosity	0.25	Representative for Gulf Coast sand
Formation Fluid and Injectate Viscosity	1.381 cp at 68°F 0.957 cp at 100°F 0.796 cp at 120°F 0.671 cp at 140°F 0.582 cp at 160°F	16% NaCl solution (Earlougher, 1977)
Regional Flow Rate	0.0	
Formation Dip	0.0	
Injection Interval Thickness	100 feet	Assumed
Fluid Compressibility	3.3 X 10^{-6} psi^{-1}	Representative for Gulf Coast
Formation Compressibility	3.3 X 10^{-6} psi^{-1}	Representative for Gulf Coast
Longitudinal Dispersivity	200 feet	Appropriate for model scale (Adams and Gelhar, 1992)
Transverse Dispersivity	20 feet	Assumed (0.1 X 200 feet)
Effective Molecular Diffusivity	1.0 X 10^{-4} ft^2/day	Representative of injectates
Injection Rate and Duration	1 well at 100 gpm for 20 years	Assumed
Depth of Center of Injection Interval	6400 feet (at well)	Typical depth
Well Radius	0.25 feet	Assumed

Table II.2 CIRF.A and SWIFT simulation input data for waste injection into a typical Texas Panhandle carbonate reservoir (with no chemical reactions).

Input Parameter	Value	Comments
Hydraulic Conductivity	0.211 ft/day	Representative for Panhandle carbonate
Intrinsic Permeability	65 md (at 96°F)	
Formation Fluid and Injectate Density 142,100 mg/l	68.2 lb/ft^3 at 68°F 67.795 lb/ft^3 at 96°F	13% NaCl solution (CRC) (Perry et al., 1984)
Porosity	0.09	
Formation Fluid and Injectate Viscosity	1.25 cp at 68°F 1.14 cp at 80°F 0.93cp at 96°F 0.74 cp at 120°F	13.0% NaCl solution (Earlougher, 1977)
Regional Flow Rate	0.0	
Formation Dip	0.0	
Injection Interval Thickness	68 feet	
Fluid Compressibility	3.3 X 10^{-6} psi^{-1}	
Formation Compressibility	3.3 X 10^{-6} psi^{-1}	
Longitudinal Dispersivity	200 feet	Appropriate for model scale (Adams and Gelhar, 1992)
Transverse Dispersivity	20 feet	Assumed (0.1 X 200 feet)
Effective Molecular Diffusivity	1.0 X 10^{-4} ft^2/day	Representative of injectates
Injection Rate and Duration	1 well at 100 gpm for 20 years	Assumed
Depth of Center of Injection Interval	4800 feet (at well)	Typical depth
Well Radius	0.25 feet	Assumed

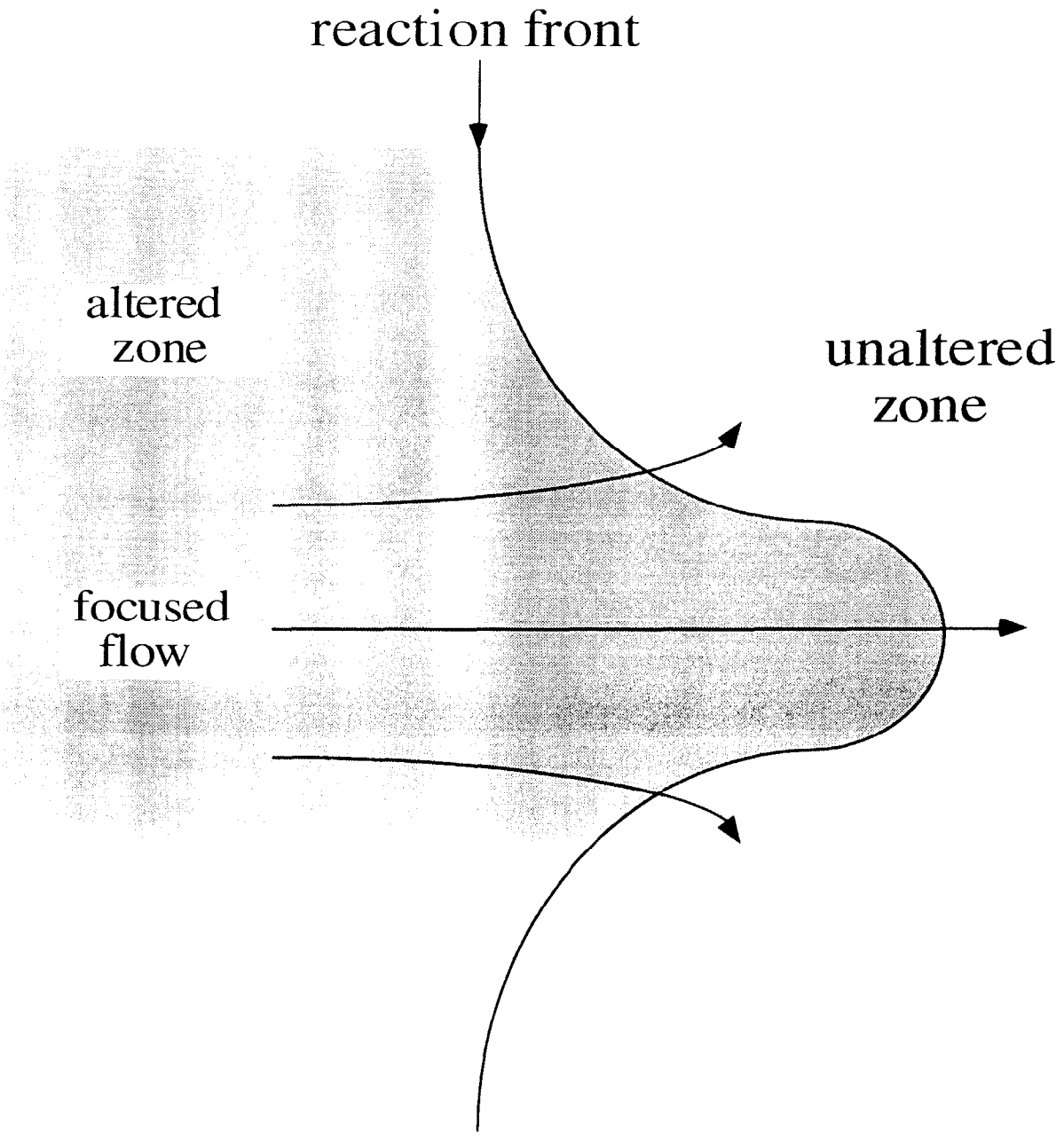

Fig. II-1 Flow self-focusing arises from the strong coupling of reaction and transport

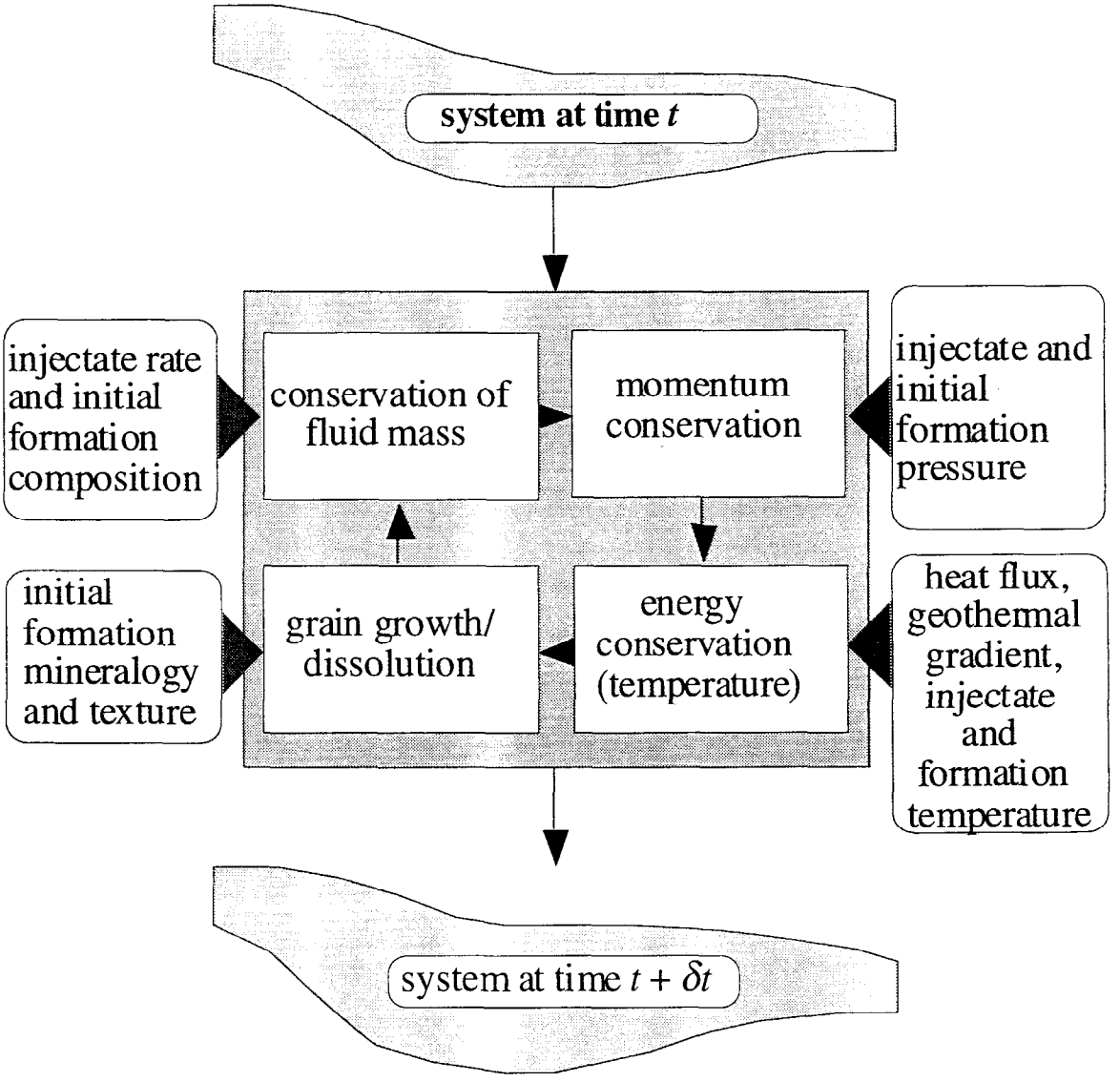

Fig. II-2 The co-evolution of all processes accounted for by CIRF.A.

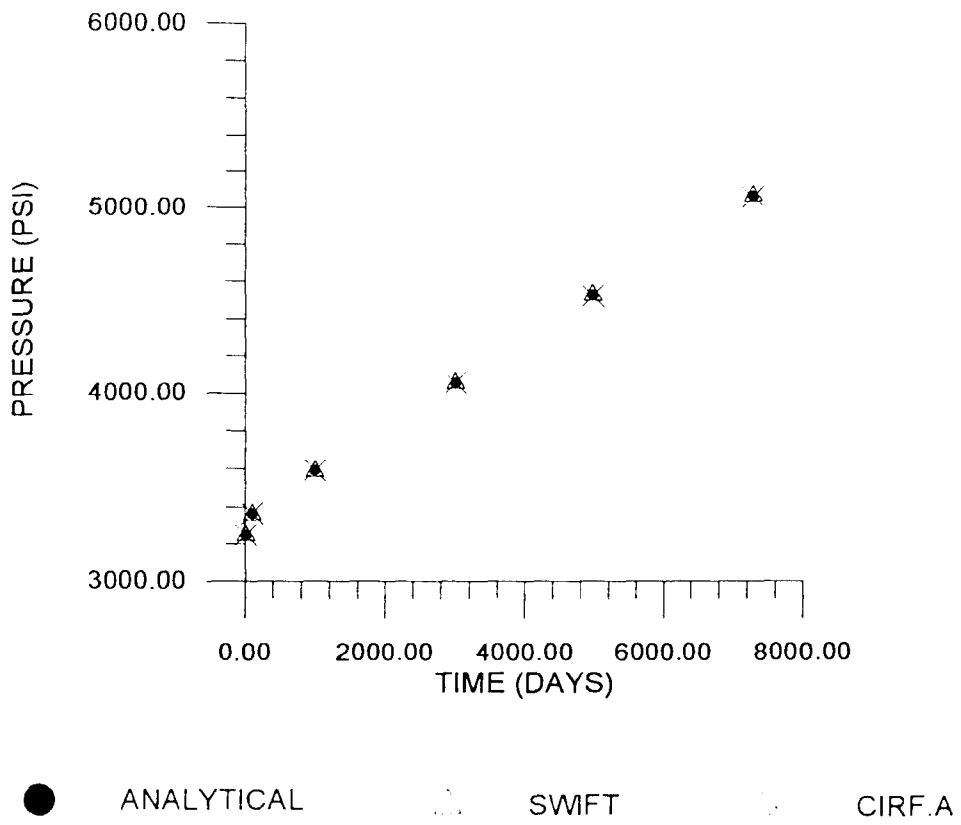

Fig. II-3 Comparison of CIRF.A, SWIFT and analytical results for waste injection into a typical carbonate reservoir with no chemical reactions. Wellbore pressures are shown as a function of injection time.

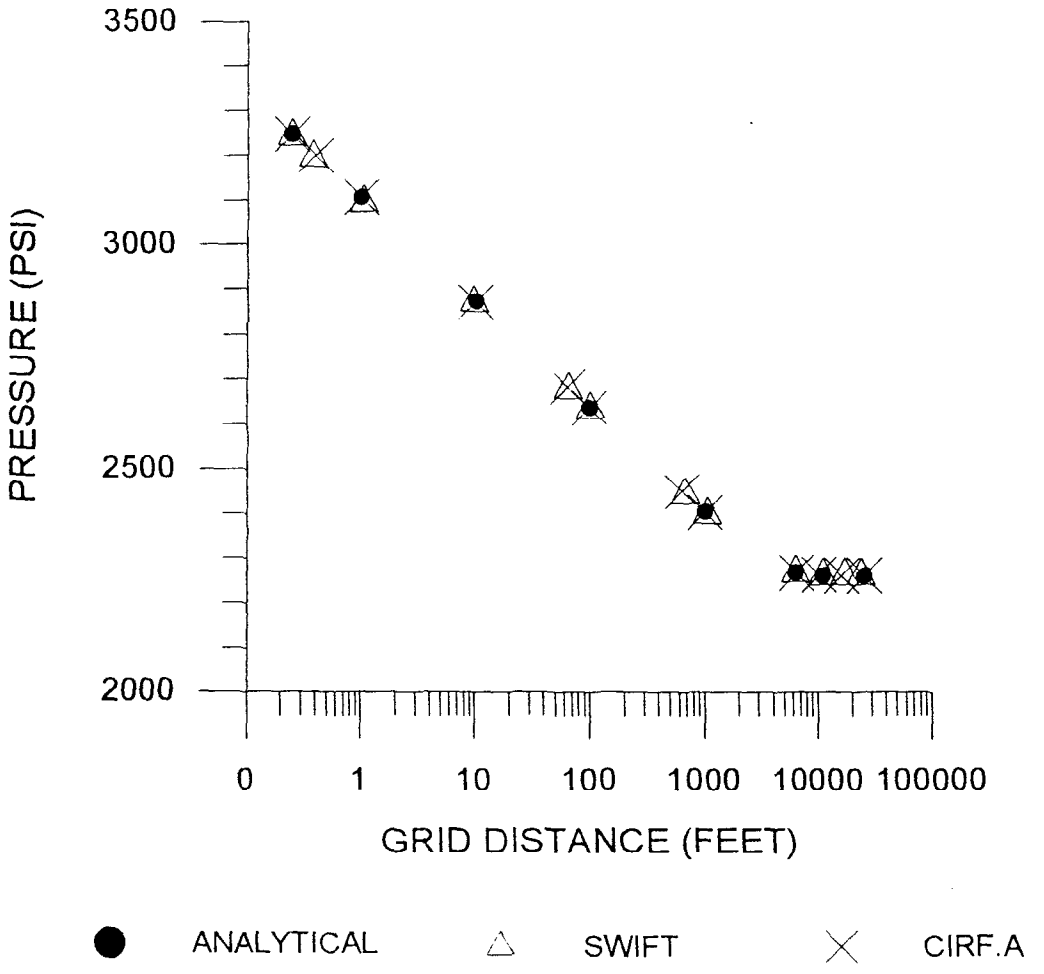

Fig. II-4 Comparison of CIRF.A, SWIFT and analytical results for waste injection into a typical carbonate reservoir with no chemical reactions. Pressures calculated after 10 days of injection are shown as a function of distance from the well.

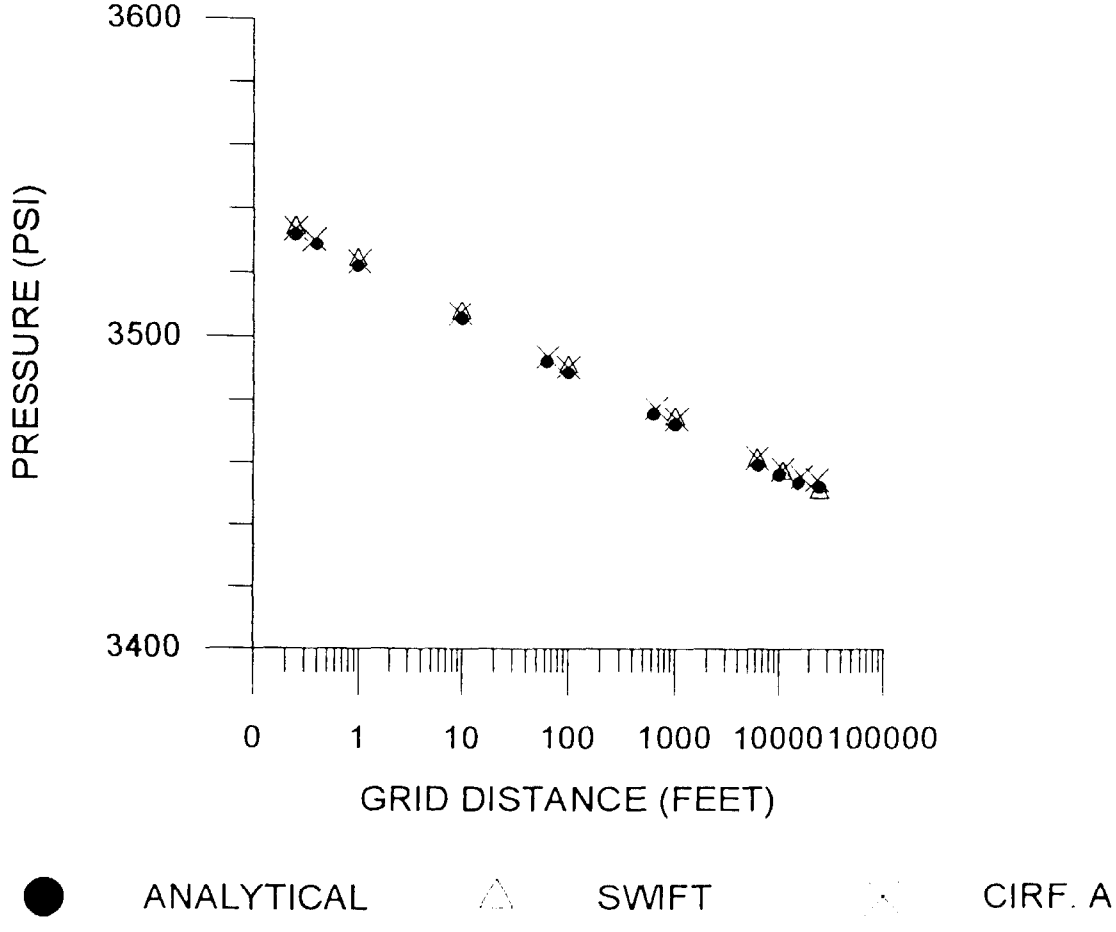

Fig. II-5 Comparison of CIRF.A, SWIFT and analytical results for waste injection into a typical sandstone reservoir with no chemical reactions. Pressures calculated after 7300 days of injection are shown as a function of distance from the well.

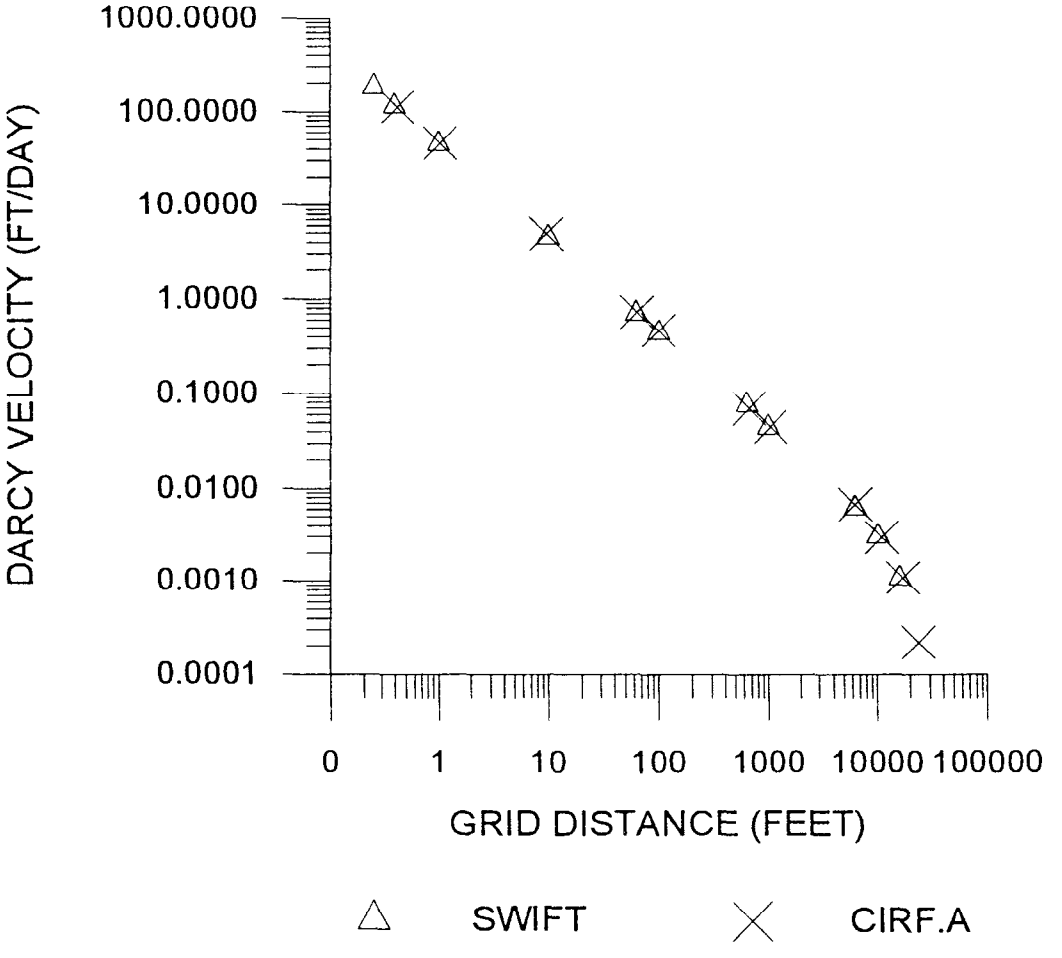

Fig. II-6 Comparison of CIRF.A and SWIFT simulation results for waste injection into a typical carbonate reservoir with no chemical reactions. Velocities calculated after 100 days of injection are shown as a function of distance from the well.

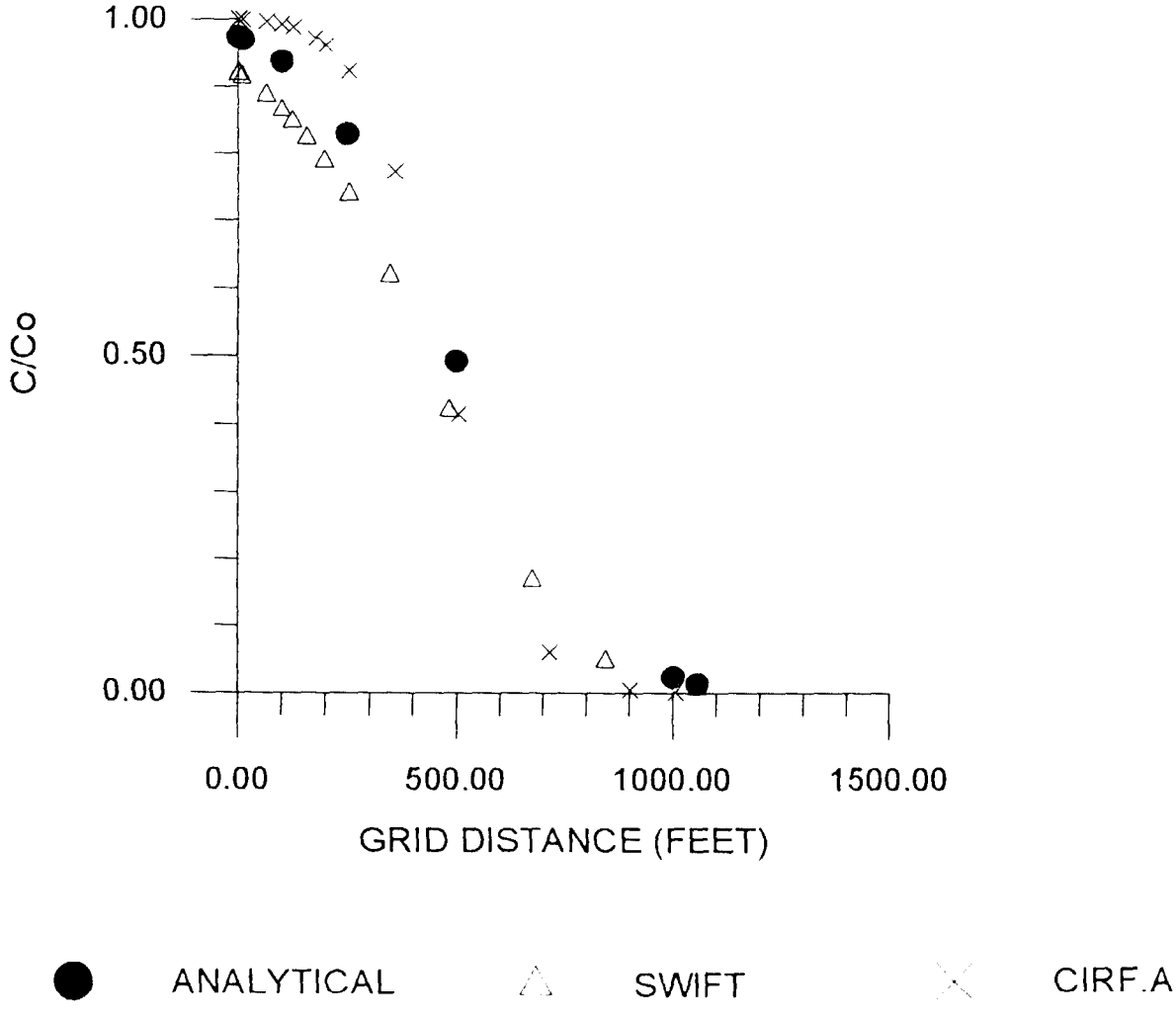

Fig. II-7 Comparison of CIRF.A, SWIFT and analytical results for waste injection into a typical sandstone reservoir with no chemical reactions. Relative concentrations calculated after 1000 days of injection are shown as a function of distance from the well.

III
Near Borehole Phenomena

A. Overview

To start our study of the appropriateness of CIRF.A for the analysis of waste disposal by deep well injection, several problems that may occur in waste injection were examined on a near-borehole scale. Here we simulated laboratory data of the injection of strong acids into rock samples, predicted precipitation-induced formation damage during injection, and studied reaction-front fingering phenomena. Detailed analysis of the problems discussed in this section is presented elsewhere (Liu et al., 1996).

B. Calibration With Laboratory Data

Laboratory core tests can be done to address several questions:

- possible formation damage (i.e., permeability-destroying precipitation or excessive dissolution leading to formation collapse);
- strategies for removing near-borehole damage due to fines migration from drilling procedures or precipitation from an earlier, ill-planned waste injection.

While core tests can address these problems, they are costly and time-consuming. CIRF.A simulations can be used to replace these tests or extend their applicability through sensitivity studies. Consider one case study as follows.

1. Experiment Summary

Long-core laboratory acidizing studies were carried out by Bartko and Newhouse (1992) to optimize an acid treatment for well stimulation and remediation of near wellbore damage in a sandstone reservoir. They determined that an optimal strength of mud acid for this sandstone is 6% HCl and 1.5% HF. In this section, a simulation of one of their core tests is presented to illustrate the complexities of rock/fluid interactions in matrix acidizing.

The experiment involved acidizing an undamaged sandstone core sample. The core was 25.4 cm in length and 2.54 cm in diameter. The rock was composed of quartz (58% by volume), kaolinite (7% by volume), illite (6% by volume), and siderite (2.5% by volume). The test was conducted at a temperature of 82^{o}C (180^{o}F). First, flow through the core was established with NH_4Cl water and the rock permeability was determined. The initial porosity and permeability of the core sample were 26.5% and 0.365 darcy, respectively. After a preflush of 5 pore volumes of 7.5% HCl, mud acid (6% HCl and 1.5% HF mixture) was injected through the core at a rate of 11 milliliter per minute for 10 pore volumes (about 31 minutes of injection).

2. Reaction Mechanisms

Major constituents in a typical sandstone are quartz and clays. Compared to the high reactivity of HF acid with clays and quartz, HCl is considered not to react with these minerals. Nevertheless, HCl is needed to maintain a low pH value in the acid and remove any calcium-bearing minerals in the formation, thereby enhancing the dissolving power of HF and reducing the precipitation of HF reaction byproducts (Williams et al., 1979). An examination of the rock minerals and acids involved in the acidizing test by Bartko and Newhouse (1992) led us to what we consider the likely reaction mechanism, as given in Table III.1.

A summary of kinetic models for acidization reactions reported by Williams et al. (1979) suggests that aluminosilicate dissolution is usually a first-order reaction with respect

to HF. Therefore, first-order dissolution reactions of HF with clays and quartz are assumed. To ensure the first-order reaction, each stoichiometric equation for the dissolution reaction by HF in Table III.1 is divided by the stoichiometric coefficient of HF. As a result, all the stoichiometric coefficients of HF become one. Under the assumption that the activity of a mineral is one, the kinetic rate laws implemented in our model as outlined in the previous section thus yield first-order dissolution reactions of HF with clays and quartz.

3. CIRF.A Simulation of Core Test

Equilibrium constants for the reactions are from the program database (i.e., essentially those of EQ3/6, Wolery, 1992). The mineral reaction rate constants were adjusted by us in an attempt to match the experimental results. The concentration profiles of total aqueous silica and aluminum as a function of distance from the injection end of the core sample after injecting 9 pore volumes of mud acid (about 28 minutes of injection) were used for comparison with the predictions of our simulator.

Fig. III-1 shows a comparison of experimental and simulated concentration profiles of total aqueous silica. It is found that the simulation results are in good agreement with the experimental results. It is interesting to note that the concentration of aqueous silica increases and reaches its maximum at about 12 cm from the injection end and then decreases. The decrease in silica concentration indicates the removal of silica from the fluid, i.e. the precipitation of hydrated silica in the rock. This represents a potential damage to rock permeability.

Fig. III-2 presents both experimental and simulated concentration profiles of total aqueous aluminum. Unlike the profile of aqueous silica, that for aqueous aluminum keeps increasing. Apparently, no aluminum precipitation occurs since it is not removed from the fluid. For aluminum, the experimental trend of monotonic increase was also predicted accurately in the simulation. Further details are found in Liu et al. (1996).

The objective of matrix acidizing is to improve rock permeability. Fig. III-3 illustrates the permeability profile after acidizing as a function of distance along the core. Compared to the initial rock permeability of 0.365 Darcy, our simulator predicts that the permeability at the core inlet has increased to about 1.22 Darcy and the permeability at the core outlet has reduced to about 0.31 Darcy. The predicted overall (averaging across the core) permeability improvement is about 22%. This is close to the measured overall permeability improvement of 19%.

In this experiment, the precipitation of hydrated silica is identified to cause acid-induced formation damage further down the core as shown in Fig. III-3. Simulation studies were carried out to minimize the acid-induced formation damage. See Liu et al. (1996) for further details.

C. Prediction of Wormholes

The stimulation efficiency of a matrix acidizing treatment for a well in a carbonate formation is enhanced by generating dissolution channels (wormholes) that advance away from the wellbore into the formation (Hoefner et al., 1987). The wormhole growth rate depends on a number of factors, including the reaction rate coefficient, acid concentration, dispersion and the rate of injection, as well as the initial porosity of the matrix. Theory (Chadam et al., 1986, 1988, 1990; Ortoleva et al., 1987a,b; Chen et al., 1990; Steefel and Lasaga, 1990; Ortoleva, 1994) and experiments (Hoefner et al., 1987; Wang et al., 1993) show that high reaction rate, high flow rate and low dispersion coefficient favor fingering or wormholing. In their experiments Wang et al. (1993) obtained a single straight wormhole in Indiana limestone by injection of 4.4 moles/liter of HCl at a flow rate of 0.01 cm/sec.

The first numerical simulation presented here corresponds to parameters which are chosen to model these experiments. Initial rock porosity and permeability were 10% and

0.04 Darcy, respectively. A constant pressure difference of 10^5 Pa was imposed across a 20 cm x 6 cm domain. An initial heterogeneity with a porosity of 100% was introduced at the inlet side (left) of the domain, as indicated by the top plot in Fig. III-4.

Fig. III-4 shows the development of a wormhole starting from the initial small heterogeneity at different injection times. At the beginning, the reaction front adjacent to the heterogeneity advances more slowly than that within the heterogeneity. When the thickness of the dissolved zone is large enough, almost all the fluid is focused into the wormhole. At this time the reaction front adjacent to the wormhole almost stops progressing, while the wormhole grows faster with time. The wormhole advancement rate increases as the system evolves.

Since the pressure is almost constant in the free fluid region, the variation in the pressure occurs in the porous medium only. As the wormhole grows, the pressure gradient and fluid velocity in the porous medium increase with time. The flow velocity has increased from its initial value of 0.024 cm/sec to 0.24 cm/sec at the end of the simulation. This phenomenon results from the feedback between reaction and transport. Streamlines are parallel to the reaction front everywhere except at the tip of the wormhole. The flow at the tip is normal to the reaction front, explaining why the front is broader there.

The influence of three parameters on the formation of wormholes was investigated. The three parameters of interest are injection rate, inlet HCl concentration and the dispersion coefficient. Table III.2 is the summary of the results of six simulations. Case 1 corresponds to Fig. III-4. The results given are in terms of the width L and initial growth rate s of the wormhole. These simulations were performed in a domain with the same size and the same initial porosity and permeability as for the simulation shown in Fig. III-4.

1. The Effect of Injection Rate

Experiments (Wang et al., 1993) show that at low injection rates the acid is spent near the core inlet surface because a planar (non-focused) reaction front advances slowly

At high injection rates, more complex wormholes form, while at intermediate rates a single wormhole penetrates the rock. In each of the six cases in our study, we obtain a single straight wormhole. Hung et al. (1989) observed a linear dependence of wormhole length on injection rate. Since the length of our simulation domain was smaller than the wormhole size for steady state conditions, in every case the wormhole reached the end of the domain before the steady state condition was obtained. Cases 1, 2 and 3 show that the growth rate increases with injection rate, as expected. More precisely, we observe that with an increase of the injection rate by a factor of 10 between Cases 1 and 2 and Cases 2 and 3, the increase in growth rate is not linear but is 11.4 and 22 times, respectively. When an increase in velocity does not have an increase in dispersion coefficient (in Cases 1, 2 and 3), the increase of velocity leads to a decrease in the wormhole width.

2. The Effect of Fluid Dispersion

As the dispersion increases, the width of a reaction front also increases. We have modeled a dispersion coefficient to be proportional to the fluid velocity and the grain size. From Cases 2 and 5 we observe that the effect of increasing dispersion on the wormhole width balances the effect of increasing velocity. From Cases 3 and 5 we observe that lower dispersion favors a narrower wormhole; this has a strong effect on the growth rate of the wormhole. In the narrower wormhole the fluid is more focused to the tip, increasing the wormhole growth rate.

3. The Effect of Acid Concentration

Comparisons of Case 1 with 6 and Case 4 with 5 show that there is a linear dependence of the growth rate of the wormhole on the concentration of acid in the inlet fluid. In Cases 4 and 5, acid concentration seems to have little influence on the width of the wormhole.

It is noteworthy that our simulations are two-dimensional while real wormholes exist in three dimensions. The flow self-focusing for the creation of wormholes is stronger in three than in two dimensions. This may explain some differences between simulations and observations.

D. CIRF.A Prediction Of Acidizing Treatments

Waste injection often induces permeability reduction near the wellbore due to solid invasion, fines migration and mineral precipitation. An effective means of restoring the rock permeability is matrix acidizing. In this section, CIRF.A is used to analyze the stimulation efficiency of matrix acidizing treatments for waste injection wells.

1. Undamaged Well Treatment

The same data as Section III.B will be used here to predict the stimulation potential of a typical acid treatment for a well in a reservoir having the same rock properties as the core. This well is thus an undamaged well since the rock used in the core test was not damaged before acidizing.

In this regard, we consider a well with a radius of 7.62 cm, a drainage radius of 200 meters, and a formation thickness of 3 meters. The formation depth is 3,000 meters. The reservoir temperature is 82^{o}C (180^{o}F), the same as the temperature used in the core test. First, 4.73 m^3 (1,250 gallons) of HCl acid (7.5% by weight) is injected from the well into the formation at a rate of 3.15x10^{-3} m^3/s (50 gallons per minute) for 25 minutes. Following that, 9.46 m^3 (2,500 gallons) of mud acid (6% HCl and 1.5% HF) is injected at the same rate for 50 minutes. CIRF.A is then used to simulate this scenario.

Simulation results illustrated in Fig. III-5 are the mineral alteration profiles for kaolinite, illite and hydrated silica as a function of the radial distance from the center of the

well at the end of the simulated operation. Note that acids have dissolved appreciable amounts of clays in the formation adjacent to the wellbore. The dissolution zone is extended from the wellbore to a radius of 80 cm. As a byproduct of the reactions of HF with clays, hydrated silica precipitates in a region from a radius of 20 cm to a radius of 100 cm, reaching a maximum value at a radius of 40 cm. Although the mineral alteration zone is extended from the wellbore to a radius of 100 cm, Fig. III-6 illustrates that most change in porosity occurs in a region from the wellbore to a radius of 60 cm. As shown in Fig. III-7, the permeability alteration zone is only extended to 40 cm away from the center of the well. This means that matrix acidizing can only enhance rock permeability in a region very close to the wellbore.

The ultimate goal of matrix acidizing is to improve well injectivity or productivity. CIRF.A also calculates the ratio of the original well productivity to the improved well productivity during the acid treatment. The productivity ratio versus operation time is presented in Fig. III-8. In the first 25 minutes of operation, the well is treated by HCl and a slight productivity improvement is contributed by the dissolution of siderite by HCl. Once a mixture of HCl and HF is injected, clays are also dissolved and a better productivity improvement is obtained. However, the productivity is only improved by about 15% at the end of the acid treatment. The calculation of well productivity under steady-state and radial flow conditions reveals that improving the productivity of this undamaged well by 50% requires the complete dissolution of all the rock minerals in a region from the wellbore to a radius of about one meter. In fact, matrix acidizing can not lead to such a complete dissolution zone around the wellbore, but will only improve the rock permeability in a region of a few tens of centimeters away from the wellbore. Therefore, a matrix acidizing treatment for an undamaged well does not provide much stimulation potential.

2. Damaged Well Treatment

To demonstrate a successful field treatment, another scenario – matrix acidizing for a

damaged well — was simulated. In this case, a clean sandstone formation (mainly composed of quartz) is assumed to have been damaged by the invasion of montmorillinite (a major constituent for some water-based drilling fluids). The clay invasion and resulting porosity and permeability alteration profiles in the formation near the wellbore are presented in Figs. III-9, 10 and 11, respectively. The maximum amount of montmorillinite invaded is 5% (by total pore volume) that occurs at the wellbore. The invasion is extended to a radius of 25 cm. The porosity at the wellbore is decreased to 20% from its original value of 25%. The permeability at the wellbore is decreased to 0.005 darcy from its original value of 0.16 darcy.

Prior to acid treatment, the formation was assumed to be saturated with formation brine that contains 9.4% NaCl (1.6 moles/liter) and 0.11% $CaCl_2$ (0.01 moles/liter). Assuming the same well and reservoir size as for the undamaged well, a field treatment is then designed. Common practice is to limit the injection rate to be consistent with the rock fracturing gradient. Here we assume that the injection rate is 1.58×10^{-3} m^3/s (25 gallons per minute).

First, 4.73 m^3 (1,250 gallons) of preflush fluid (6% HCl) is injected for 50 minutes, followed by the injection of 9.46 m^3 (2,500 gallons) of mud acid (6% HCl and 1.5% HF) for 100 minutes. After that, 4.73 m^3 (1,250 gallons) of afterflush fluid (6% HCl) is injected for 50 minutes. In the end, all the injected fluids are withdrawn. The reaction mechanism involved in this case is given in Table III.3. CIRF.A is then used to simulate this treatment.

During the period of mud acid treatment, invaded montmorillinite is dissolved as injection proceeds. The temporal evolution and the spatial distribution of montmorillinite in the formation is illustrated in Fig. III-12. Consequently, porosity and permeability change with time and space. As indicated in Figs. III-13 and 14, porosity and permeability in the formation have been fully recovered at the end of mud acid injection.

The productivity ratio as a function of the operation time shown in Fig. III-15 provides the productivity improvement in response to each treatment step. A few interesting phenomena are observed in this figure. Further details are in Liu et al. (1996). Fig. III-16 illustrates the distribution profiles of the precipitation of hydrated silica at the end of the mud acid treatment (150 minutes) and at the end of the operation (400 minutes). The productivity ratio at the end of the operation has been increased from 0.31 to 0.97, and hence this treatment has increased the productivity of the damaged well by about a factor of three.

E. Effects of Multi-Phase Flow on Acidizing

Acid treatments are often conducted to improve the productivity of oil or gas wells. In these cases, multi-phase flow of aqueous fluids with oil or gas is then encountered. In multi-phase flow, other parameters such as fluid saturations, capillary pressure and relative permeabilities come into play. In the literature, most acidizing studies focused on the single-phase flow of aqueous acidic fluids.

To determine the effects of multi-phase flow on acidizing results, we also carried out simulation studies for the above core test, undamaged well and damaged well in two-phase flow conditions. We assumed that before acid injection all the rocks involved in the three cases were initially saturated with oil in the presence of connate water. Our simulation results indicated that multi-phase flow had little influence on mineral dissolution and porosity and permeability alteration if the amount of injected acid was the same and oil was completely displaced. This is because the saturation front advances much faster than mineral reaction fronts. If the treatment pressure was kept constant, the amount of acid that could be injected at a given time was lower in the two-phase flow due to the effects of

relative permeability. In this situation, the permeability enhancement was correspondingly less.

Rock wettability is a major factor when ascertaining the location and distribution of fluids in a formation. In an oil-wet formation, oil contacts most of the rock surfaces. When acid displaces oil, thin oil films still exist on the pore surfaces. If the oil films do not break during acidizing, the chances for the acid to contact the pore surfaces and react with rock minerals are then greatly reduced. Further theoretical and modeling studies are being undertaken to understand the complexities of acid treatments in multi-phase flow.

Another interesting phenomenon – viscous fingering — may develop when a less viscous acid solution displaces a more viscous oil fluid (Ortoleva et al., 1994). It is found that the coupling between the viscous fingering and reaction-front fingering leads to very complex fingering patterns (Liu and Ortoleva, 1995). These effects are difficult to predict without a multi-phase, reaction-transport simulator.

Table III.1. Reaction mechanism for core acidizing

Mineral dissolution reactions:

1. SiO_2 (quartz) + 6HF = H_2SiF_6 + $2H_2O$
2. $Al_2Si_2O_5(OH)_4$ (kaolinite) + 18HF = $2H_2SiF_6$ + $2AlF_3$ + $9H_2O$
3. $K_{.6}Mg_{.25}Al_{2.3}Si_{3.5}O_{10}(OH)_2$ (illite) + 29HF = $0.6K^+$ + $0.25Mg^{2+}$ + $1.2AlF_3$ + $1.1\,AlF_4^-$ + $3.5H_2SiF_6$ + $12H_2O$
4. $FeCO_3$ (siderite) + H^+ = Fe^{2+} + HCO_3^-

Mineral precipitation reactions:

1. H_2SiF_6 + $4H_2O$ = $Si(OH)_4$ (ppt.) + 6HF
2. $2K^+$ + SiF_6^{2-} = K_2SiF_6 (ppt.)

Aqueous reactions:

1. HF = H^+ + F^-
2. HCl = H^+ + Cl^-
3. AlF_2^+ = Al^{3+} + $2F^-$
4. AlF_3 = Al^{3+} + $3F^-$
5. AlF_4^- = Al^{3+} + $4F^-$
6. H_2SiF_6 = $2H^+$ + SiF_6^{2-}
7. $CO_2(aq)$ + H_2O = H^+ + HCO_3^-

Table III.2. The effects of injection velocity u, diffusion/dispersion coefficient D and inlet acid concentration [HCl] on the wormhole growth rate s and width L. The simulations were performed with the same initial conditions as in Fig. III-3.

Case #	u (cm/sec)	[HCl] (mol/l)	D (cm^2/sec)	L (cm)	s (cm/sec)
1	0.024	4.0	5×10^{-5}	1.5	1.40×10^{-3}
2	0.24	4.0	5×10^{-5}	1.2	1.60×10^{-2}
3	2.4	4.0	5×10^{-5}	1.1	0.325
4	2.4	1.0	1×10^{-4}	1.2	6.17×10^{-2}
5	2.4	4.0	1×10^{-4}	1.2	0.257
6	0.024	1.0	5×10^{-5}	1.2	3.83×10^{-4}

Table III.3. Reaction Mechanism for Damaged Well Acidizing

Mineral dissolution reactions:

1. SiO_2 (quartz) + 6HF = H_2SiF_6 + $2H_2O$
2. $Na_{.33}Mg_{.33}Al_{1.67}Si_4O_{10}(OH)_2$ (montmorillinite) + 30HF = $0.33Na^+$ +$0.33Mg^{2+}$ + $0.68AlF_3$ + $0.99\ AlF_4^-$ + $4H_2SiF_6$ + $12H_2O$

Mineral precipitation reactions:

1. $H_2SiF_6 + 4H_2O = Si(OH)_4$ (ppt.) + 6HF
2. $2Na^+ + SiF_6^{2-} = Na_2SiF_6$ (ppt.)
3. $Ca^{2+} + 2F^- = CaF_2$ (ppt.)

Aqueous reactions:

1. $HF = H^+ + F^-$
2. $HCl = H^+ + Cl^-$
3. $AlF_2^+ = Al^{3+} + 2F^-$
4. $AlF_3 = Al^{3+} + 3F^-$
5. $AlF_4^- = Al^{3+} + 4F^-$
6. $H_2SiF_6 = 2H^+ + SiF_6^{2-}$
7. $NaCl = Na + Cl^-$
8. $CaCl_2 = Ca^{2+} + 2Cl^-$

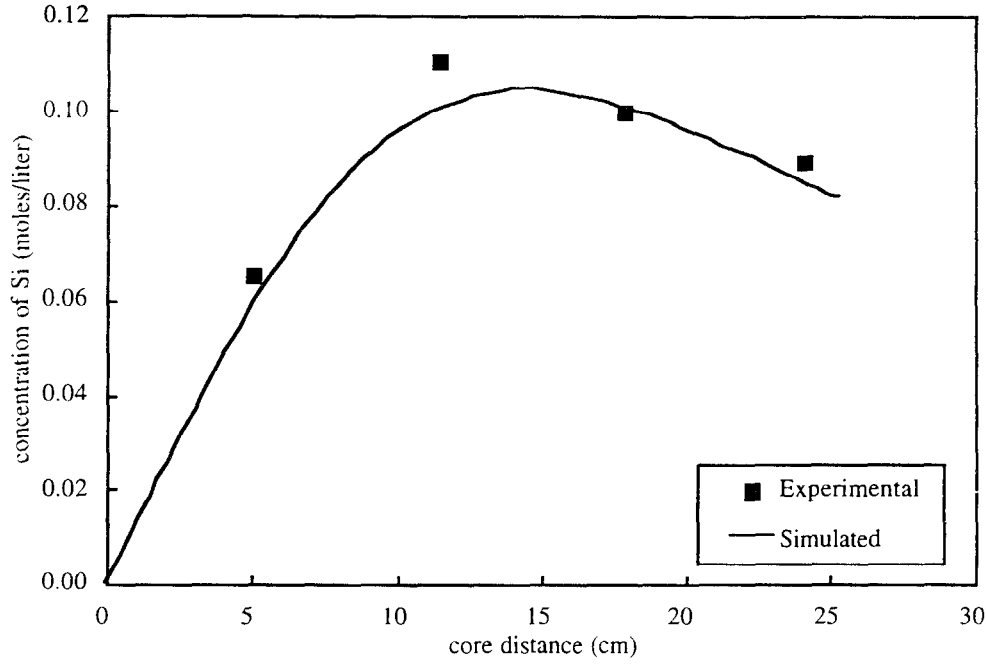

Fig. III-1 Comparison of simulated and observed results of a core acidizing test: total aqueous silica concentration versus core distance after 9 pore volumes of mud acid treatment.

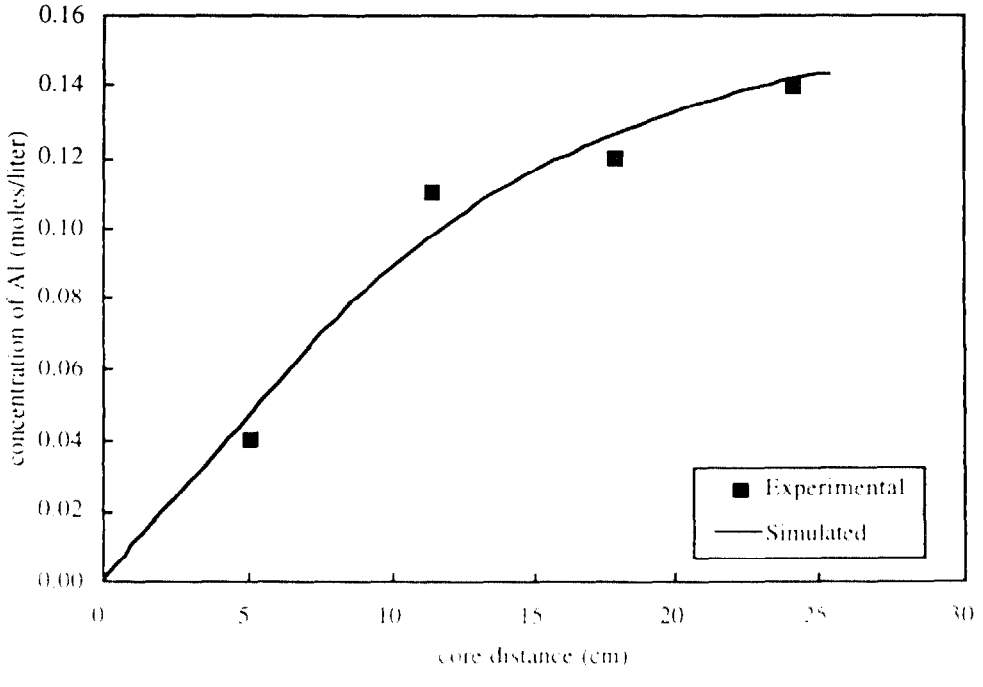

Fig. III-2 Comparison of simulated and observed results of a core acidizing test: total aqueous aluminum concentration versus core distance after 9 pore volumes of mud acid treatment

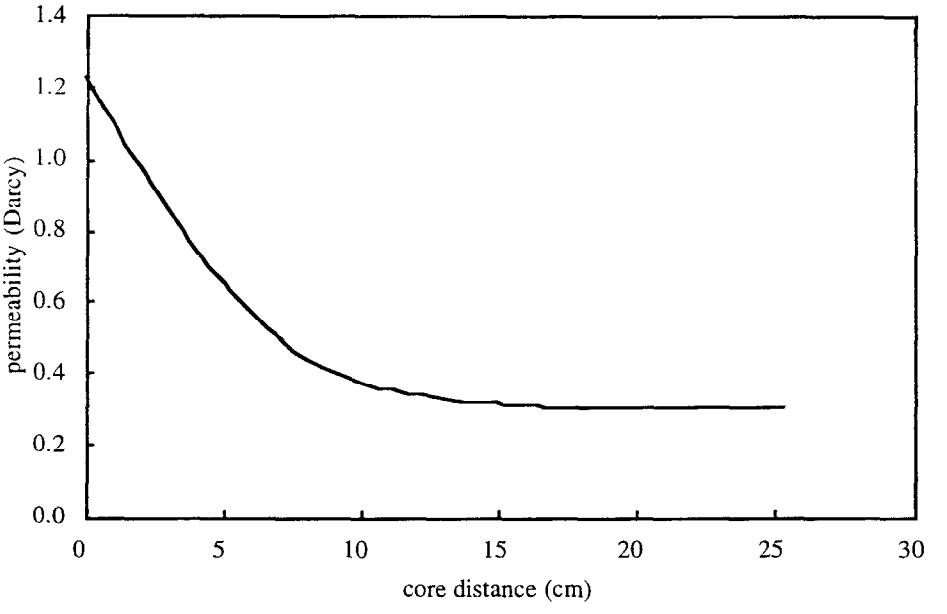

Fig. III-3 Predicted permeability alteration profile from the core acidizing test after 10 pore volumes of mud acid treatment.

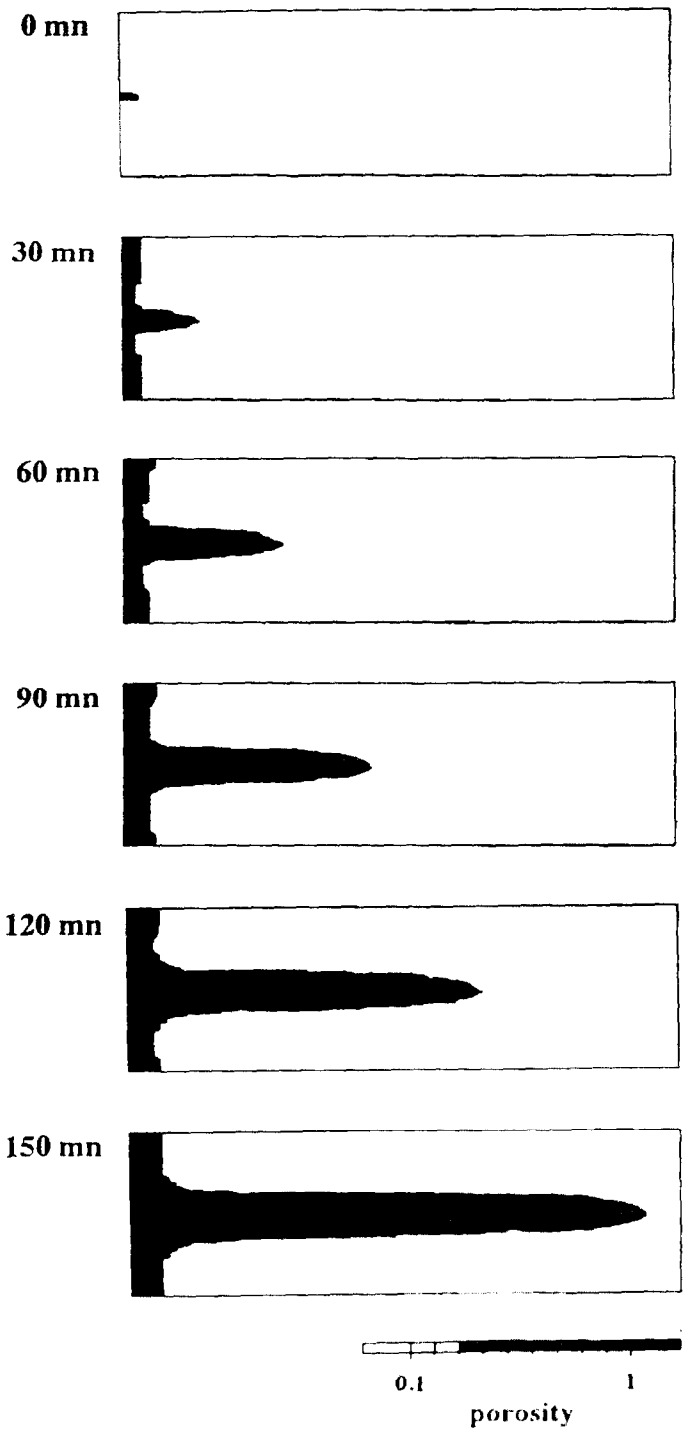

Fig. III-4 Evolution of the porosity distribution in a limestone formation with the initial porosity of 10%. HCl acid (15%) was injected at a differential pressure $\Delta p = 10^5$ Pa across a 6 cm × 20 cm domain with no-flow top and bottom boundaries.

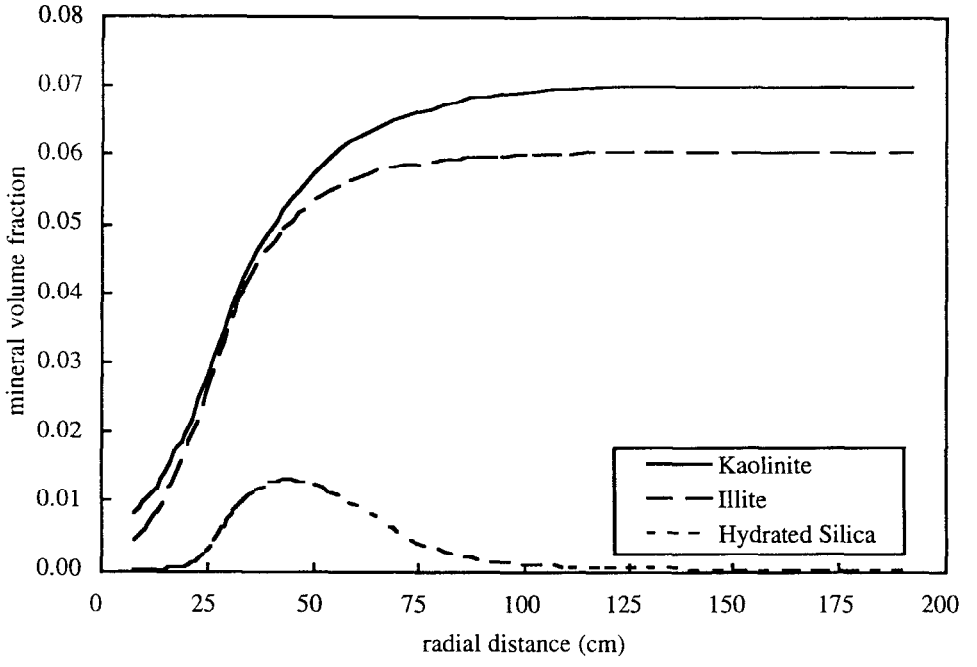

Fig. III-5 Predicted mineral alteration profiles from the acidizing treatment of a undamaged well. Volume fractions of kaolinite, illite and hydrated silica are shown as a function of radial distance after the treatment.

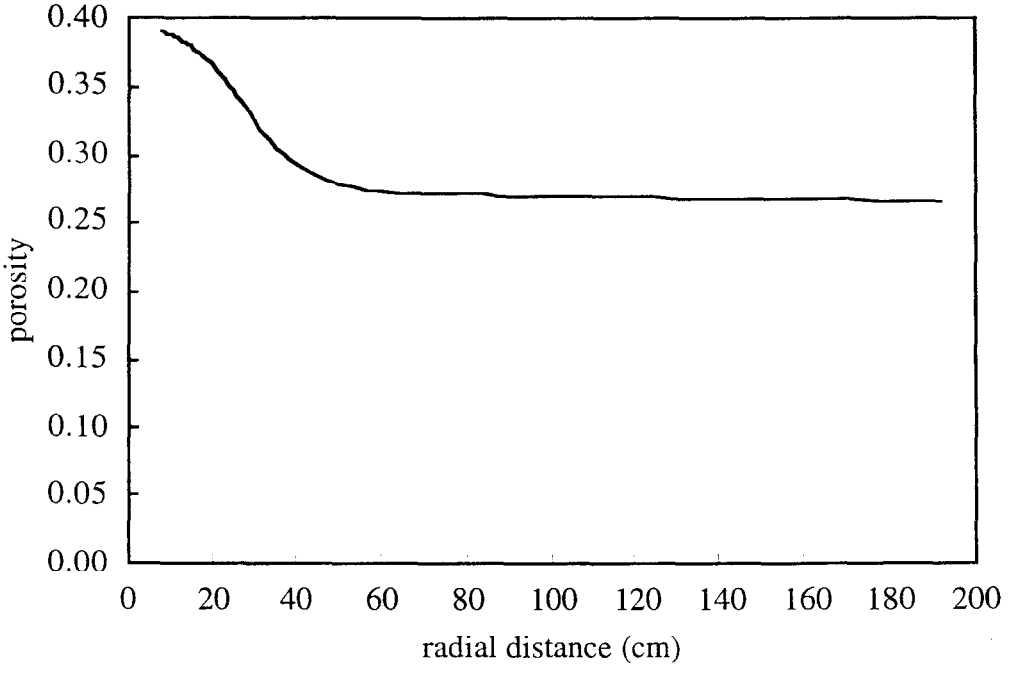

Fig. III-6 Predicted porosity alteration profile from the acidizing treatment of a undamaged well.

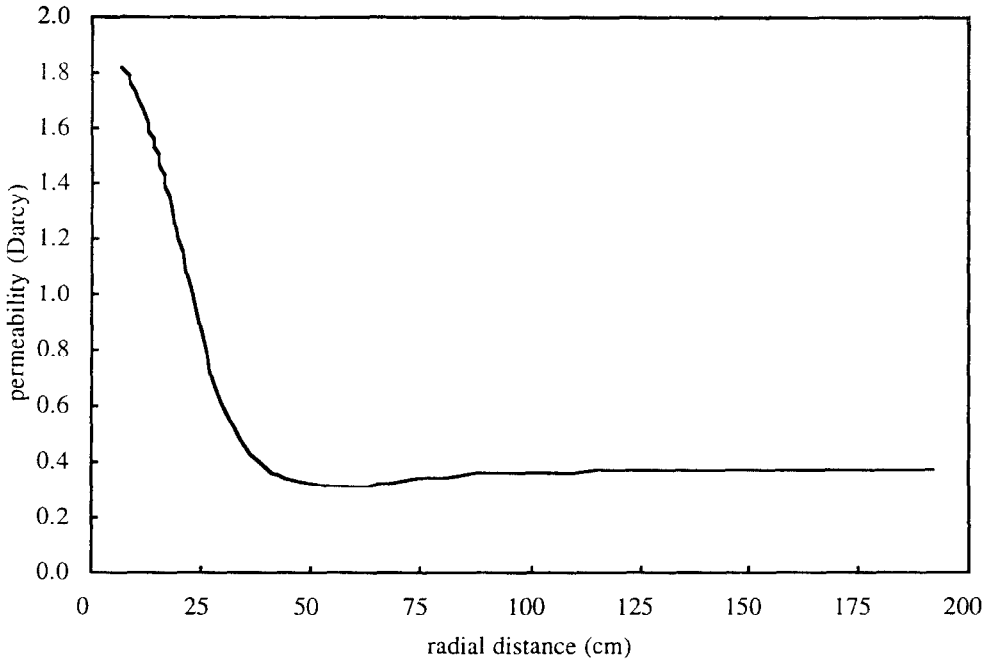

Fig. III-7 Predicted permeability alteration profile from the acidizing treatment of a undamaged well.

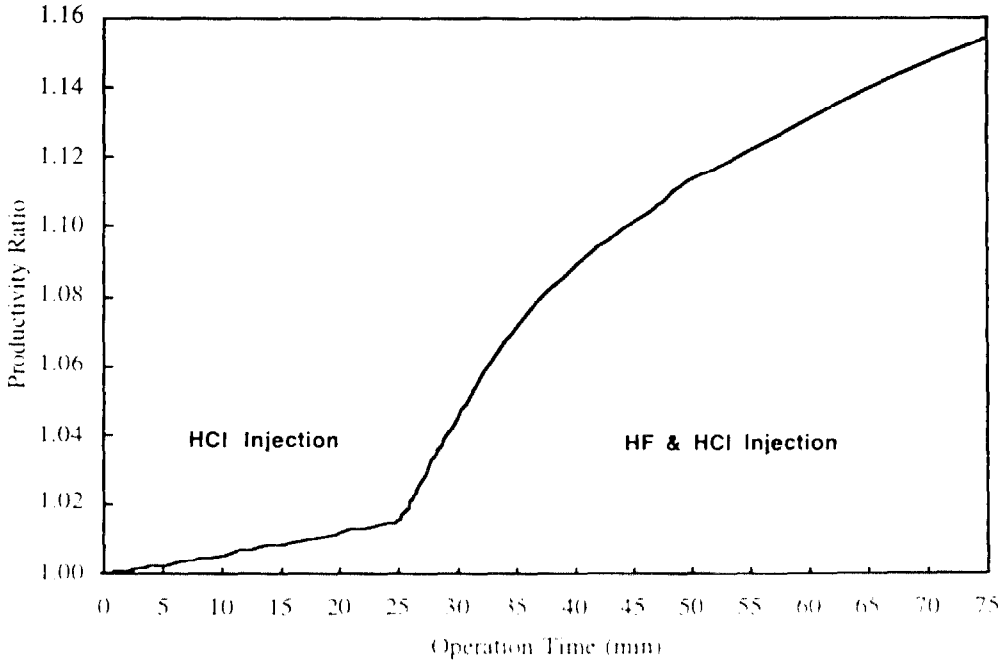

Fig. III-8 Stimulation potential for the undamaged well: the ratio of the well productivity during acidizing to the original well productivity is shown as function of the treatment time.

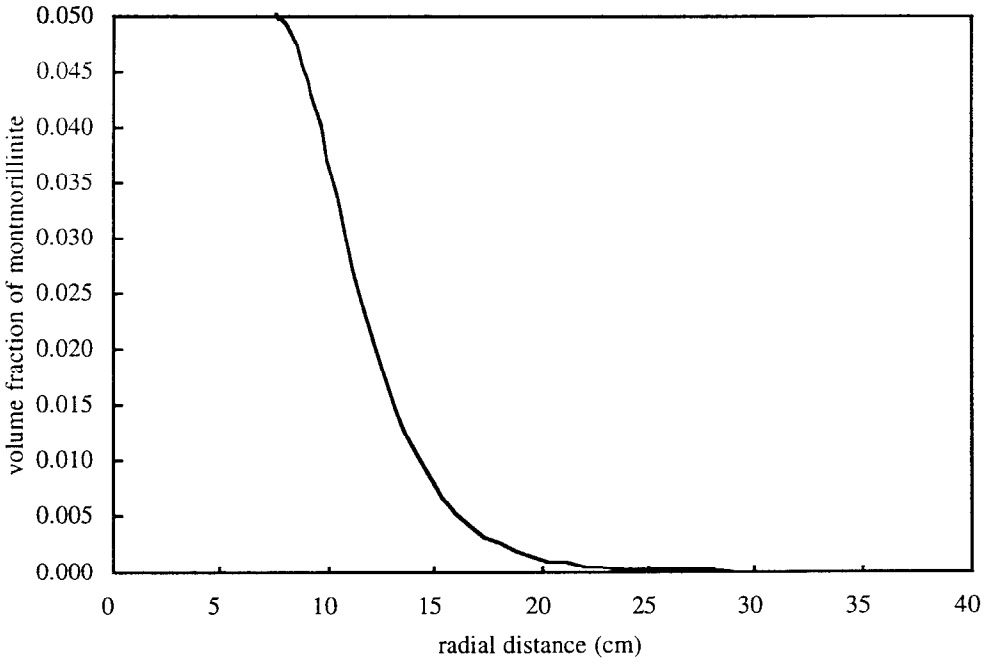

Fig. III-9 Clay invasion profile for the damaged well: the volume fraction of invaded montmorillinite versus the radial distance from the center of the well.

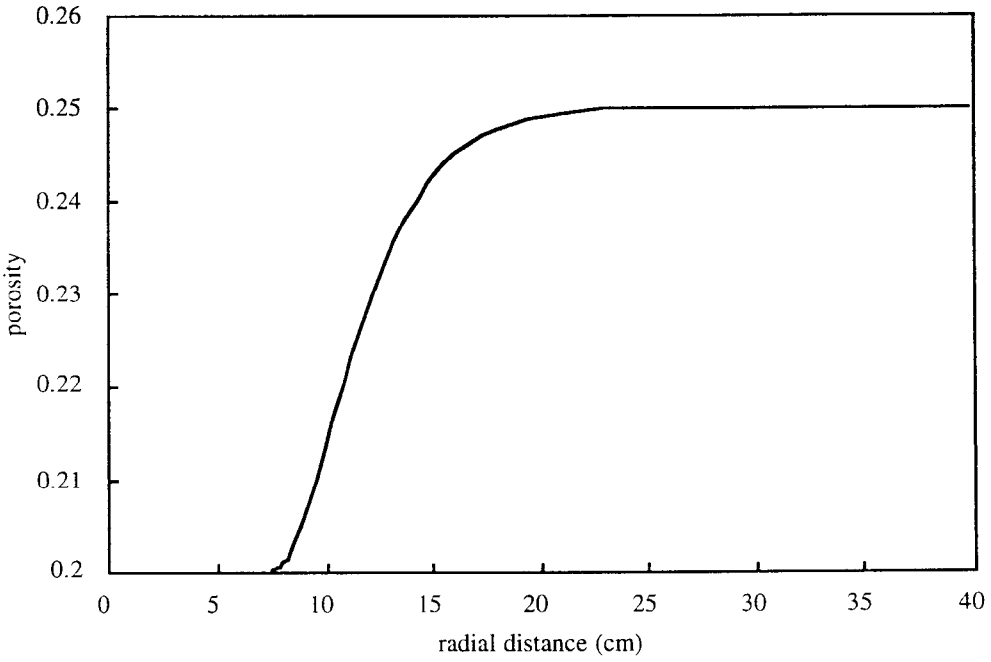

Fig. III-10 Porosity distribution near wellbore resulting from the invasion of montmorillinite.

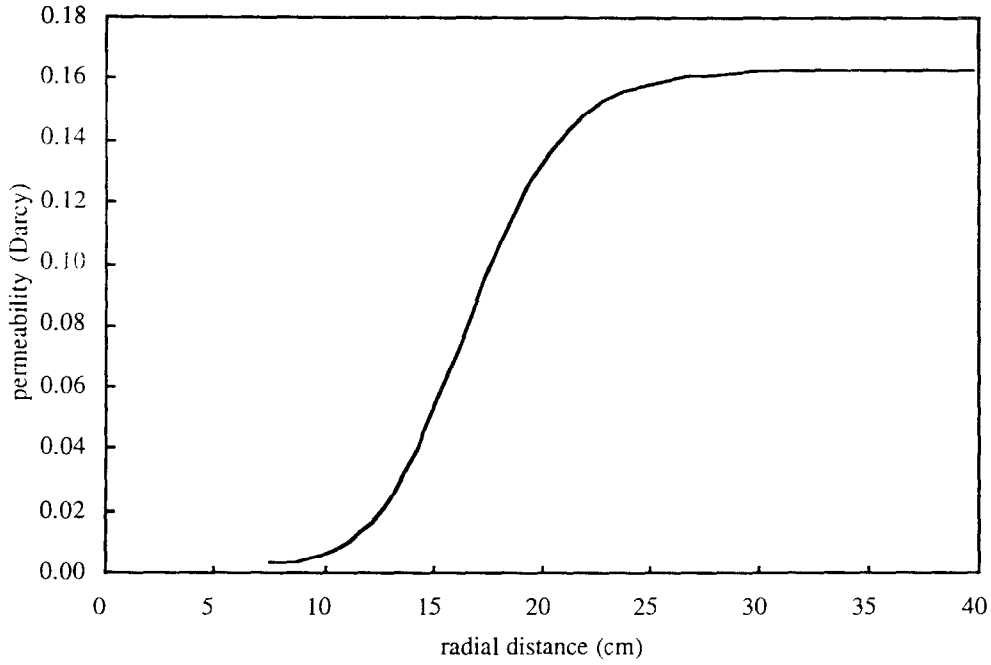

Fig. III-11 Permeability distribution near wellbore resulting from the invasion of montmorillinite.

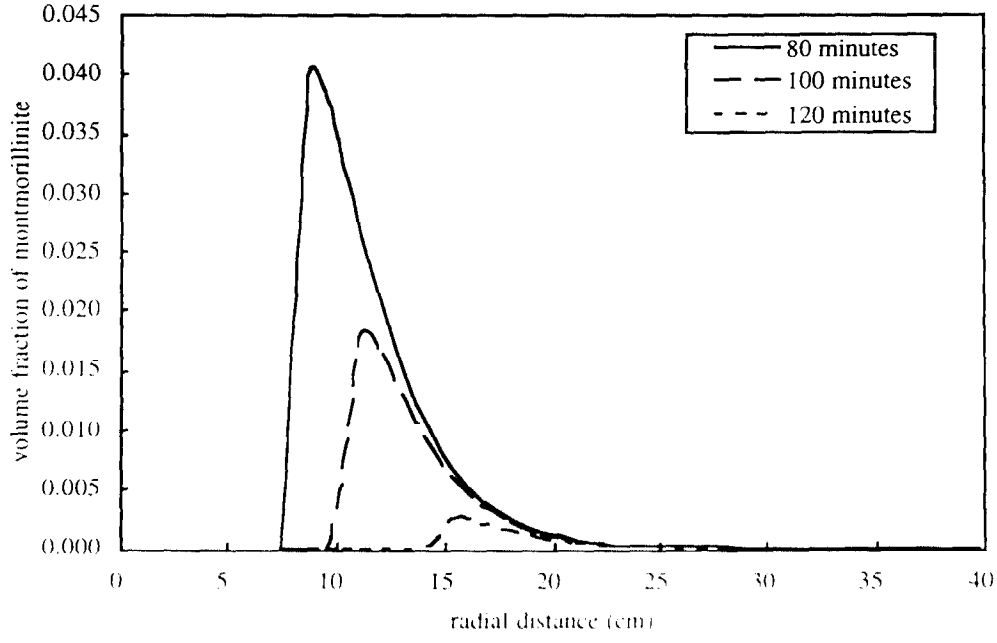

Fig. III-12 The volume fraction of montmorillinite versus radial distance at different acid treatment times

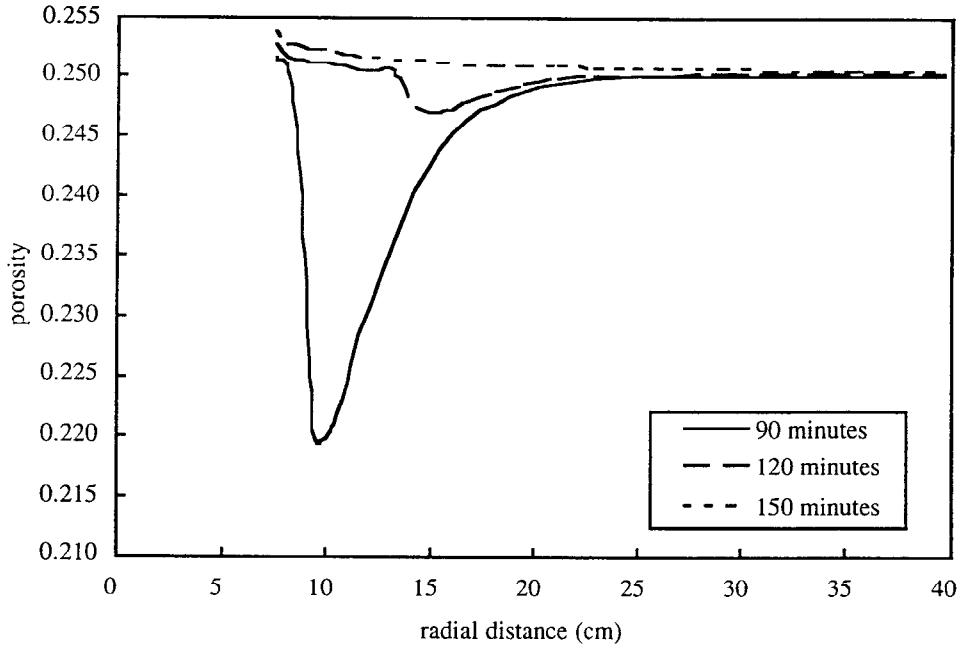

Fig. III-13 Evolution of the porosity alteration profile during the acid treatment of the damaged well.

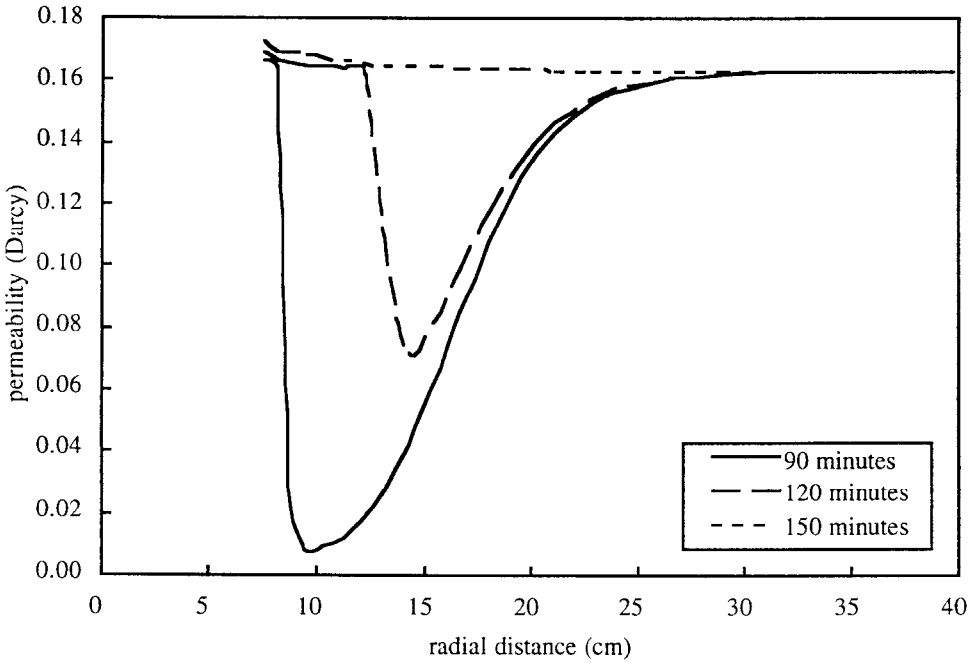

Fig. III-14 Evolution of the permeability alteration profile during the acid treatment of the damaged well.

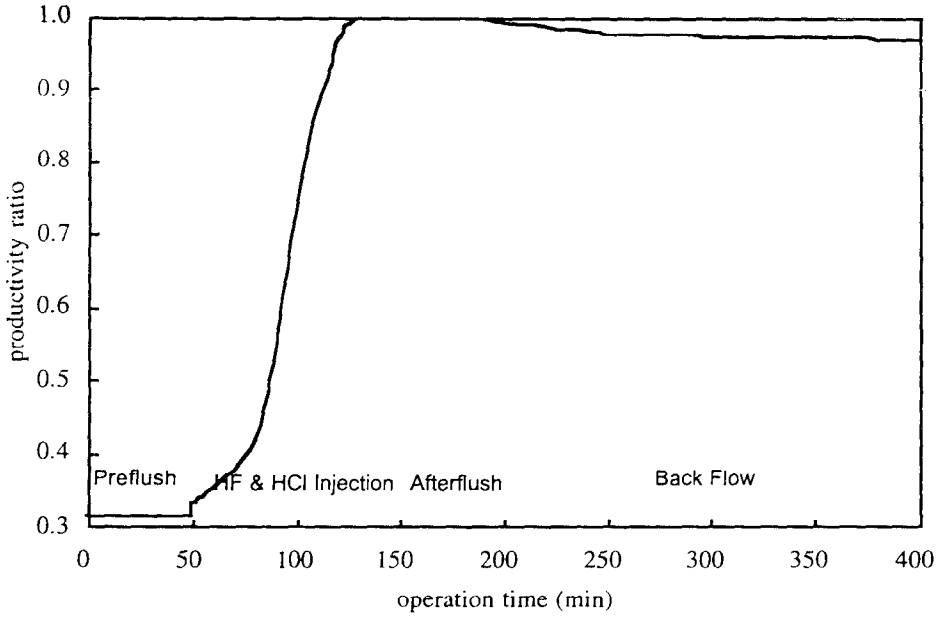

Fig. III-15 Stimulation potential for the damaged well: the ratio of the well productivity during acidizing to the productivity of the well without formation damage is shown as function of treatment time.

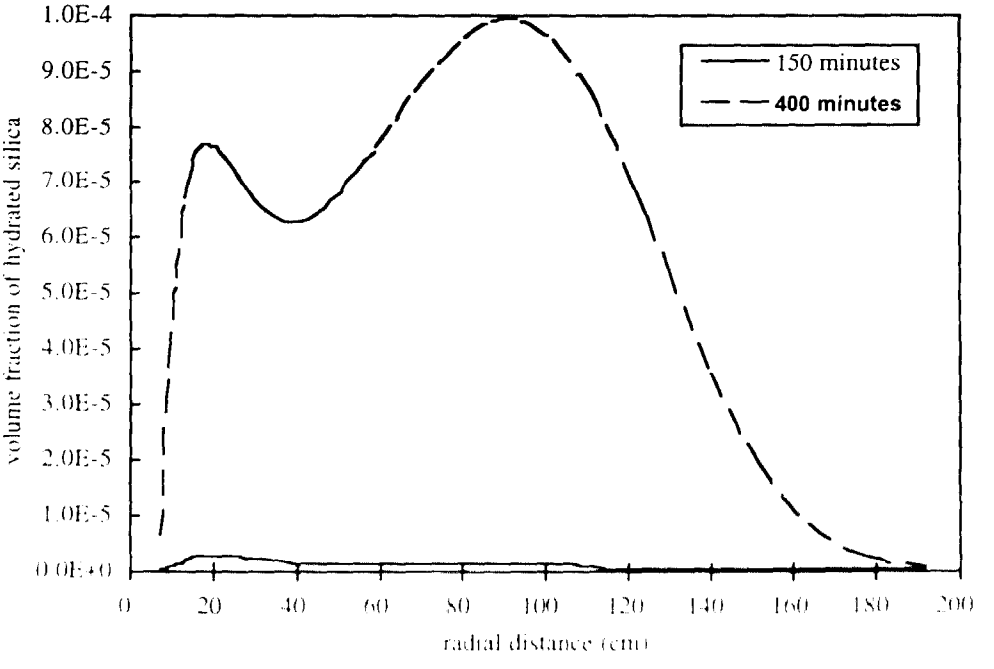

Fig. III-16 The volume fraction of hydrated silica precipitated versus radial distance at different treatment times

IV
Field Scale Simulation: Operation and 10,000 Year Fate Analysis of Waste Injection

A. Overview

A key element of waste repository management is a quantitative model for predicting the fate of injected waste fluids. This involves knowing the chemical evolution of the waste fluid and the viability of the repository to either contain waste fluids over an acceptable period of time or render them neutral through fluid/rock interaction or thermal decomposition (as for organic waste). Environmental regulations require a knowledge of these factors for over 10,000 years from the time of waste emplacement.

Prediction has three elements. First, one must acquire an accurate characterization of the pre-injection state of the repository. Then an accounting of the reaction, transport and mechanical processes and the related physico-chemical data must be acquired (this includes reaction rate, equilibrium, thermodynamic parameters and data on transport and rock mechanical laws). Finally, one must have a forward model. Because of the complexity of these systems, forward modeling requires computational modeling approach

Features such modeling should consider are the increase/decrease in waste toxicity over time through reactions; the compromising of natural or engineered seals or barriers for containments due to waste-rock/cement interaction; the evolution of the mechanical viability of the reservoir and its confining units.

B. Simulating the Operation Period

In order to simulate the operation period of waste injection, it was necessary to compile data required by CIRF.A from operating Class I disposal well facilities. The data were obtained from publicly available information on reservoir and waste fluid composition and reservoir rock properties. This information is available from facilities located in the Texas Gulf Coast, the Texas panhandle, Louisiana, and the Midwestern portion of the United States. In this section, simulations using CIRF.A were performed for two field examples of waste injection: one carbonate reservoir and one sandstone reservoir. Data for the two cases were collected from Texas Natural Resources Conservation Commission (TNRCC, 1993).

1. Carbonate Reservoir

a. Problem Description

This specific case involved the injection of waste fluid into a carbonate reservoir. The basic input data for the simulation of this case are given in Table IV.1. A single injection well located in the center of a cylindrical region representing the reservoir was considered. In this region, a no-flow condition was specified at a radial extent of 52,800 feet (10 miles). Detailed injection rate history for the well of interest is provided in Table IV.2. However, for the purpose of simplicity, an average injection rate of 105.7 gallons per minute was used in the study.

The formation interval that receives waste fluid was considered homogeneous and isotropic before injection. This formation interval is composed of dolomite, anhydrite and a small amount of calcite. The rock mineralogy and texture of this formation is given in Table IV.3. In this table, the grain radii for all the minerals were determined by fitting the original rock permeability according to a correlation relating permeability to grain radii and volume fractions of minerals, shape factor, geometry factor, and porosity (see Eqn. II.18).

In addition, formation fluid characteristics and waste stream composition are provided in Tables IV.4 and 5, respectively. For the waste stream constituents in Table IV.5, some species are in small quantity and are not expected to directly react with the formation minerals. Neglecting these minority species and examining the waste fluid speciation and the rock mineralogy led us to the reaction network as shown in Table IV.6.

b. Simulation Results and Discussion

One of our goals for this project is to delineate the effects of salinity, temperature, and pressure on waste fluid/rock interactions. The phenomenology in CIRF.A is based on activity corrected thermodynamics and mass action rate laws. Salinity effects are implemented by the extended Debye-Huckel theory for the correction of the activities of aqueous species. Thermal effects contribute to reaction rate coefficients, equilibrium constants, temperature dependence of activities of solutes and solids, and energy transport. Pressure only enters the reaction dynamics through the equilibrium constant. To correctly reflect the reaction processes, all simulations were performed by including salinity effects on activities.

i) Pressure Effects on Waste Fluid/Rock Interactions

To illustrate the effects of pressure, two simulation studies were carried out at the reservoir temperature of 106.8 °F. For one simulation, no pressure correction was considered, i.e., the equilibrium constants for the reactions were treated under standard pressure (14.7 psi). The other simulation was performed under the actual fluid pressure in the reservoir. The

pressure effects on mineral dissolution, porosity and permeability are shown in Figs. IV-1, 2, 3,4 and 5.

As shown in Fig. IV-1, anhydrite was dissolved faster at a higher pressure (the reservoir pressure). The pressure effect on anhydrite dissolution was diminished as all the anhydrite in the formation adjacent to the wellbore was dissolved. However, Figs. IV-2 and 3 indicate that pressure has no marked effect on the dissolution of the other two minerals (dolomite and calcite). This is because the pressure effects as calculated using the partial molar volumes for all these aqueous species involved in the dissolution of dolomite and calcite are small. Since the pressure effects are only reflected by the dissolution of anhydrite, the pressure effects on porosity and permeability variations at the wellbore in Figs. IV-4 and 5 are similar to that of anhydrite dissolution.

ii) Temperature Effects on Waste Fluid/Rock Interactions

To examine the effects of temperature on the reaction-transport process, results from three simulations under the actual reservoir pressure were compared: one at the reservoir temperature of 106.8 ^{o}F, one at a temperature of 88.8 ^{o}F (18 ^{o}F or 10 ^{o}C lower than the reservoir temperature), and the other at a temperature of 124.8 ^{o}F (18 ^{o}F or 10 ^{o}C higher than the reservoir temperature). The temperature effects on mineral dissolution, porosity and permeability are shown in Figs. IV-6, 7, 8, 9 and 10.

Fig. IV-6 reveals that increasing temperature leads to a decrease in the dissolution rate of anhydrite. The volume fraction of anhydrite dissolved from the rock adjacent to the wellbore at the three different temperatures eventually attains a constant value. This value represents the amount of anhydrite originally present in the rock (in terms of volume fraction). The effects of temperature on the dissolution of dolomite and calcite is opposite to that of anhydrite. As illustrated in Figs IV-7 and 8, an increase in temperature results in an increase in the dissolution rate of dolomite and calcite.

The effects of temperature on porosity and permeability at the wellbore are given in Figs. IV-9 and 10, and are explained as follows. At the earliest times, the variations of

porosity and permeability are dominated by the dissolution of anhydrite. During this period, increasing the temperature results in smaller rates of porosity and permeability enhancement. Calcite in the rock near the wellbore was completely dissolved in less than 1,000 days. At about 2,000 days of injection, all the anhydrite in the rock near the wellbore was dissolved. However, as injection continued dolomite was still being dissolved and the change of porosity and permeability at the wellbore was controlled only by the dissolution of dolomite. As a result, increasing temperature exhibits an increase in porosity and permeability.

The results presented above clearly demonstrate that the pressure and temperature in the reservoir have significant impacts on waste fluid/rock mineral interactions, rock properties, and contaminant transport. However, these effects, in general, are very complex and are dependent on the waste fluid/reservoir system of interest. This implies that any simulation performed under simplified conditions may give misleading results. The results presented here can only be obtained by coupled reaction-transport modeling.

iii) Spatial and Temporal Variations of Mineral and Rock Properties

During the injection of waste fluid into the formation, the reaction-transport processes as well as the variations of rock properties are time and space dependent. Simulations were performed at the actual reservoir temperature and pressure to investigate the effects of temporal and spatial variations on the simulation results.

It is interesting to note in Fig. IV-11 that anhydrite was dissolved in a region adjacent to the wellbore and was precipitated in an intermediate region. This phenomenon can be explained as follows. The waste fluid is under-saturated with respect to anhydrite and thus has a tendency to dissolve anhydrite when it enters the formation from the wellbore. As injection proceeds, "fresh" waste fluid is continuously fed to the formation and anhydrite continues to be dissolved in the near-wellbore region. As seen from the reaction network in Table IV.6, the dissolution of anhydrite leads to the formation of Ca^{2+} and SO_4^{2-} ions. The injection of waste fluid and the dissolution of anhydrite provide

calcium and sulfate while the dissolution of dolomite and calcite provides calcium. Ca^{2+} and SO_4^{2-} are carried away into the formation due to transport. At some distance, the concentrations of calcium and sulfate are sufficiently high that the fluid becomes super-saturated with respect to anhydrite. As a result, anhydrite starts to precipitate and yields the portion of the curve below zero in Fig. IV-11. In this particular case, the amount of anhydrite precipitated is very small and not enough to plug the formation. However, if the concentrations of sulfate and/or calcium in the waste fluid are very high and a significant amount of calcium is additionally provided by mineral dissolution, this phenomenon can cause severe formation damage problems.

The dissolution of dolomite and calcite with respect to radial distance and injection time is illustrated in Figs. IV-12 and 13. As injection proceeds, the zone of dissolution of dolomite and calcite extends deeper into the formation. Although both dolomite and calcite react with the acids in the waste fluid, calcite is quickly dissolved due to its relatively small amount present in the reservoir rock.

As shown in Figs. IV-14 and 15, during waste injection porosity increases from 7% to about 30% while permeability increases from 0.69 to more than 30 darcy near the wellbore. Away from the wellbore, porosity and permeability gradually decrease to their original values as the waste fluid is neutralized by mineral dissolution. This reaction-transport process significantly alters porosity and permeability in a region extending 40 feet from the wellbore. Such a high increase in porosity near the wellbore may risk formation collapse when the formation can no longer sustain the overburden stress. Formation collapse can destroy the rock permeability on the one hand, but may also destroy well integrity and cause waste fluid to travel vertically.

iv) Acid Neutralization

When the waste fluid is injected into the formation, calcite and dolomite serve as major reactants to neutralize the acids. The effects of acid neutralization by rock minerals are demonstrated in Fig. IV-16. The pH value of the waste fluid is increased from 1.7 at

wellbore to about 6.5 at some distance in the reservoir. As injection continues, the acids invade deeper into the formation. However, after 6,000 days (more than 16 years) of injection the waste fluid remains acidic in a region of only 300 feet from the wellbore.

c. Comparison with Field Measurements

i) Skin Factor

Hawkins (1956) first introduced the concept of skin factor to describe the effects of formation damage or stimulation around the wellbore. A skin region is represented as a zone of altered permeability adjacent to the wellbore as illustrated in Fig. IV-17. In this diagram, r_w is the wellbore radius, r_s is the radius of the skin region, k_s is the average altered permeability in the skin region, and k_0 is the unchanged permeability in the reservoir. The skin factor, s, is then calculated by

$$s = (k_0/k_s - 1) \ln (r_s/r_w) \qquad \text{(IV.1)}$$

A positive skin factor indicates permeability reduction or formation damage in the near-wellbore region. On the other hand, a negative skin factor represents permeability increase near the wellbore or well stimulation. CIRF.A can be used to predict the skin factor. One advantage of using CIRF.A to model waste injection is as follows. Although the skin factor can be determined by well testing techniques, the permeability and the radius of the skin region can not be estimated. CIRF.A thereby provides a unique means of determining these two parameters.

Our simulation results demonstrate that the waste fluid can cause dissolution of rock minerals and a significant increase in porosity and permeability in the near-wellbore region. This is the case during the actual operation of waste injection. Field information (TNRCC, 1993) indicates that a negative skin factor of -6.2 was associated with this injection well. CIRF.A predicts an ultimate negative skin factor of -6.04 as shown in Fig. IV-18. Reaction-front fingering and worm-holing phenomena are likely to develop in this problem, causing higher permeability increase and therefore, a more negative skin factor. This

simulation result demonstrates the capability and potential of CIRF.A for modeling deep well waste injection in the near wellbore region.

ii) Pressure Variation at the Wellbore

Fig.IV-19 indicates that site wellbore pressure data (TNRCC, 1993) are in good agreement with the pressure predicted by CIRF.A. A parameter sensitivity study indicates that pressure data is very sensitive to skin factor, reservoir size, and reservoir rock compressibility. The simulation result shown in Fig. IV-19 was obtained upon increasing the rock compressibility (given in Table IV.1) by 1.5 times.

The variation of pressure at the wellbore with respect to time is explained as follows. At the earliest times after injection, the pressure at the wellbore is dominated by transient flow. This results in an increase of the wellbore pressure. During this time, the waste fluid quickly dissolves rock minerals and increases permeability. Since the waste is injected at a constant flow rate, the increase in permeability will decrease the pressure at the wellbore. Before dissolution-induced permeability increase counter-acts the effect of the transient flow, the pressure at the wellbore will still increase. However, once the effect of the permeability increase becomes dominant, the pressure at the wellbore starts to drop. At the end of the transient flow period, pressure variations due to injection reach the reservoir outer boundary. For a closed reservoir as studied here, no fluid can escape from the boundary. Since we treat both the fluid and the reservoir rock matrix as slightly compressible, continued injection increases the pressure at the wellbore and elsewhere in the reservoir.

2. Sandstone Reservoir

a. Simulation Description

In this section, simulation studies of the disposal of acidic waste fluid into a sandstone formation are presented. The assumptions about the reservoir extent and geometry in addition to well location were the same as those used for the carbonate case.

Basic parameter inputs necessary for the simulations are provided in Table IV.7. The injection rate history data for this well is given in Table IV.8. An average rate of 48.0 gallons per minute was used in the simulation.

Core analysis indicates that the formation consisted of quartz, illite, and calcite. Table IV.9 gives bulk volume fraction and grain radius for each mineral. In this table, the grain radii for quartz, illite and calcite were determined by fitting the original rock permeability to the permeability correlation implemented in CIRF.A as shown in Eqn. II.18. For simplicity, we assumed all the three minerals to be the same size.

Injection records (TNRCC, 1993) indicate that this well had severe formation damage problems within a few years of injection. Up to April 1992, several stimulation operations were required to recover the injection capability for this well. No information is currently available about when these stimulation operations were conducted.

Formation and waste fluid compositions are given in Tables IV.10 and 11, respectively. An examination of the constituents of the formation and waste fluids in Tables IV.10 and 11 indicates that the concentration of sulfate in the waste and the concentration of calcium in the formation fluid are high. The precipitation of anhydrite in the formation due to waste injection is believed to cause formation damage in this system. Although all natural waters used in industrial processes contain calcium, calcium was not given in the waste fluid as noted in Table IV.11. In order to carry out simulation studies, the concentration of calcium in the waste fluid is assumed to be 0.002 moles/liter. At this concentration, the waste fluid is slightly over-saturated with respect to anhydrite at surface temperature. Since anhydrite is less soluble at higher temperature, the waste fluid becomes more over-saturated at the formation temperature.

Since the types of organic acids in the waste fluid were not given, we used acetic acid for simulation. A study of waste injection in North Carolina indicate that organic acids may be converted to methane by microorganisms (Leenheer et al., 1976). In summary, major aqueous and mineral reactions assumed in this study are provided in Table IV.12

b. Simulation Results and Discussion

The simulation procedures in the sandstone reservoir were similar to those used for the carbonate reservoir. Salinity, pressure and temperature effects on thermodynamic constants and species activities were included. Spatial and temporal variations of flow and rock properties due to waste fluid/rock mineral interactions were investigated at the actual reservoir temperature and pressure.

Fig. IV-20 indicates that the zone of calcite dissolution extends deeper into the formation with time. Fig. IV-21 illustrates how the precipitation of anhydrite varies with respect to time and radial distance from the wellbore. As injection continues, the zone of precipitation of anhydrite extends deeper into the formation. Fig. IV-22 shows that porosity has been reduced to 0.16 from its original value of 0.317 after 700 days of injection. However, severe porosity reduction occurred in a region of less than 7 feet away from the center of the well.

Porosity alteration reflects permeability change, but they are not equivalent. This is demonstrated by the permeability alteration profile in Fig. IV-23. Formation damage in this case was mainly caused by the precipitation of anhydrite. Although the dissolution of calcite has stimulation effects, it did not counter-act the effects of formation damage due to anhydrite precipitation. After 700 days of injection, the rock permeability adjacent to the wellbore has been reduced to about 0.01 darcy from the original permeability of 0.695 darcy. Formation damage accelerated at about 700 days of injection. This is indicated by the skin factor as shown in Fig. IV-24. The skin factor has increased to 87. Severe near-wellbore formation damage leads to a significant increase in the wellbore pressure as shown in Fig. IV-25. High wellbore pressure may fracture the formation and affect reservoir integrity. Simulation was ceased at 700 days of injection.

Simulation results indicate that mineral reactions did not lead to appreciable change of quartz and illite and their contents in the rock remained almost unchanged. Although the waste fluid is very acidic, it contains sulfuric acid only. Clay and quartz are usually very

reactive with hydrofluoric acid (HF) as noted in Chapter III, however. Thus more dramatic effects would be expected when the injectate contains an appreciable amount of HF (and similarly for highly alkaline fluids).

c. Minimizing Formation Damage

Our simulation study and field evidence in the sandstone reservoir indicate that injection practices may cause formation damage. CIRF.A can be used to predict this problem before it happens, and to design injection procedures to minimize it as much as possible. A simple solution to this problem is to dilute the concentrations of sulfate and calcium prior to injection. This approach was demonstrated by a simulation using CIRF.A. The simulation was performed by reducing the concentrations of sulfate and calcium in the waste fluid. The concentration of sulfate was reduced from 2.22 moles/liter to 1.11 moles/liter and the concentration of calcium was reduced from 0.002 moles/liter to 0.001 moles/liter.

Since the waste fluid is diluted, the acid strength is also reduced. As a result, calcite dissolution is decreased as well. This is clearly demonstrated by the evolution of calcite dissolution in the formation as shown in Fig. IV-26. We note that the diluted waste becomes under-saturated with respect to anhydrite at both the surface and formation temperature. However, calcite dissolution by acid releases calcium into the fluid when it is injected into the formation. The addition of calcium makes the fluid over-saturated in a certain region of the formation and leads to anhydrite precipitation there. This is demonstrated by Fig. IV-27. This region starts at 5 feet away from the well and extends to over 100 feet during the injection period of 700 days. As shown in Fig. IV-27, the maximum precipitation occurs at 20 feet away from the well. As injection continues, more anhydrite is precipitated.

The dissolution of calcite and precipitation of anhydrite change the formation porosity and permeability. Fig. IV-28 indicates that porosity in the near-wellbore region is first increased and then decreased. The increase in porosity is caused by calcite dissolution

and the decrease results from anhydrite precipitation. Fig. IV-29 shows similar characteristics for permeability alteration. The rock permeability is enhanced in the formation adjacent to the wellbore and damaged beyond 10 feet away from the well. The overall effects on the well flow efficiency can be analyzed by the skin factor as shown in Fig. IV-30. In the first 350 days of injection, a negative value of the skin factor indicates that the well is stimulated. The smallest value of the skin factor is -0.4 at 50 days of injection. After 350 days, the skin factor becomes positive and increases as injection proceeds. A positive value of the skin factor indicates formation damage. At the end of simulation (730 days of injection), the skin factor is 0.58. This number indicates that the formation is only slightly damaged. The resulting evolution of the pressure at the wellbore versus injection time is shown in Fig. IV-31.

C. Predicting The 10,000 Year Fate

In this facet of our study, the goal here is to predict the 10,000 year fate of the injected waste by extending our simulations of the two field injection cases beyond the operation period. In particular, we investigate whether certain wastes may be transformed over time. We determine the evolution in geometry and composition of the waste fluid while in residence in the repository for various injectate fluid compositions and initial formation mineralogies. The escape of waste fluids from a normally pressured compartment over 10,000 years is discussed in Chapter V.

1. Carbonate Reservoir

To predict the 10,000 year fate of waste in the formation, we re-simulate the case of waste injection into the carbonate reservoir in a two-dimensional, rectangular system. The system is 20 kilometers by 5 kilometers with a thickness of 15.24 meters (50 feet). The boundaries on the top and bottom are assumed to be sealed and those on the left and right

are taken to be open. The injection well is located in the center of the system and waste is injected at 105.7 gallons per minute for 17 years. Other data necessary for the simulation are given in Tables IV.1, 3, 4, 5 and 6.

Fig. IV-32 shows the concentration distributions of acid, sodium and arsenic after 17 years of injection. Since acid is consumed through reaction with carbonate minerals in the formation, the acid is not spread and remains localized. The waste fluid contains less sodium than the formation fluid. The sodium concentration distribution indicates that the formation fluid is displaced by the waste fluid in a region around the well. Arsenic is spread in the reservoir around the well and becomes less concentrated (toxic) farther away from the well.

The distribution of porosity, permeability and pressure at the end of injection (17 years) is illustrated in Fig. IV-33. For the rock/fluid system we investigate here, the waste fluid remains reactive only in a region close to the well. This was already demonstrated by the radial flow simulations in the previous section. The radial flow results indicate that significant change in porosity and permeability occurs in a region about 13 meters (40 feet) away from the well. Such a small region is well within the size of one grid block in the two-dimensional simulation. Since numerical solutions are discrete, simulation results are represented by grid block solutions. As shown in Fig. IV-33, the porosity and permeability alteration reflects the simulation results of the grid block where the well is located. The pressure distribution in the reservoir indicated that the pressure in the vicinity of the well is 1,600 psi. This pressure represents the average pressure within the computational cell containing the well and not the pressure at the wellbore.

When injection stops, the waste migration is dominated by diffusion transport. The extent of the waste plume at different simulation times is discussed as follows. Fig. IV-34 shows the waste plume in the reservoir at 55 years, 38 years after the end of injection; waste injection occurred in the first 17 years. A comparison between Figs. IV-32 and 34 indicates that there is not much change in sodium and arsenic concentration profiles. The

notable change is that acid has completely neutralized. Fig. IV-35 shows that the waste has migrated to a significant extent at 5,000 years. At 10,000 years, sodium and arsenic has migrated about 5 kilometers in each side of the well, as illustrated in Fig. IV-36.

2. Sandstone Reservoir

The injection of waste into the sandstone reservoir studied in the previous section is used for 10,000 year fate prediction. The simulation is carried out in a two-dimensional system. The system is 2,000 meters by 500 meters with a thickness of 45.72 meters (150 feet). The well located at the center of the system is injected at 48 gallons per minute for 700 days (1.9 years). Other data necessary for the simulation are given in Tables IV.7, 9, 10, 11 and 12. In particular, the transformation of acetic acid is assumed to be governed by microorganisms and the chemical formulation is given in Table IV.12.

Fig. IV-37 shows the concentration distributions of sulfate, acetate and methane at 55 years since the beginning of injection. Sulfate is the major component of the waste fluid and its concentration is as high as 2.2 moles/liter in the original waste stream. Since the injection period is relatively short, the concentration of sulfate is quickly reduced after injection stops. This is demonstrated by the top plot in Fig. IV-37. During waste injection, the pH value of the waste fluid is low and acetic acid exists mostly in its complex form. When injection stops, the acidity (mostly from sulfuric acid) becomes neutralized by reacting with calcite. Once the pH rises, the acetic acid starts to dissociate into hydrogen and acetate ions. This is illustrated by the middle plot in Fig. IV-37. The bottom plot in Fig. IV-37 indicates that methane already evolves from the acetic acid.

The evolution of the waste plume after 10,000 years is shown in Fig. IV-38. Sulfate is diminished due to diffusion transport. Most acetate is converted to methane. The produced methane concentration has increased to 0.072 moles/liter. Over a certain time frame, the change in the geological environment may accelerate waste transformation.

Certain wastes may be rendered non hazardous over time. In particular, in the model chosen here, neutralization took place via boiremediation.

D. Reservoir-Scale Reaction Fingering

When a reactive fluid is injected into a reservoir, a pattern of mineral alteration may develop in the reservoir as a result of fluid/rock interaction. As short-scale effects can take place near the well, accurate simulation requires a refined grid there. An example of such gridding is seen in Fig. IV-39 for a five-spot production/injection scenario.

Consider the injection of 0.1 moles/liter HCl acid into a tight, calcite-cemented sandstone reservoir having an initial porosity of 1%. The system of interest is 200 meters by 200 meters with a thickness of 3 meters. Here we simulate a system with an injection well at the left bottom and a production well at the right top. One would expect the development of an alteration zone that expands from the injection well as time of injection advances. However, due to the flow self-focusing instability, the alteration pattern after 3,000 days injection is seen to be fingered as shown in Fig. IV-40. In this way, the alteration can extend much further from the injection well than would have been predicted via the average alteration front location.

Table IV.1 CIRF.A simulation input for waste injection into a carbonate reservoir.

Input Parameter	Value	Comments
Hydraulic conductivity	Kx = 0.236 ft/day	Equivalent to 69.2 md
Formation fluid density	68.3 lb/ft^3 at 104° F	Assumes TDS = 14.35% NaCl
Injectate fluid density	62.824 lb/ft^3 at 104°F	Assumes TDS =16.8% NaSO4
Porosity	0.07	
Formation fluid viscosity	1.475 at 60°F 1.157 cp at 80°F 0.893 cp at 104°F 0.768 cp at 120°F 0.643 cp at 140°F	Assumes TDS = ppm NaCl
Injectate fluid viscosity	1.143 cp at 60°F 0.879 cp at 80°F 0.668 cp at 104°F 0.579 cp at 120°F 0.467 cp at 140°F	Assumes TDS = ppm NaCl
Initial pressure	966 psi at 4090 feet	
Pressure gradient	0.4743 psi/ft	
Skin factor	-6.2	
Well radius	0.255 feet	
Injection interval thickness	50 feet (constant)	
Fluid compressibility	3.3 X 10^{-6} psi^{-1}	
Formation compressibility	4.7 X 10^{-6} psi^{-1}	
Longitudinal dispersivity	150 feet	
Transverse dispersivity	15 feet	
Temperature gradient	0.00732 °F/ft	
Effective molecular diffusivity	4.465 X 10^{-4} ft^2/day	
Depth of center of injection	4090 feet at 106.8°F	Measurement datum

Table IV.2 Injection rate history for a well in the carbonate reservoir.

Year	Yearly Average Rate (gpm)
1976	159.5
1977	120.5
1978	108.1
1979	108.0
1980	89.7
1981	99.6
1982	56.2
1983	68.7
1984	104.7
1985	144.2
1986	109.8
1987	101.3
1988	120.1
1989	73.8
1990	108.2
1991	110.2
1992	114.5

Table IV.3 Rock mineralogy and texture in the carbonate reservoir.

Mineral	Bulk volume fraction*	Grain radius (cm)
Dolomite	0.7163	0.02000
Anhydrite	0.1953	0.00635
Calcite	0.0186	0.00010

* Summation of all mineral volume fractions and rock porosity equals one.

Table IV.4 Characteristics of formation fluid for the carbonate reservoir.

Parameter		Concentration (mg/l)	Concentration (meq/l)
pH		-	-
H_2S		-	-
TSS		-	-
TDS		-	-
TDS (Calculated)		158,405	-
SpG		-	-
Total Hardness		-	-
Bicarb	$HC0_3$	403	7
Chlorides	Cl	95,471	2,689
Sulfates	SO4	1,415	29
Calcium	Ca	7,724	386
Magnesium	Mg	1,475	121
Sodium	Na	51,890	2,256
Potassium	K	N/D	0
Iron	Fe	2.8	0
Barium	Ba	0.3	0
Strontium	Sr	0	0

Table IV.5 Characteristics of waste fluid for injection into the carbonate reservoir.

Parameter		Concentration (mg/l)
Sulfuric Acid	H_2S0_4	11,900
Total suspended solids	TSS	74
Total dissolved solids	TDS	15,152
Sulfate	$S0_4^=$	12,011
Chloride	Cl^-	1,296
Calcium	Ca	110
Sodium	Na	2,672
Copper	Cu	134
Selenium	Se	7.8
Telurium	Te	11.3
Lead	Pb	1.2
Arsenic	As	70
Antimony	Sb	1.3
Nickel	Ni	1.8
Silver	Ag	<0.2
Cadmium	Cd	0.2
Chromium	Cr	17.8
Iron	Fe	11.6
pH	(standard units)	1.7
Specific Gravity	(dimentionless)	1.0116**

Table IV.6 Reaction mechanisms assumed for describing the dynamics of waste injection into the carbonate reservoir.

Mineral reactions

$$CaMg(CO_3)_2 \text{ (dolomite)} + 2\ H^+ = Ca^{++} + Mg^{++} + 2\ HCO_3^-$$

$$CaSO_4 \text{ (anhydrite)} = Ca^{++} + SO_4^{--}$$

$$CaCO_3 \text{ (calcite)} + H^+ = Ca^{++} + HCO_3^-$$

Aqueous reactions

$$H_2SO_4 = 2\ H^+ + SO_4^{--}$$

$$H_2O = H^+ + OH^-$$

$$NaCl = Na^+ + Cl^-$$

Table IV.7 CIRF.A simulation input for waste injection into a sandstone reservoir.

Input Parameter	Value	Comments
Hydraulic conductivity	K = 3.06 ft/day (695.4 md)	Average sidewall core data
Formation fluid density	68.33 lb/ft^3 at 77°F 67.74 lb/ft^3 at 131°F	Fluid analysis
Injectate fluid density	76.13 lb/ft^3 at 68°F 74.62 lb/ft^3 at 131°F	Waste analysis
Porosity	0.317	Average sidewall core data
Formation fluid viscosity	1.286 cp at 68°F 0.92 cp at 100°F 0.686 cp at 131°F 0.646 cp at 140°F	Assumes 142,186 ppm TDS = ppm NaCl (Earlougher)
Injectate fluid viscosity	2.282 cp at 68°F	Assumes 371,311.5 ppm TDS = ppm $(NH_4)_2SO_4$ (CRC)
	1.63 cp at 100°F	Estimated
	1.216 cp at 131°F	Estimated
	1.147 cp at 140°F	Estimated
Initial pressure	2809.4 psig at 6098 feet	
Pressure gradient	0.4745 psi/ft	
Skin factor	0.0	
Well radius	0.4375 feet	
Injection interval thickness	164 feet	
Fluid compressibility	3.3 X 10^{-6} psi^{-1}	
Formation compressibility	3.3 X 10^{-6} psi^{-1}	
Longitudinal dispersivity	150 feet	
Temperature gradient	0.00922 °F/ft	
Surface Temperature	75 °F	
Effective molecular diffusivity	4.465 X 10^{-4} ft^2/day	
Depth of center of injection	6098 feet at 131.2°F	Measurement datum

Table IV.8 Injection rate history for a well in the sandstone reservoir

Year	Yearly Average Rate (gpm)
1986	46.88
1987	36.93
1988	50.11
1989	67.88
1990	38.27
1991	N/A
1992	53.37
1993	42.38

Table IV.9 Rock mineralogy and texture for the sandstone reservoir

Mineral	Bulk volume fraction	Grain radius (cm)
Quartz	0.546	2.638×10^{-3}
Illite	0.103	2.638×10^{-3}
Calcite	0.034	2.638×10^{-3}
Anhydrite*	0.0	5.0×10^{-4}

* Anhydrite did not exist in the formation prior to waste injection.

Table IV.10 Characteristics of formation fluid for the sandstone reservoir

Parameter	Value
SiO_2	18.3 ppm
HCO_3^-	177.8 ppm
Cl^-	87,053.3 ppm
Ca^{++}	3,464.5 ppm
Ba^{++}	66.3 ppm
Mg^{++}	1,155.4 ppm
$Na^+(K^+)$	50,335.3 ppm
Total Solids	142,186.0 ppm
Specific Gravity (25 °C)	1.0953
pH (25 °C)	7.33

Table IV.11 Characteristics of waste fluid for injection into the sandstone reservoir.

Parameter	Value
Sulfate	213,000.0 mg/L
Ammonia Nitrogen	30,600.0 mg/L
Chemical Oxygen Demand	8,620.0 mg/L
Chloride	600.0 mg/L
Cyanide Amenable to Chlorination	17.4 mg/L
Organic Acids	5,340.0 mg/L
Total Solids	453,000.0 mg/L
Specific Gravity	1.22
pH (20 °C)	< 1.0

Table IV.12 Reaction mechanisms assumed for describing the dynamics of waste injection into the sandstone reservoir.

Mineral reactions

SiO_2 (quartz) = SiO_2 (aq)

$K_{.6}Mg_{.25}Al_{2.3}Si_{3.5}O_{10}(OH)_2$ (illite) + 8 H^+ = 5 H_2O + 0.6 K^+ + 0.25 Mg^{++} + 2.3 Al^{3+} + 3.5 SiO_2 (aq)

$CaCO_3$ (calcite) + H^+ = Ca^{++} + HCO_3^-

$CaSO_4$ (anhydrite) = Ca^{++} + SO_4^{--}

Fast aqueous reactions

H_2SO_4 = 2 H^+ + SO_4^{--}

H_2O = H^+ + OH^-

NH_3 + H_2O = NH_4^+ + OH^-

Slow aqueous reactions

CH_3COOH = CH_4 + CO_2

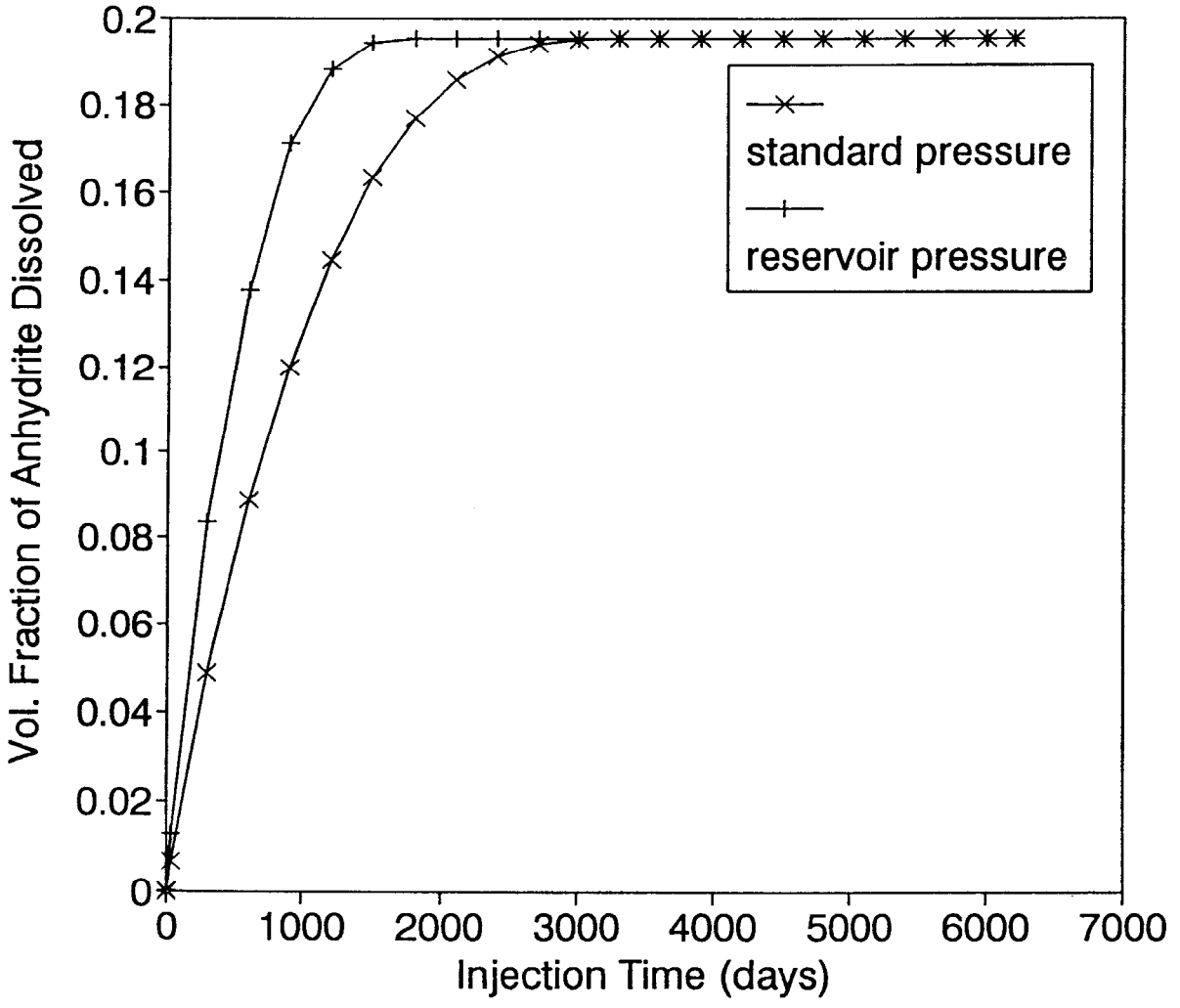

Fig. IV-1 Anhydrite dissolution at the wellbore for the carbonate reservoir as calculated at two different pressures at the reservoir temperature of 106.8 ^{o}F is shown as a function of waste injection time.

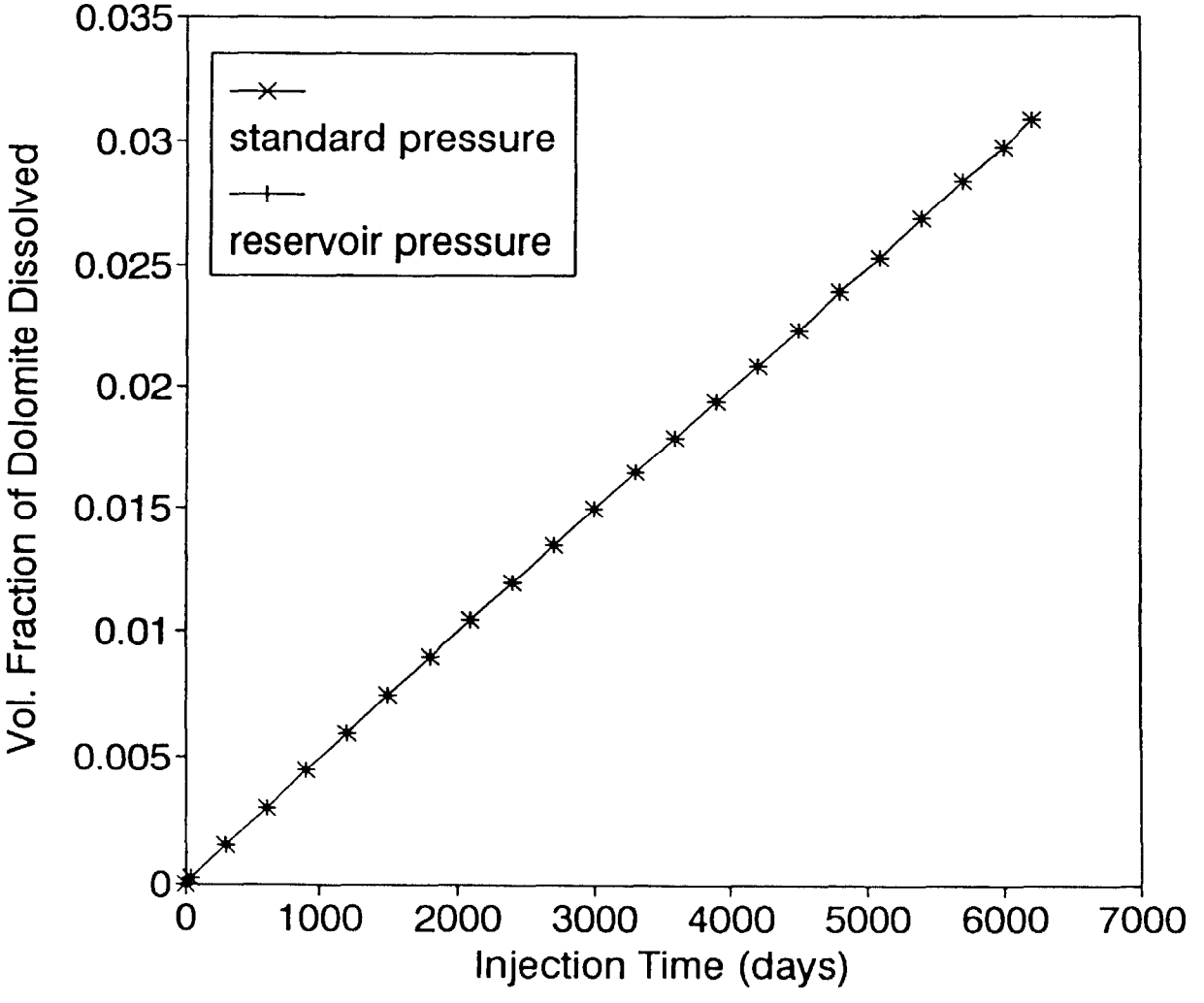

Fig. IV-2 Dolomite dissolution at the wellbore for the carbonate reservoir as calculated at two different pressures at the reservoir temperature of 106.8 °F is shown as a function of waste injection time.

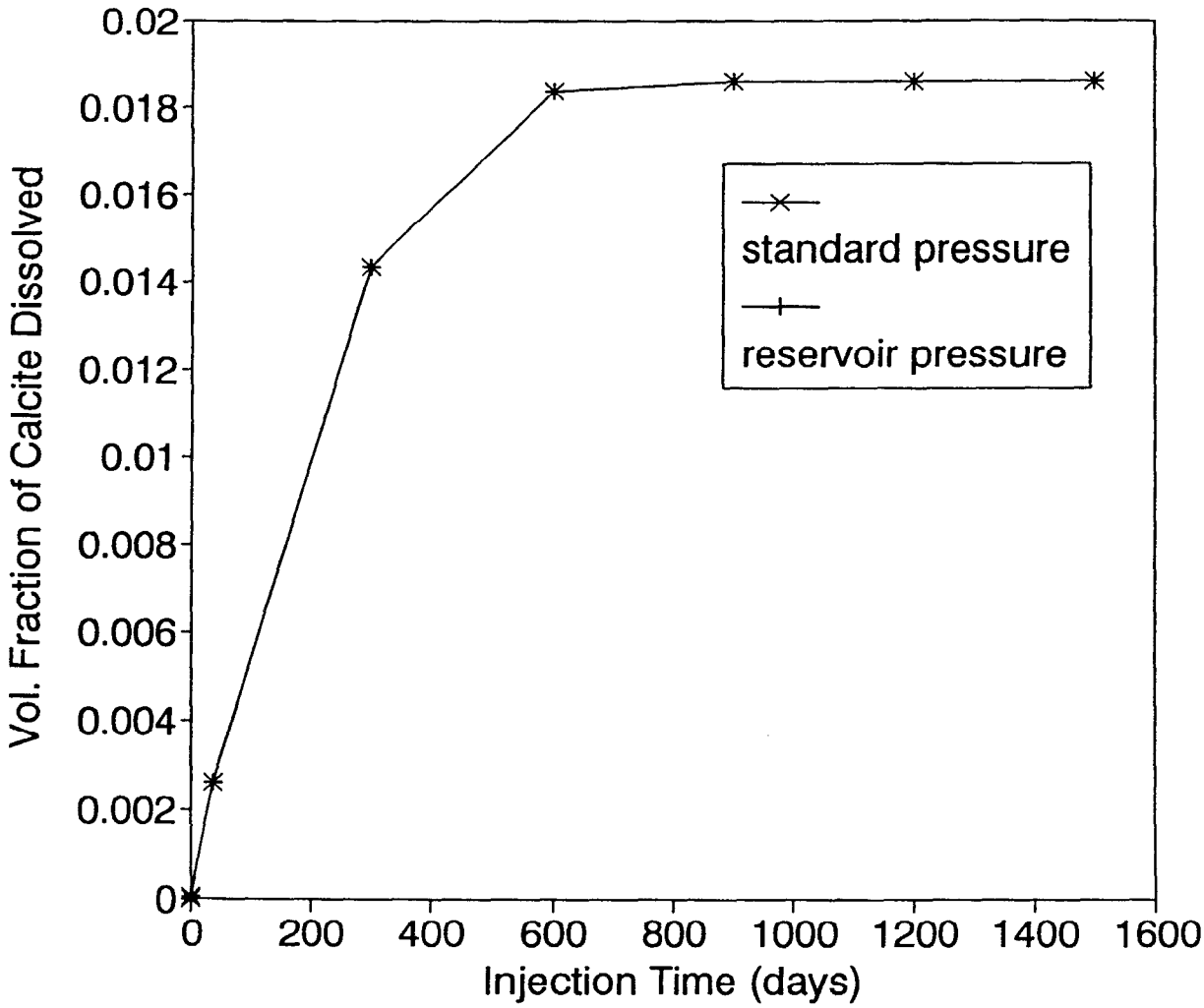

Fig. IV-3 Calcite dissolution at the wellbore for the carbonate reservoir as calculated at two different pressures at the reservoir temperature of 106.8 °F is shown as a function of waste injection time.

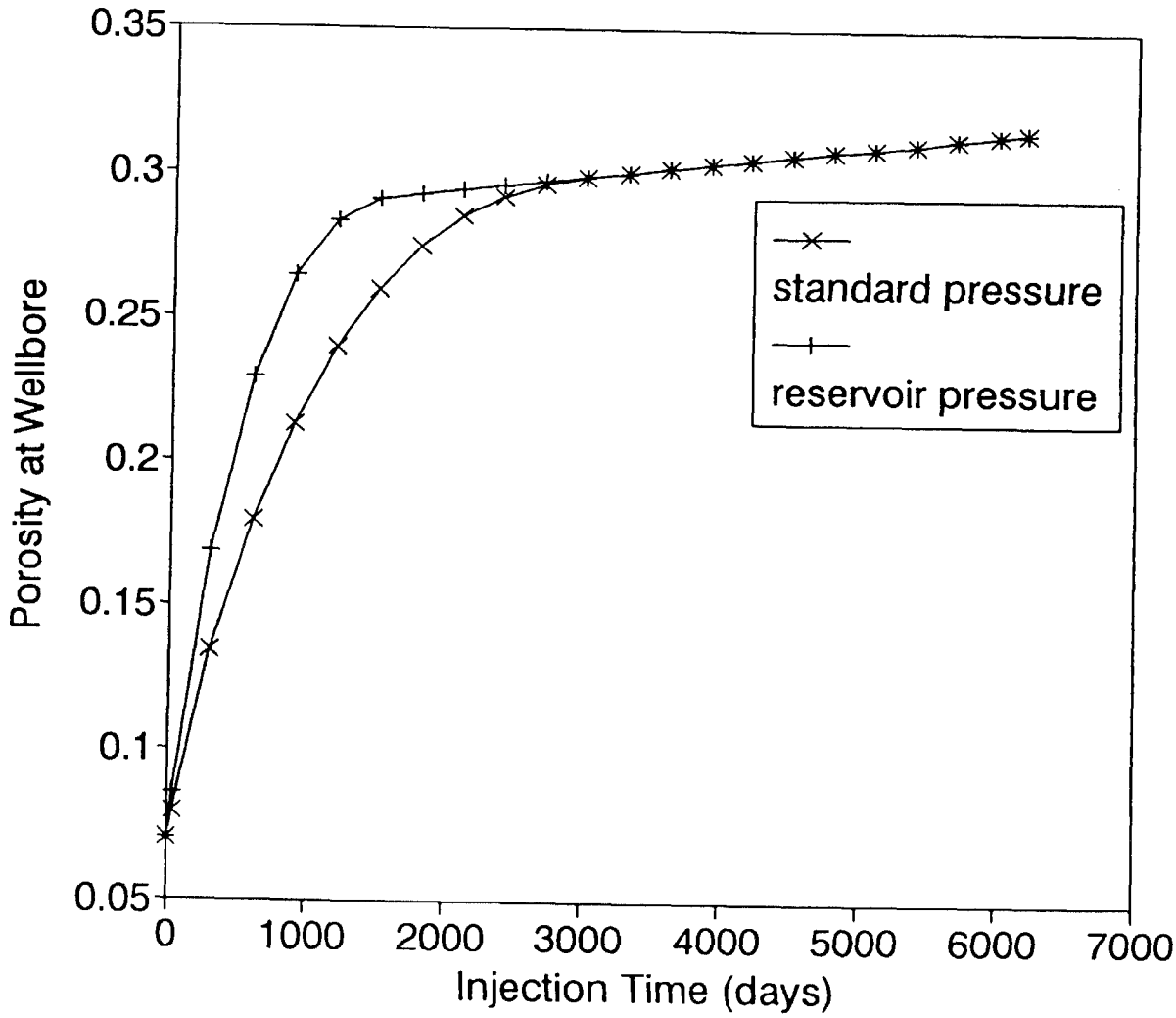

Fig. IV-4 Porosity change at the wellbore for the carbonate reservoir resulting from mineral reactions at two different pressures at the reservoir temperature of 106.8 °F is shown as a function of waste injection time.

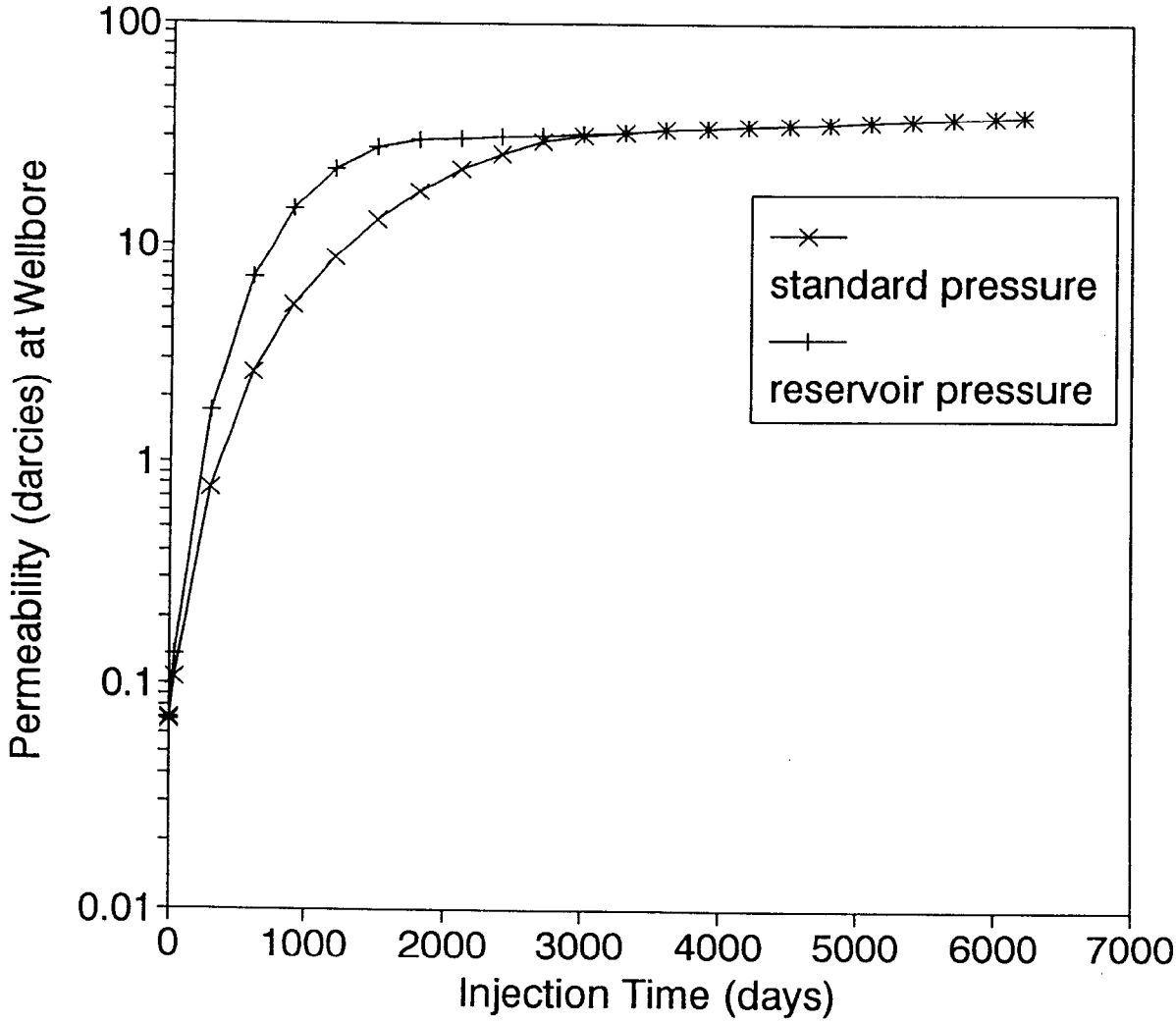

Fig. IV-5 Permeability change at the wellbore for the carbonate reservoir resulting from mineral reactions at two different pressures at the reservoir temperature of 106.8 °F is shown as a function of waste injection time.

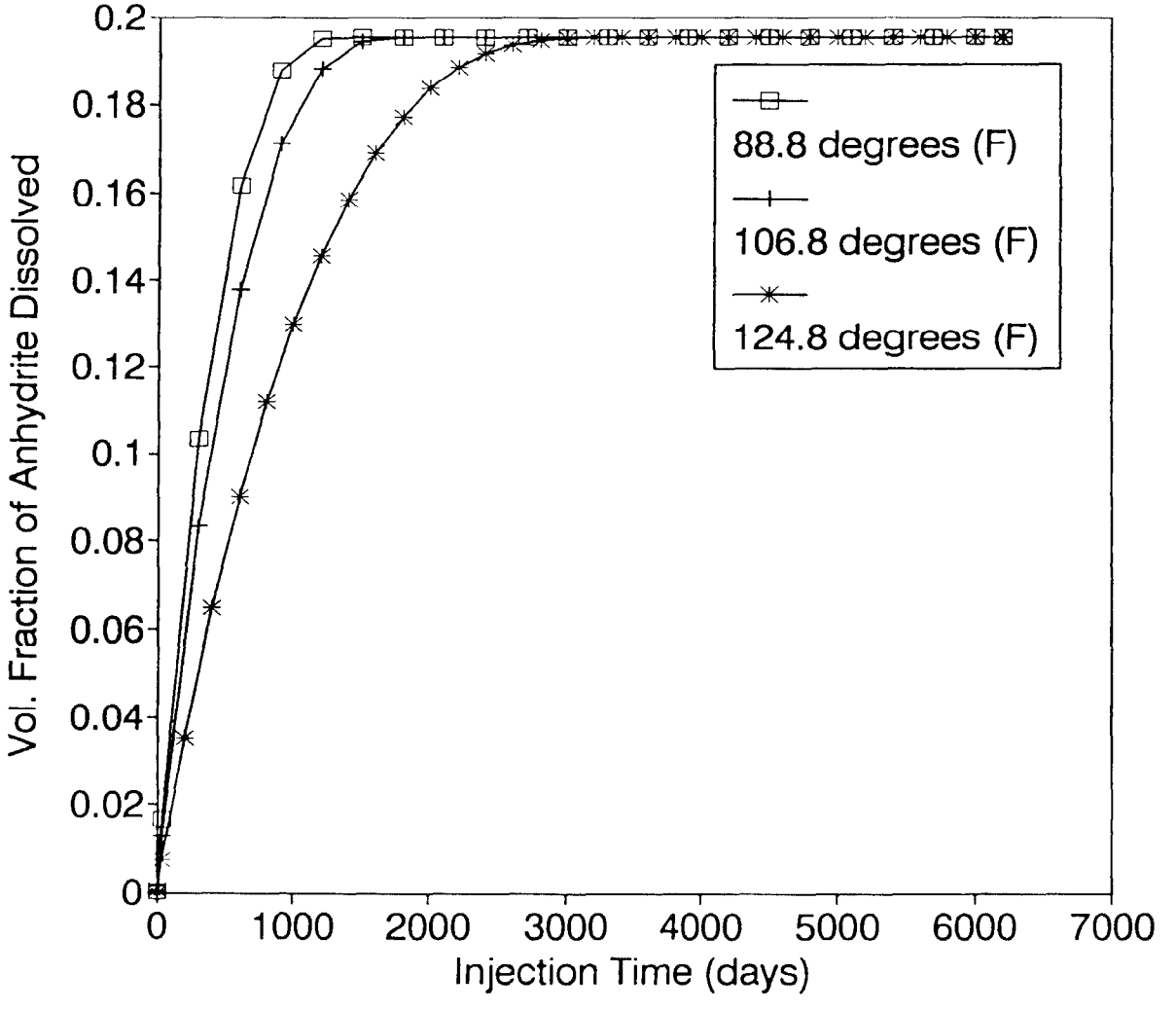

Fig. IV-6 The effect of temperature on anhydrite dissolution at the wellbore for the carbonate reservoir is shown as a function of waste injection time.

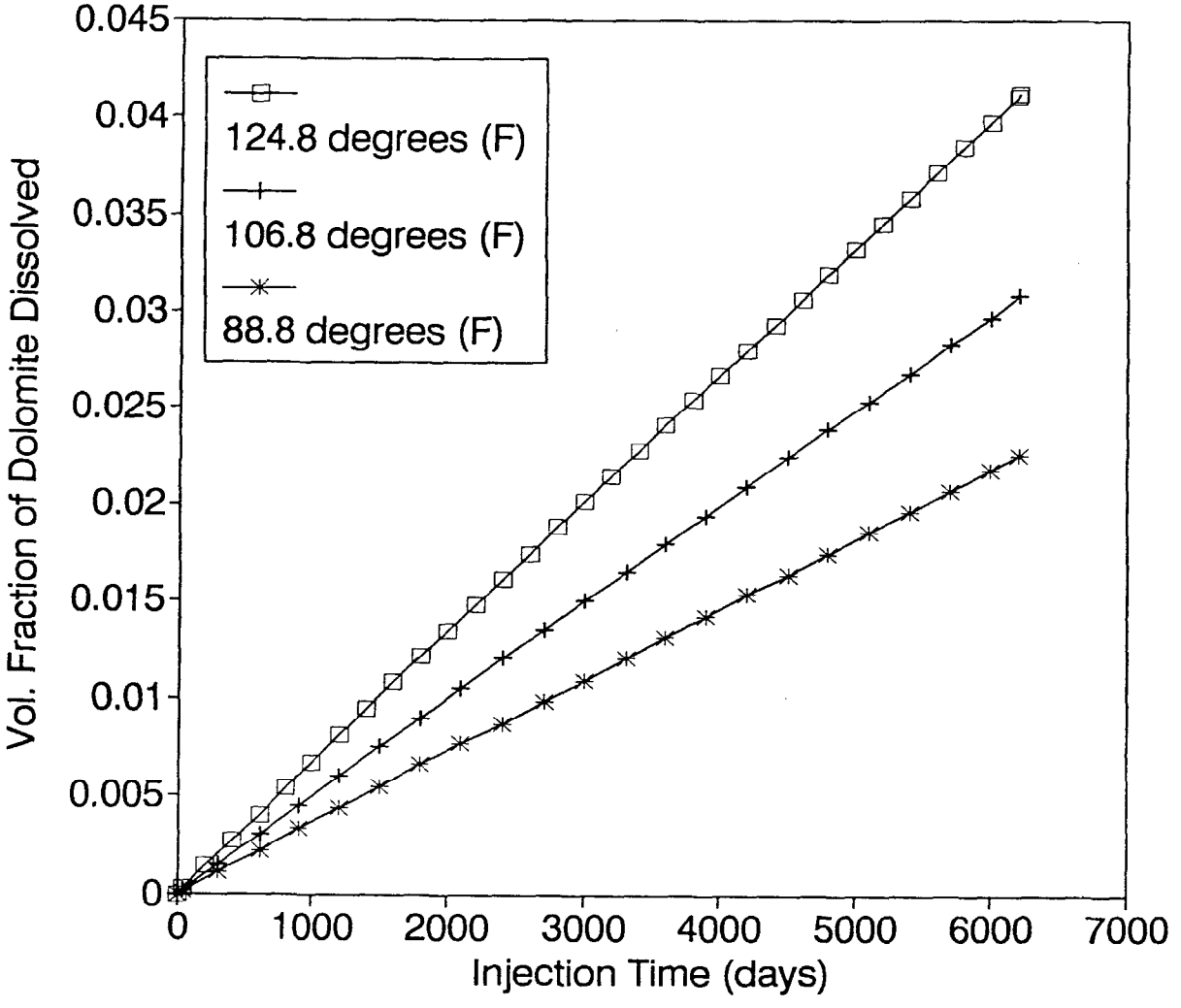

Fig. IV-7 The effect of temperature on dolomite dissolution at the wellbore for the carbonate reservoir is shown as a function of waste injection time.

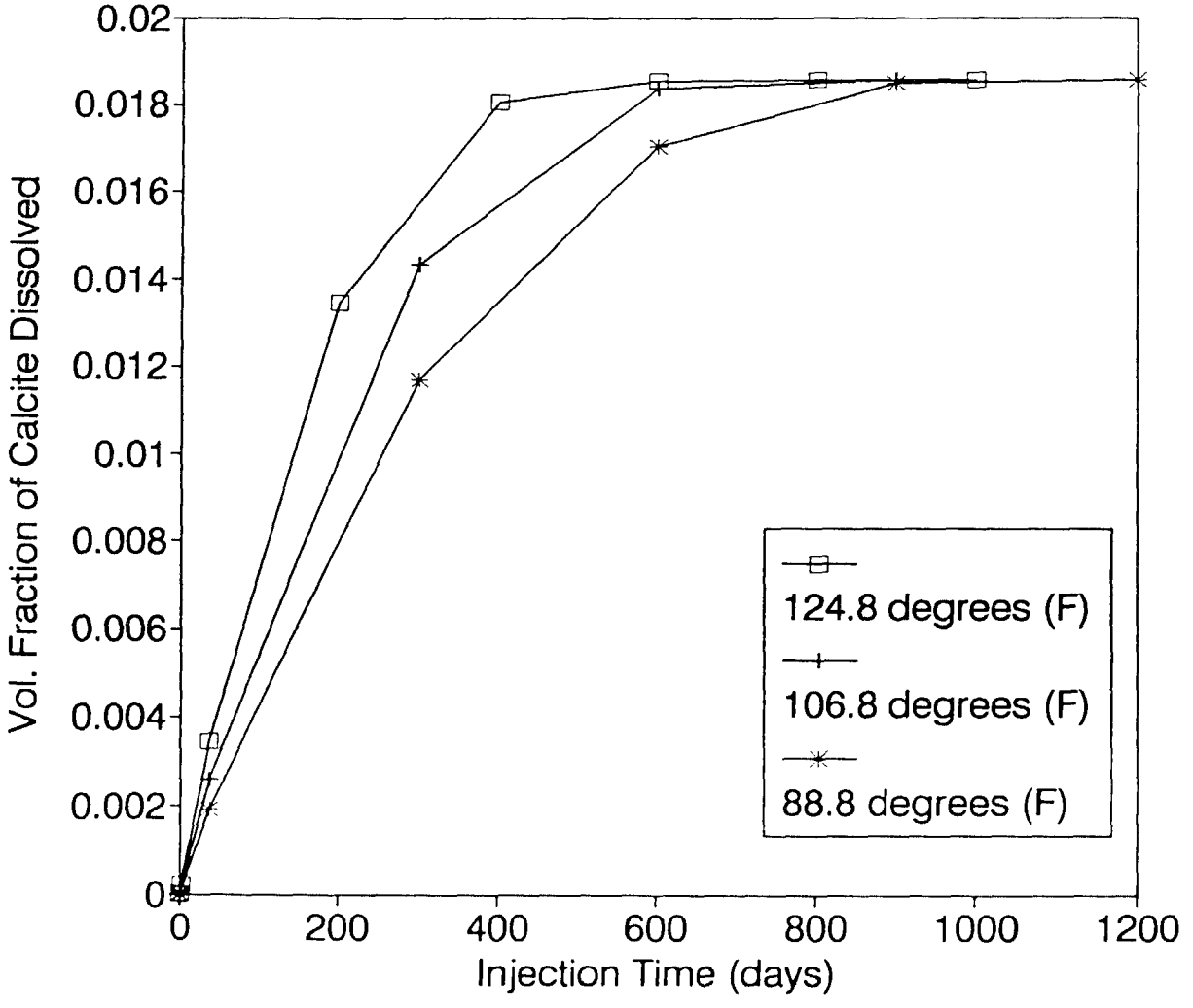

Fig. IV-8 The effect of temperature on calcite dissolution at the wellbore for the carbonate reservoir is shown as a function of waste injection time

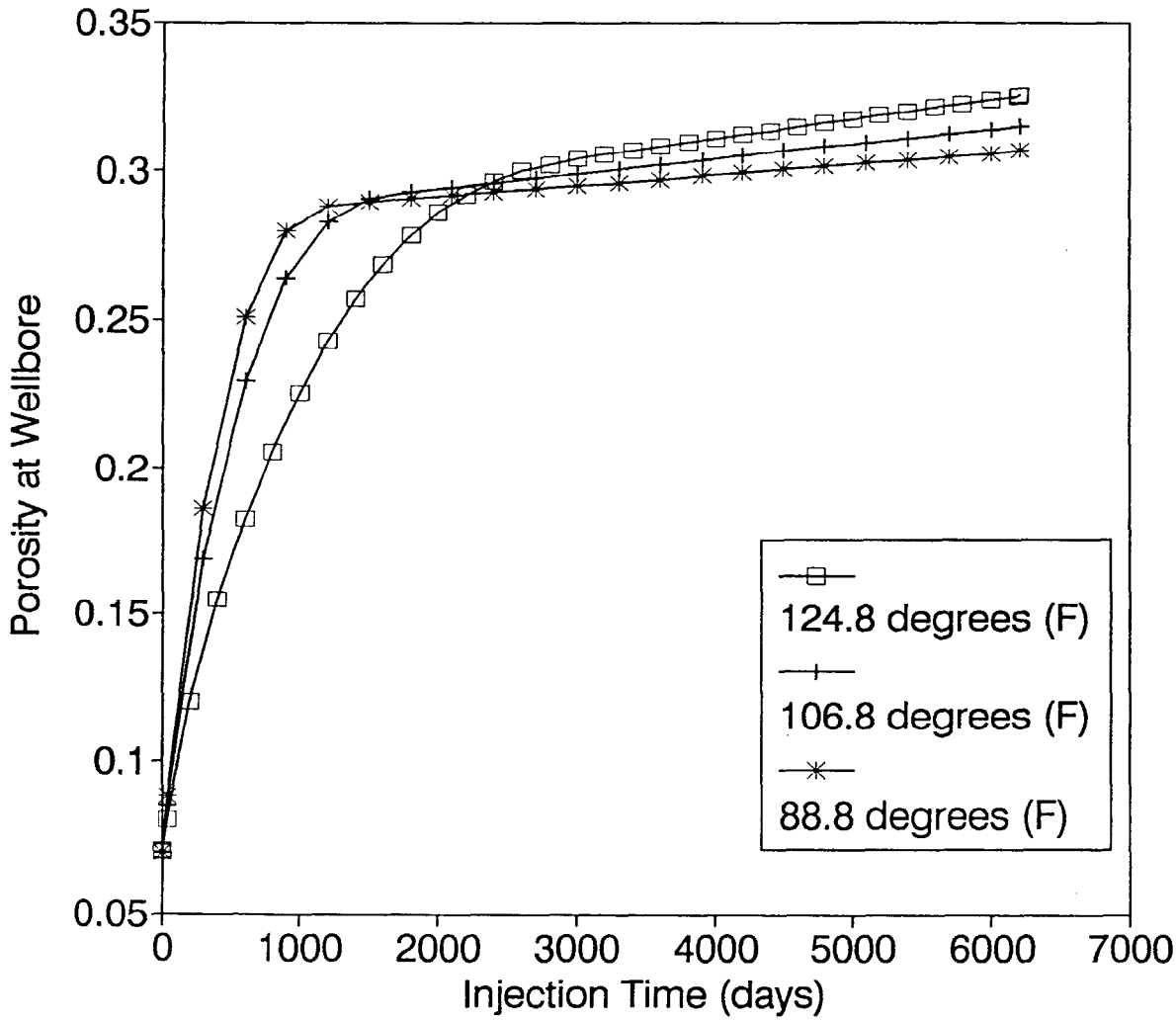

Fig. IV-9 The effect of temperature on porosity variation at the wellbore for the carbonate reservoir is shown as a function of waste injection time.

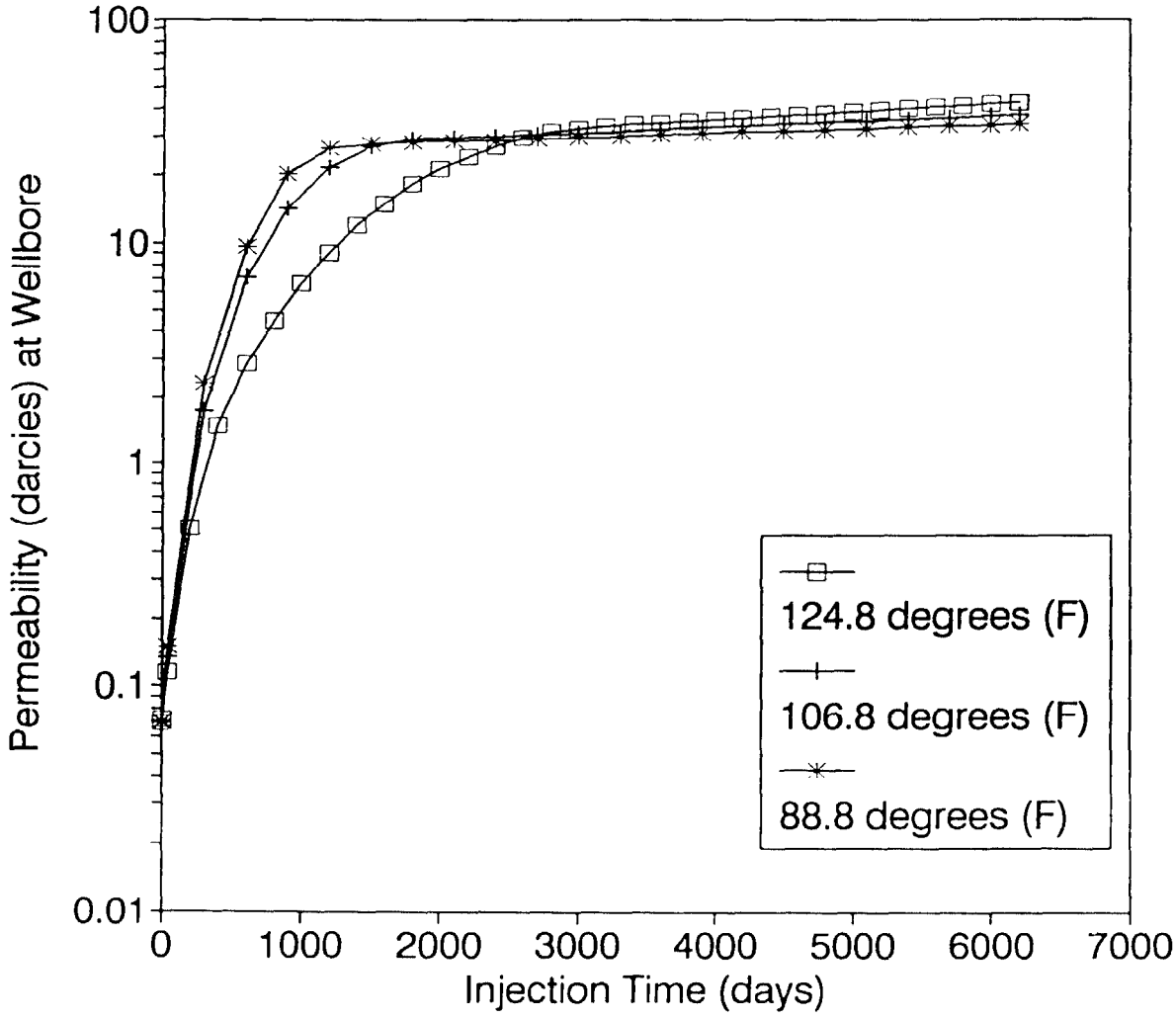

Fig. IV-10 The effect of temperature on permeability variation at the wellbore for the carbonate reservoir is shown as a function of waste injection time.

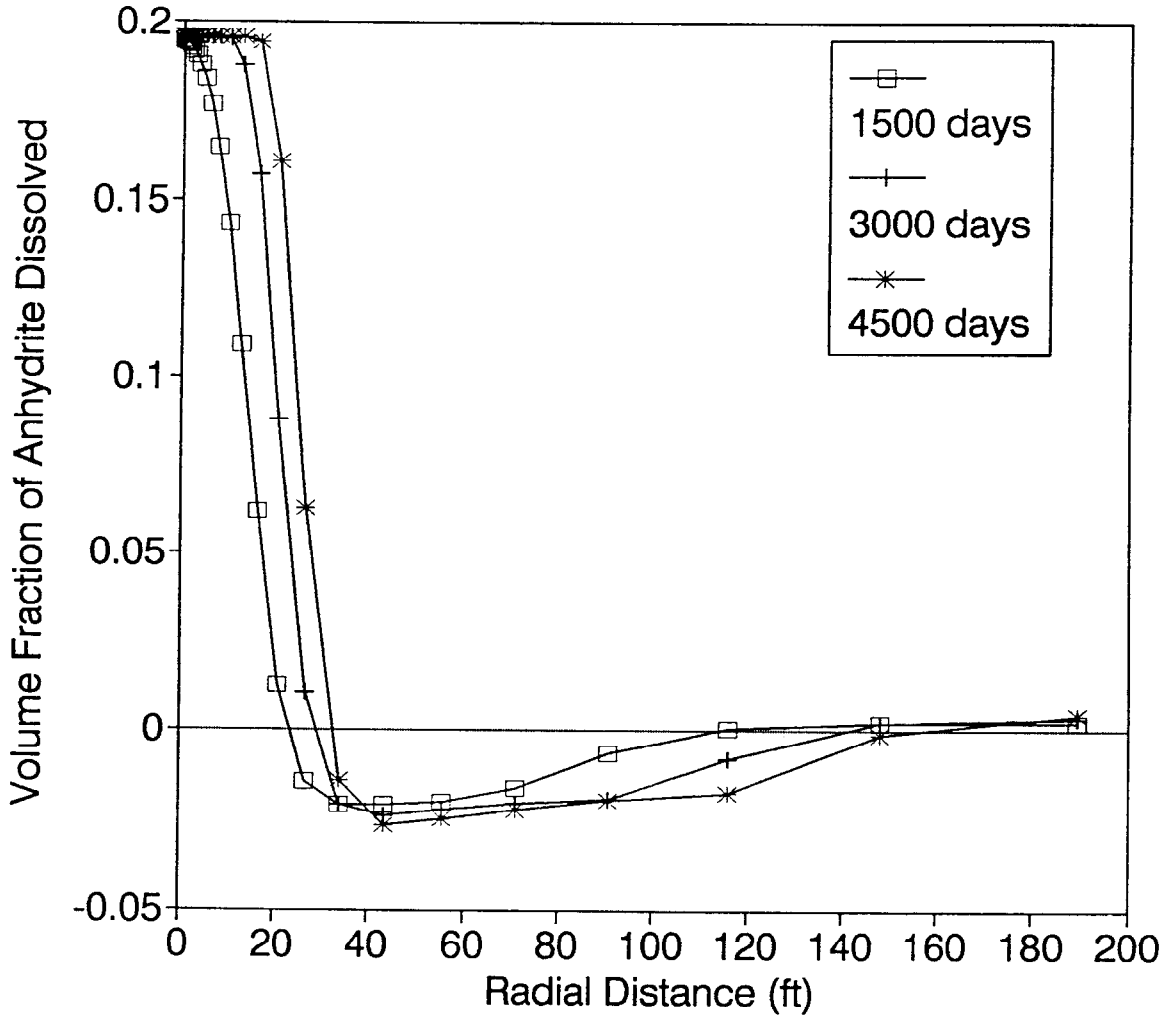

Fig. IV-11 Temporal evolution of the spatial profile of the volume fraction of anhydrite dissolved under the conditions of reservoir temperature and pressure during waste injection in the carbonate reservoir.

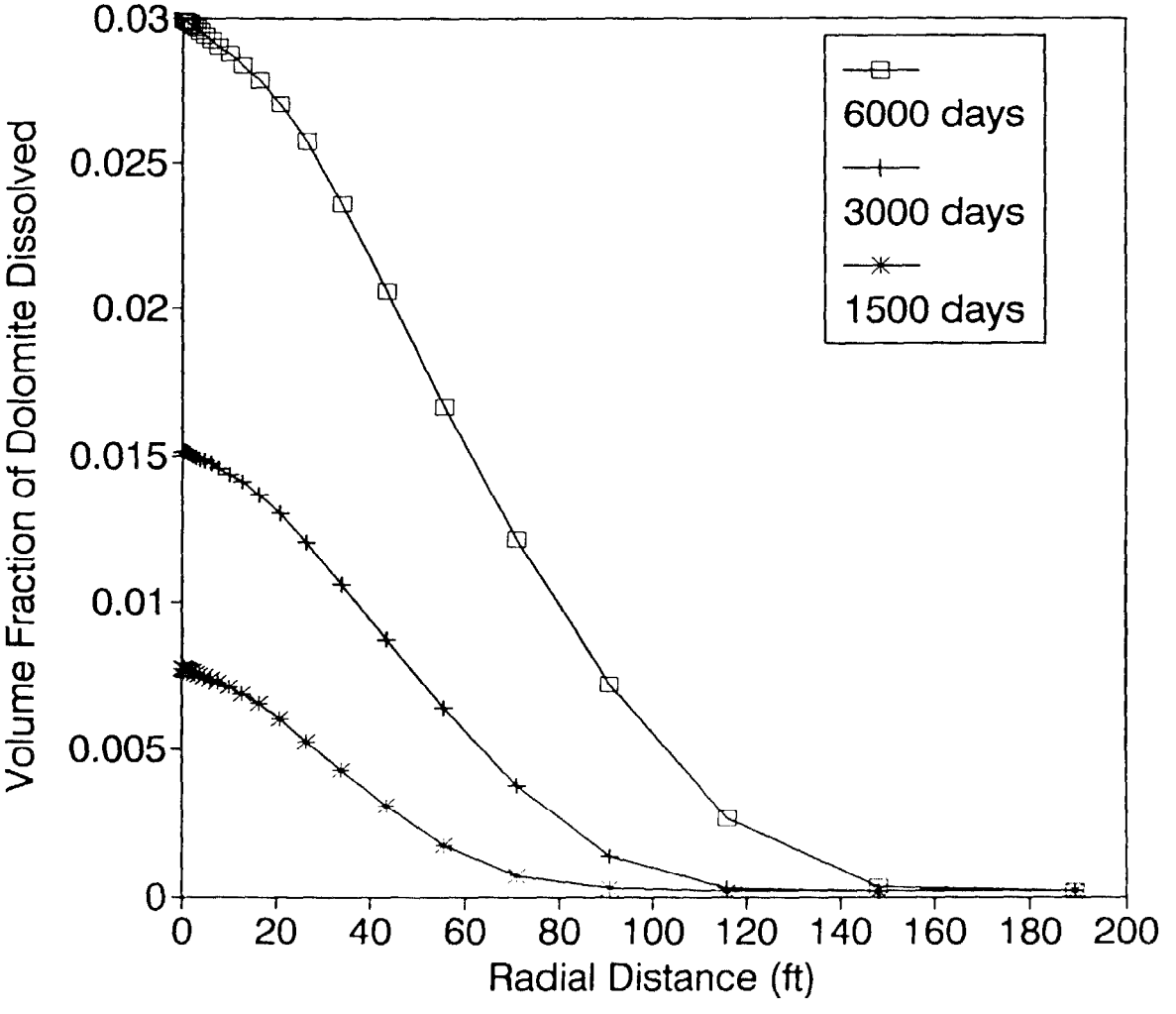

Fig.IV-12 Temporal evolution of the spatial profile of the volume fraction of dolomite dissolved under the conditions of reservoir temperature and pressure during waste injection in the carbonate reservoir.

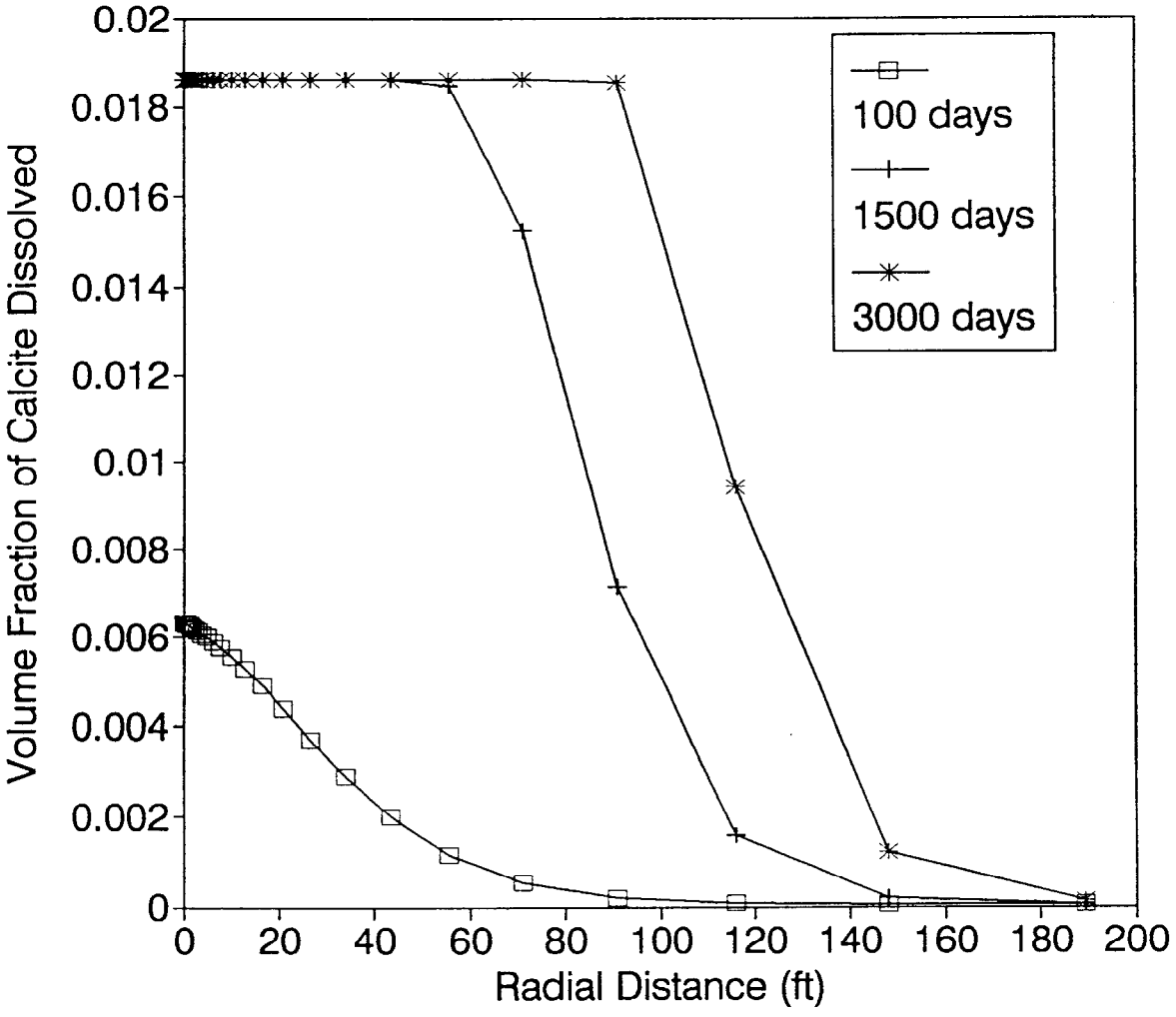

Fig. IV-13 Temporal evolution of the spatial profile of the volume fraction of calcite dissolved under the conditions of reservoir temperature and pressure during waste injection in the carbonate reservoir.

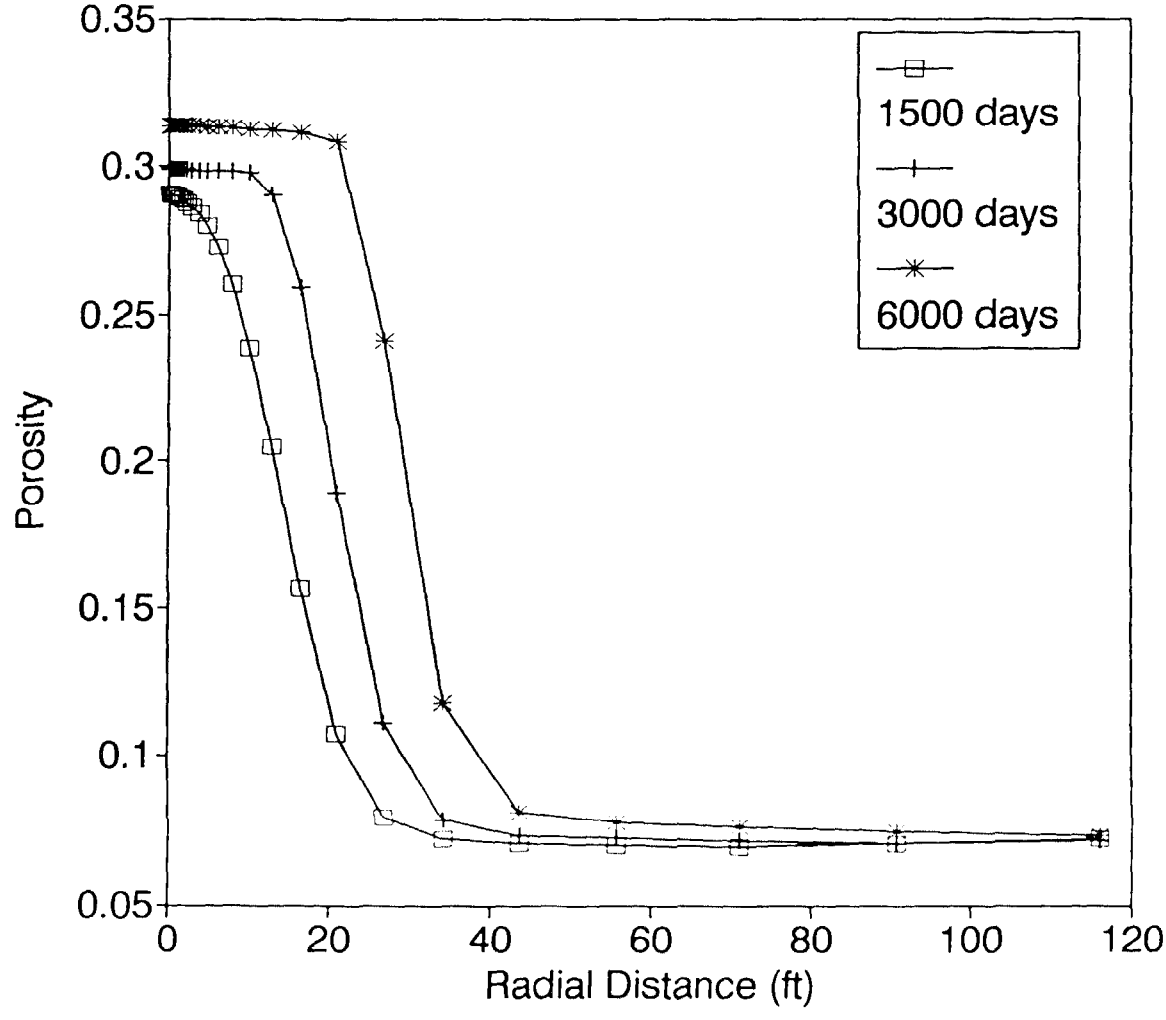

Fig. IV-14 Temporal evolution of the spatial profile of porosity under the conditions of reservoir temperature and pressure during waste injection in the carbonate reservoir

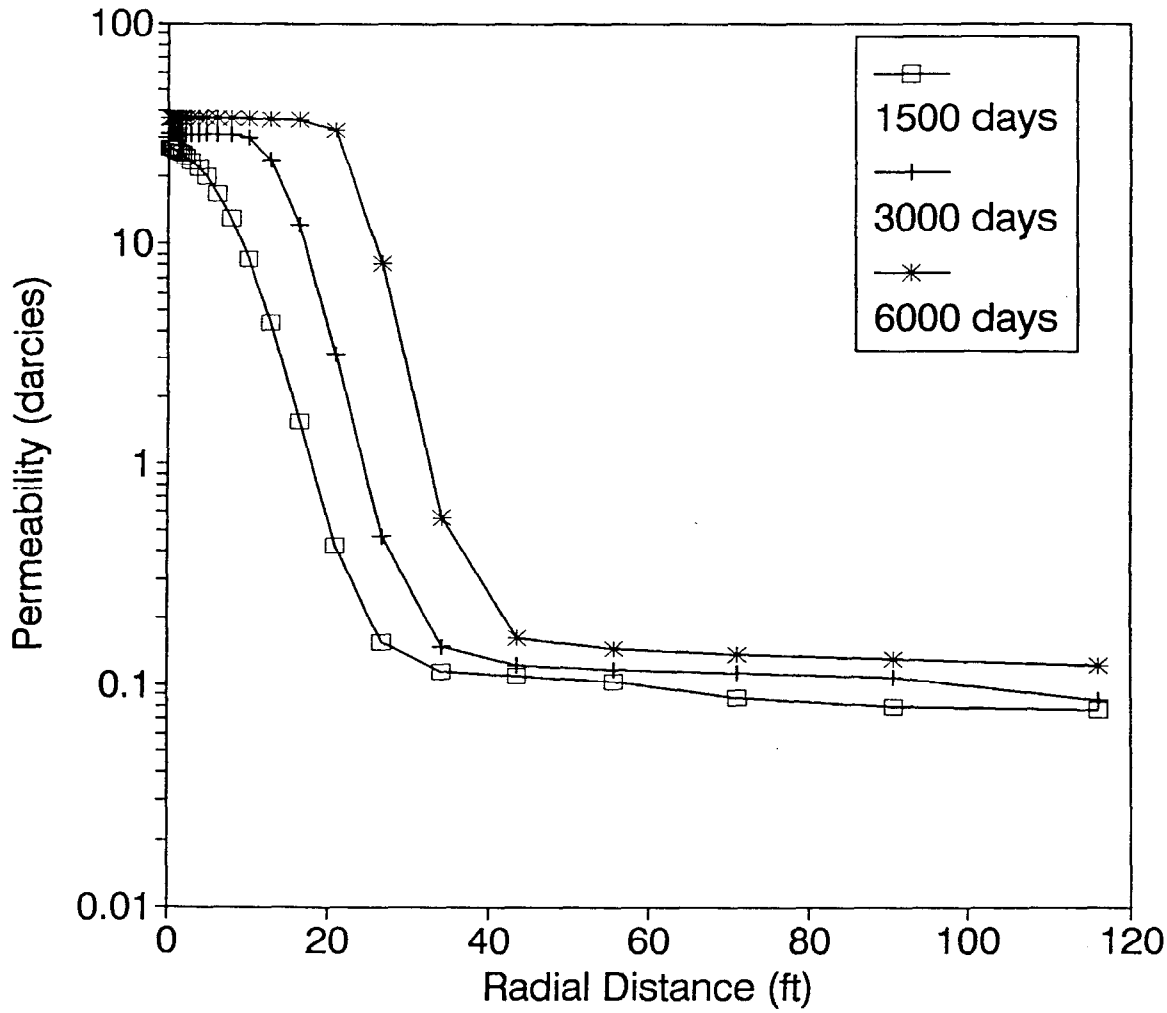

Fig. IV-15 Temporal evolution of the spatial profile of permeability under the conditions of reservoir temperature and pressure during waste injection in the carbonate reservoir.

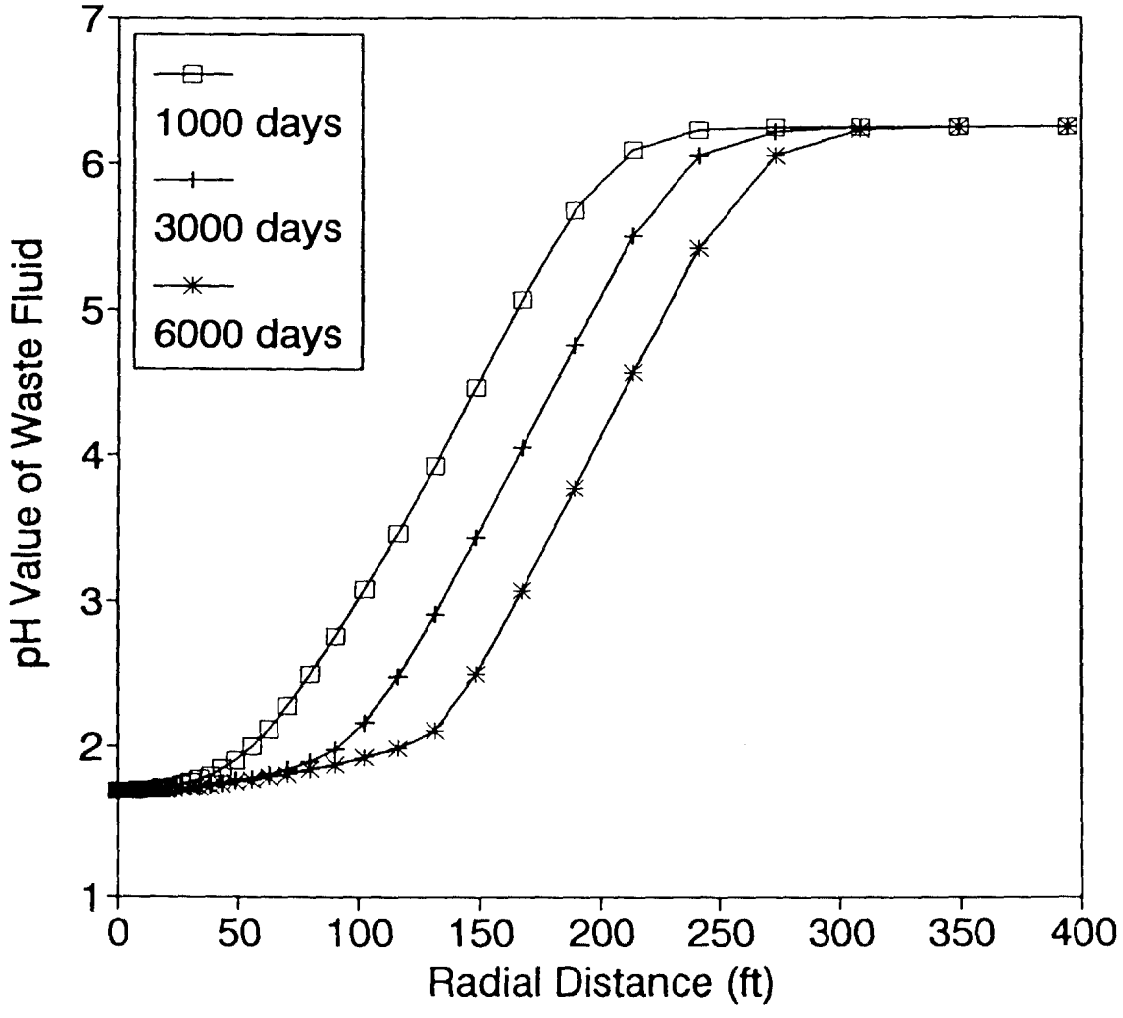

Fig. IV-16 Effects of acid neutralization by mineral reactions shown as the temporal evolution of the spatial profile of pH.

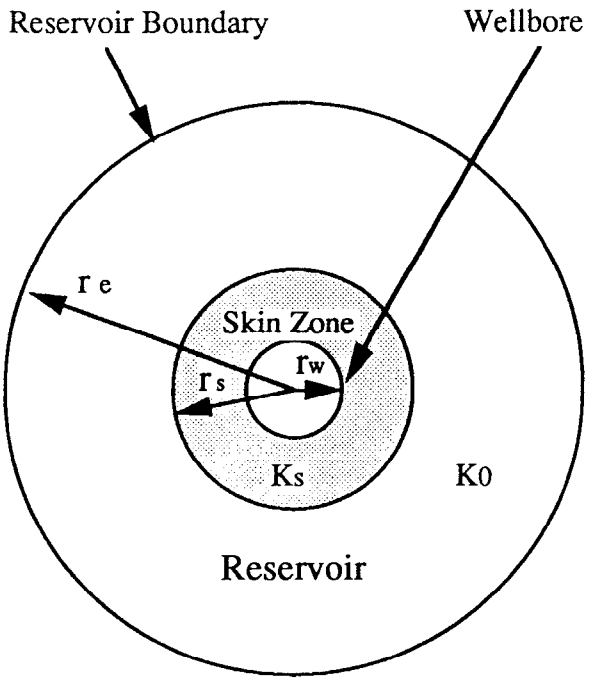

Fig. IV-17 Schematic depiction of a skin region around the wellbore.

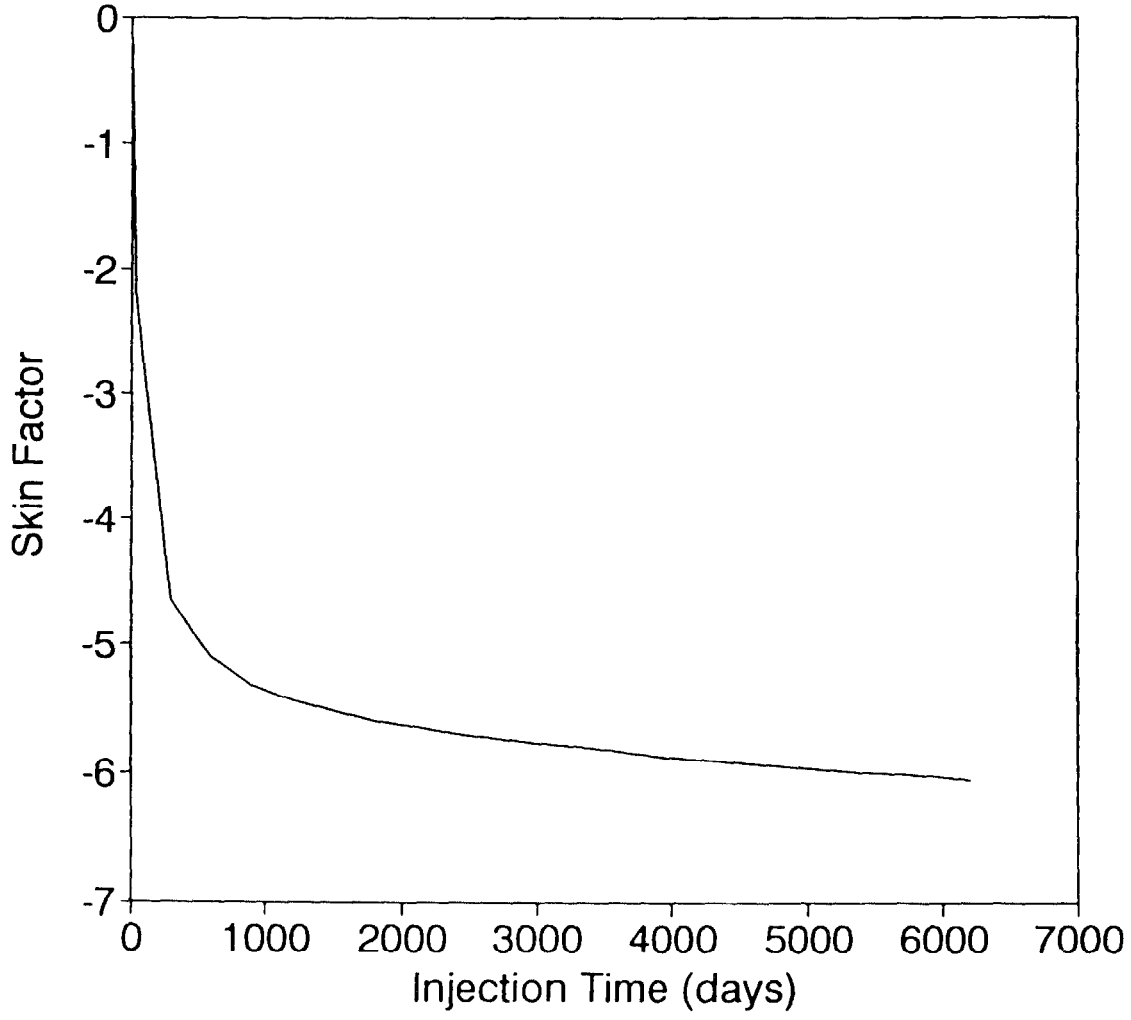

Fig. IV-18 Predicted skin factor is shown as a function of waste injection time for the carbonate reservoir.

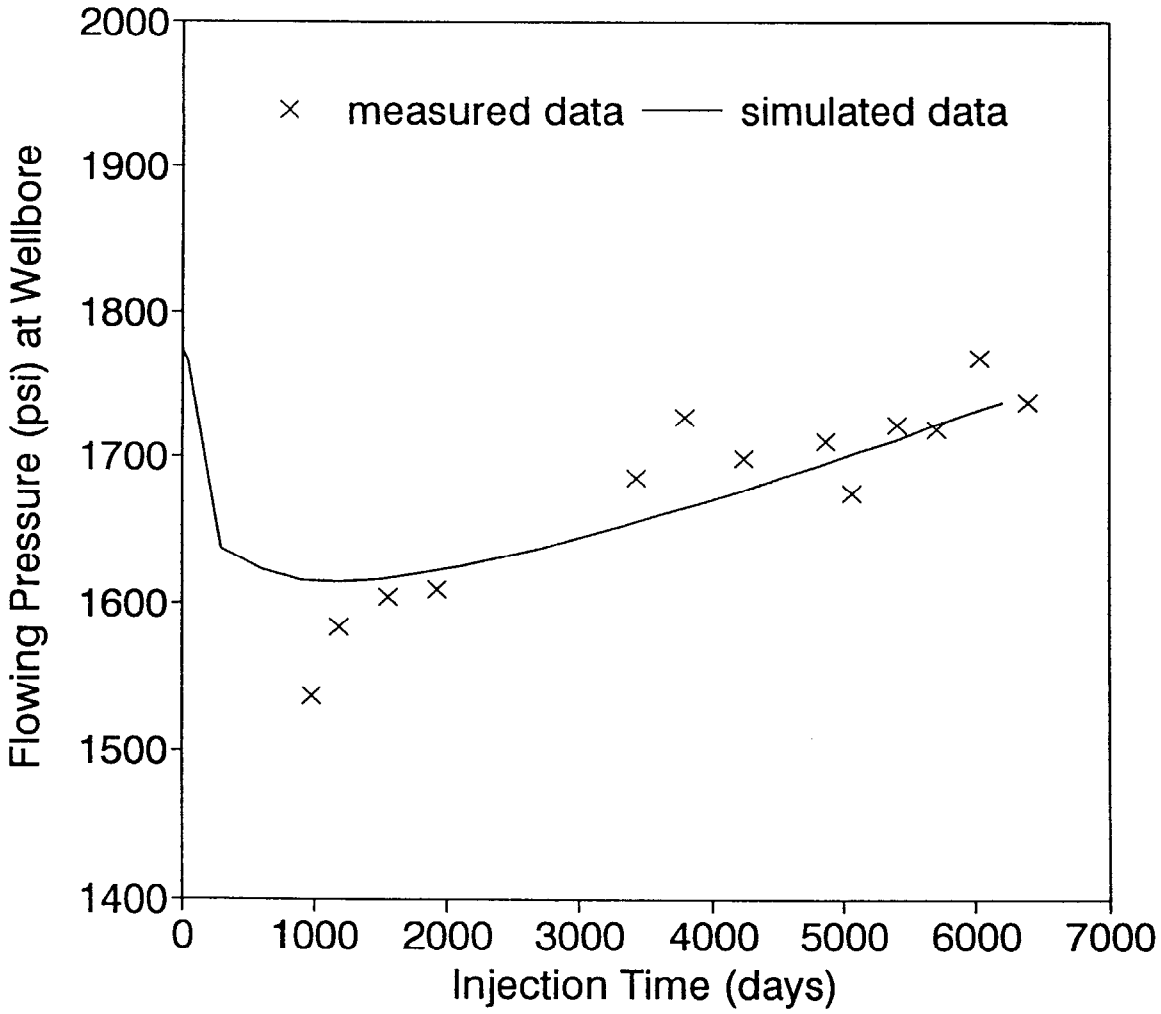

Fig. IV-19 Comparison of simulation results and field measurements of the flowing pressure of fluid at the wellbore during waste injection into the carbonate reservoir.

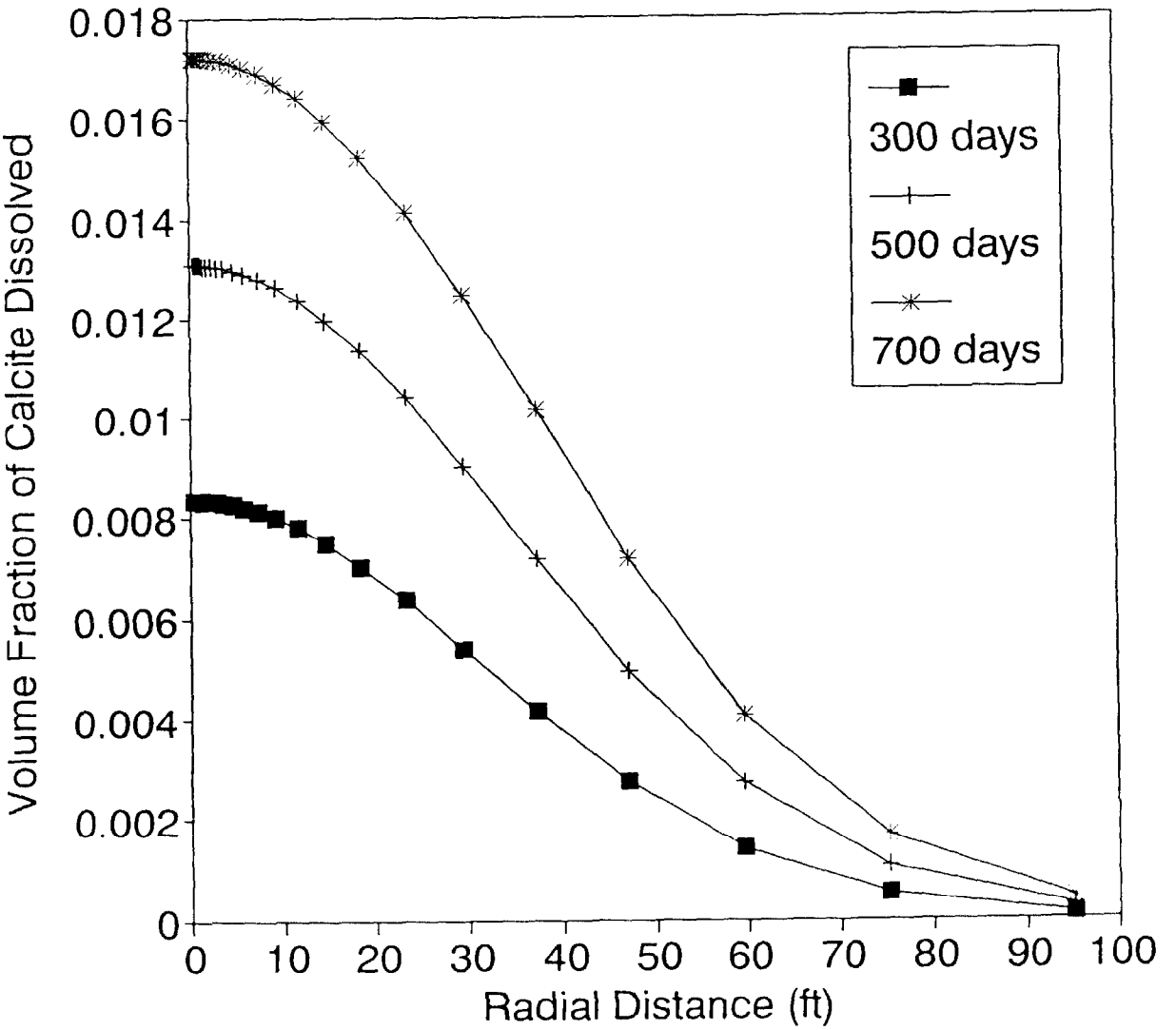

Fig. IV-20 Temporal evolution of the spatial profile of the volume fraction of calcite dissolved under the conditions of reservoir temperature and pressure during waste injection in the sandstone reservoir.

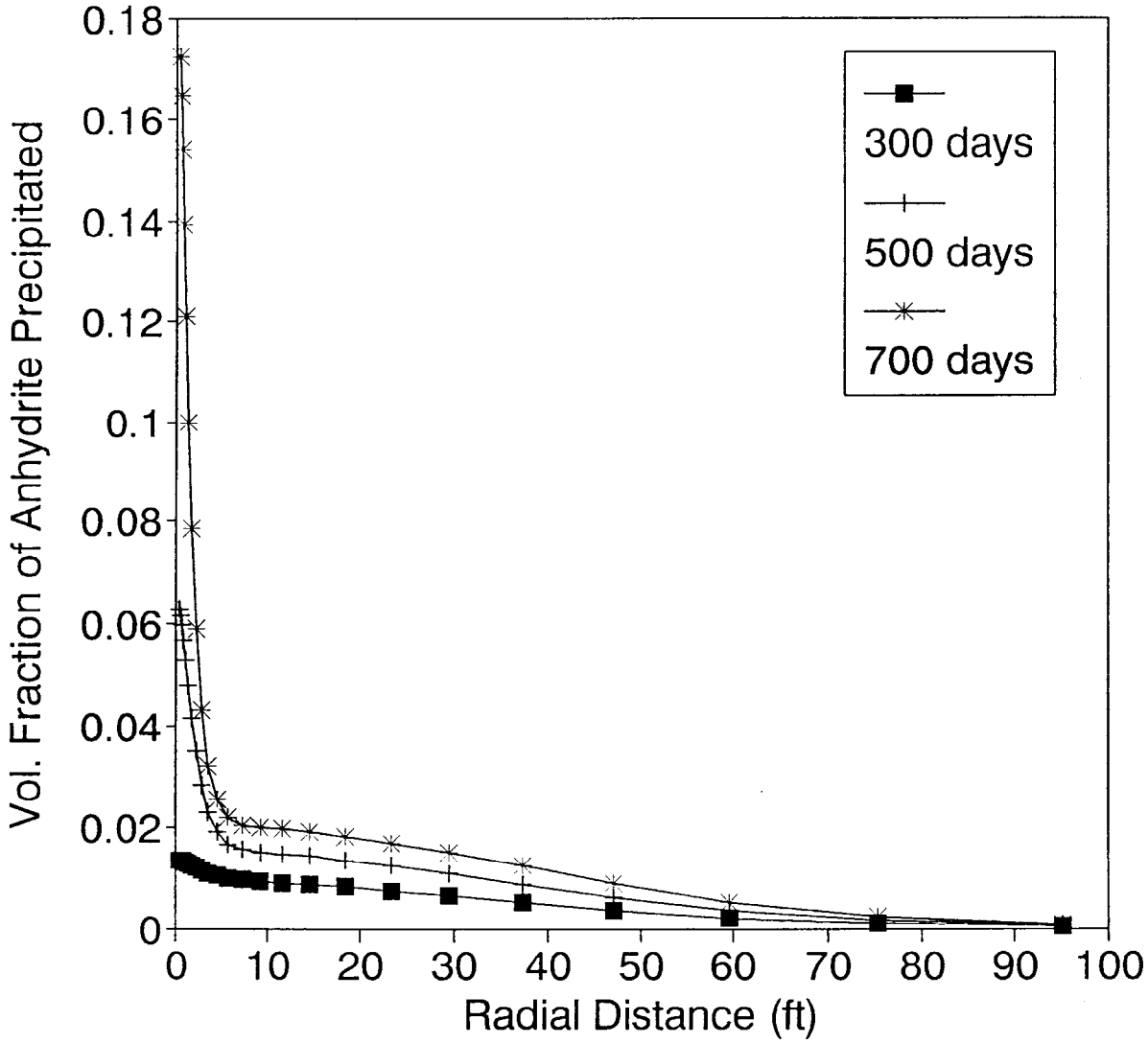

Fig. IV-21 Temporal evolution of the spatial profile of the volume fraction of anhydrite precipitated under the conditions of reservoir temperature and pressure during waste injection in the sandstone reservoir.

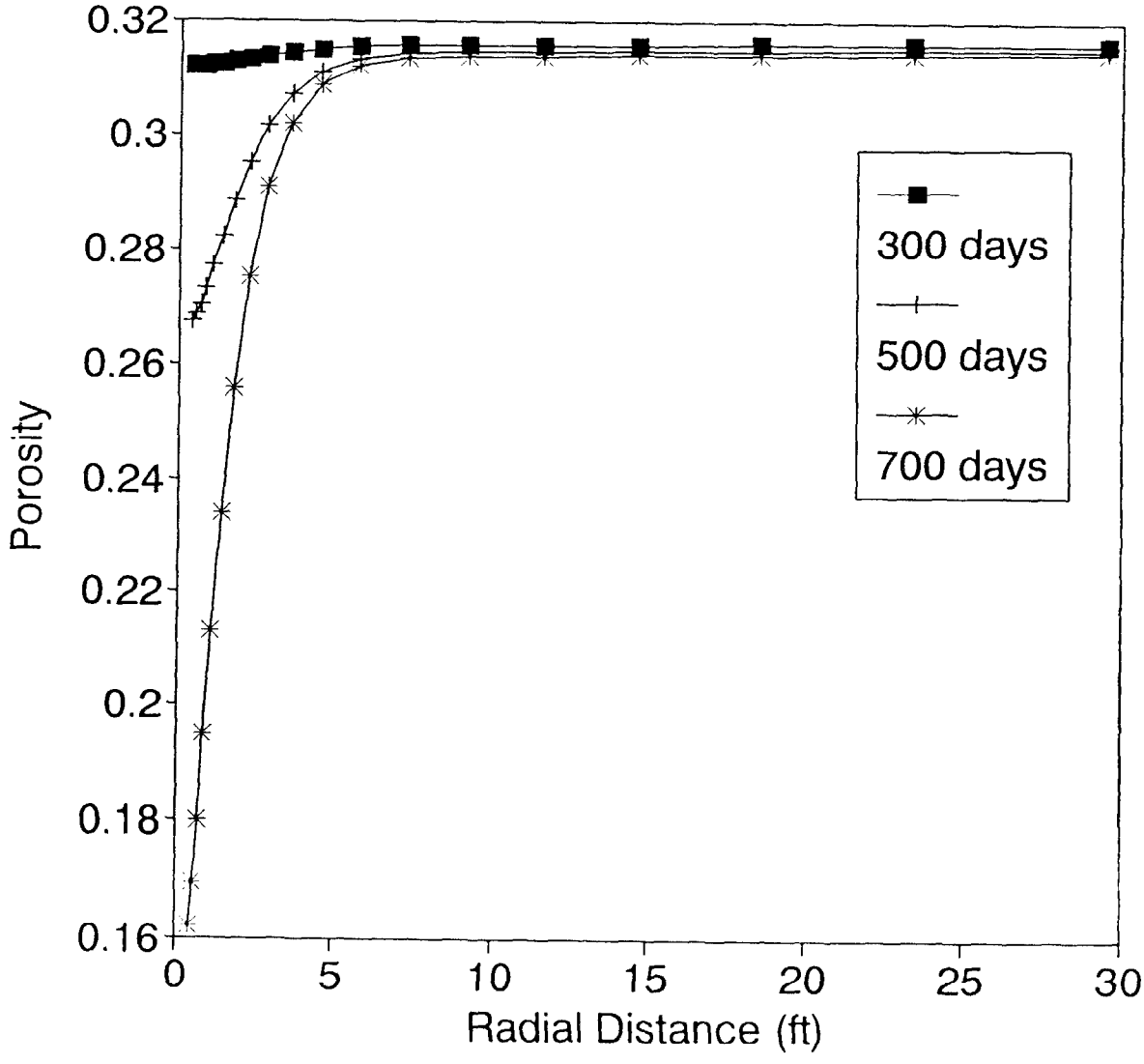

Fig. IV-22 Temporal evolution of the spatial profile of porosity under the conditions of reservoir temperature and pressure during waste injection in the sandstone reservoir.

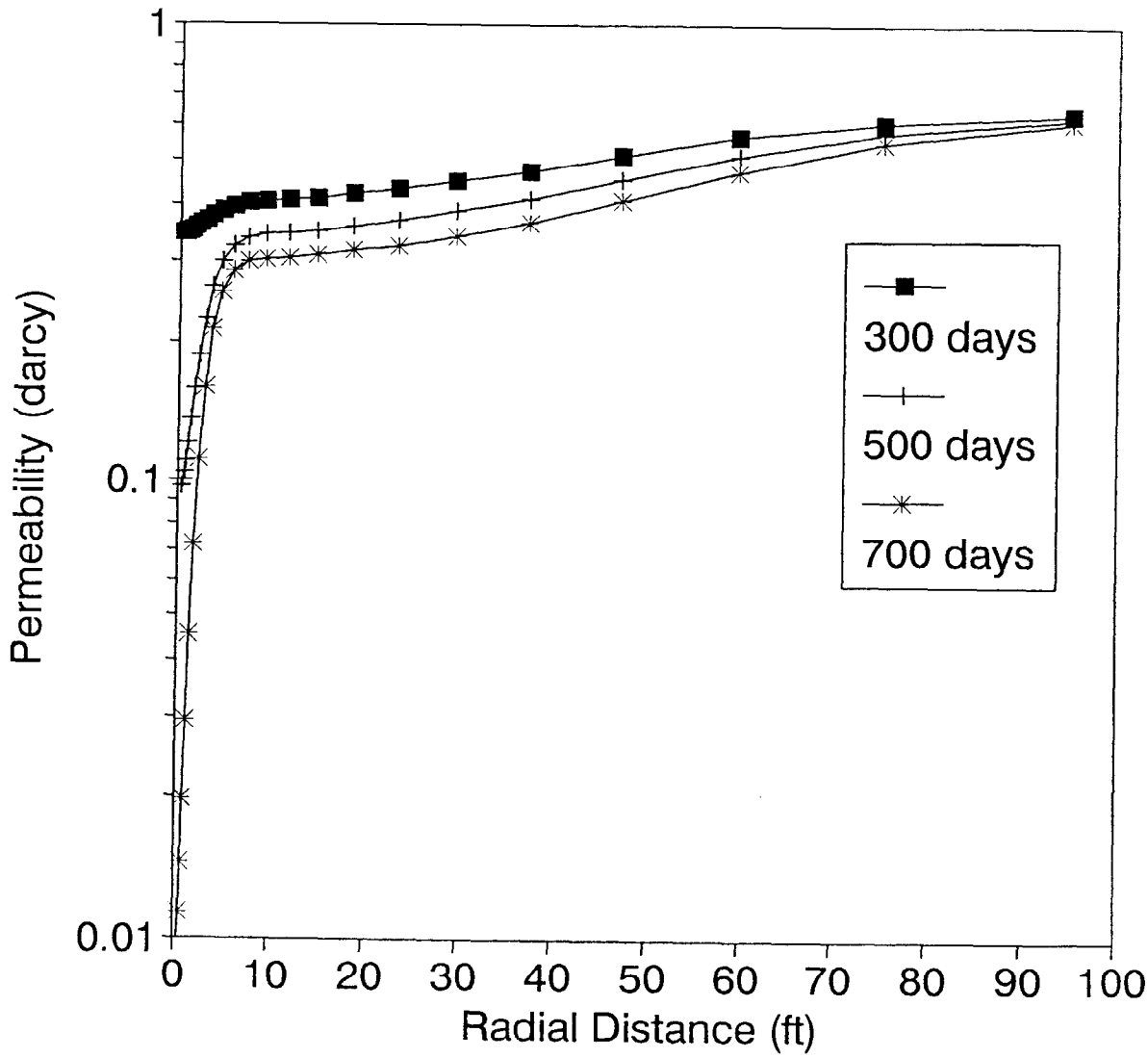

Fig. IV-23 Temporal evolution of the spatial profile of permeability under the conditions of reservoir temperature and pressure during waste injection in the sandstone reservoir.

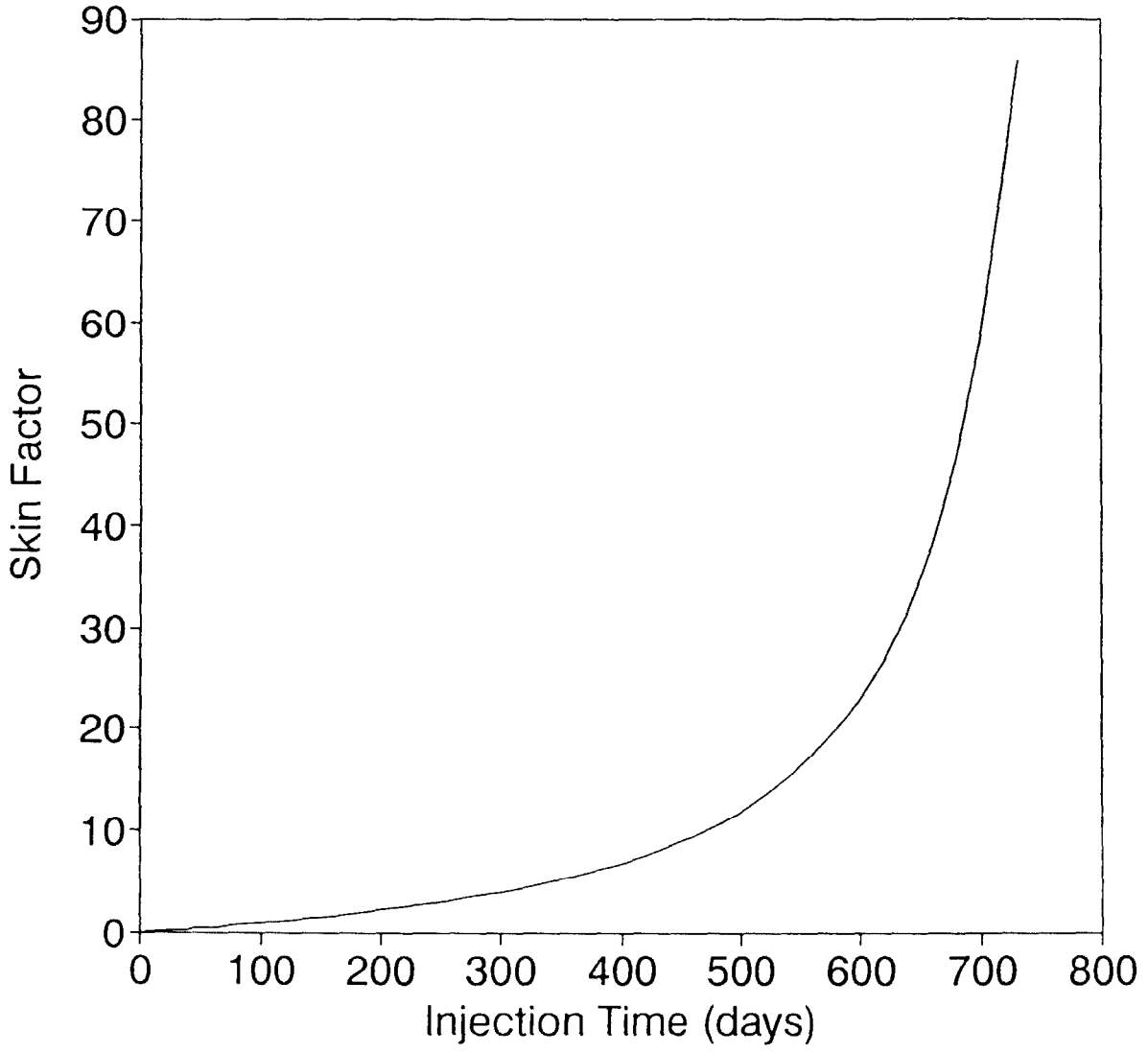

Fig. IV-24 Predicted skin factor is shown as a function of waste injection time for the sandstone reservoir.

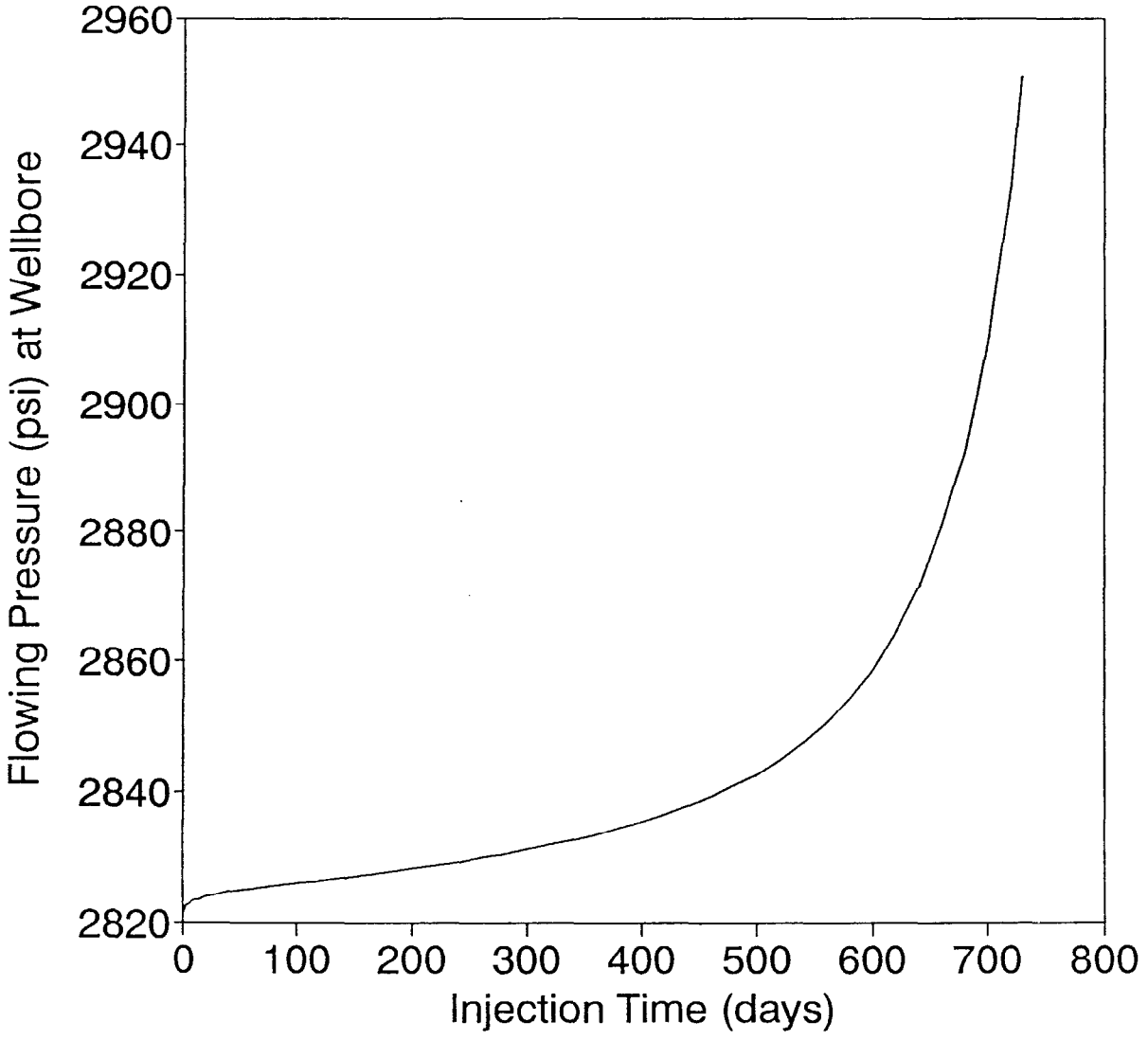

Fig. IV-25 Predicted flowing pressure of fluid at the wellbore for the sandstone reservoir is shown as a function of waste injection time.

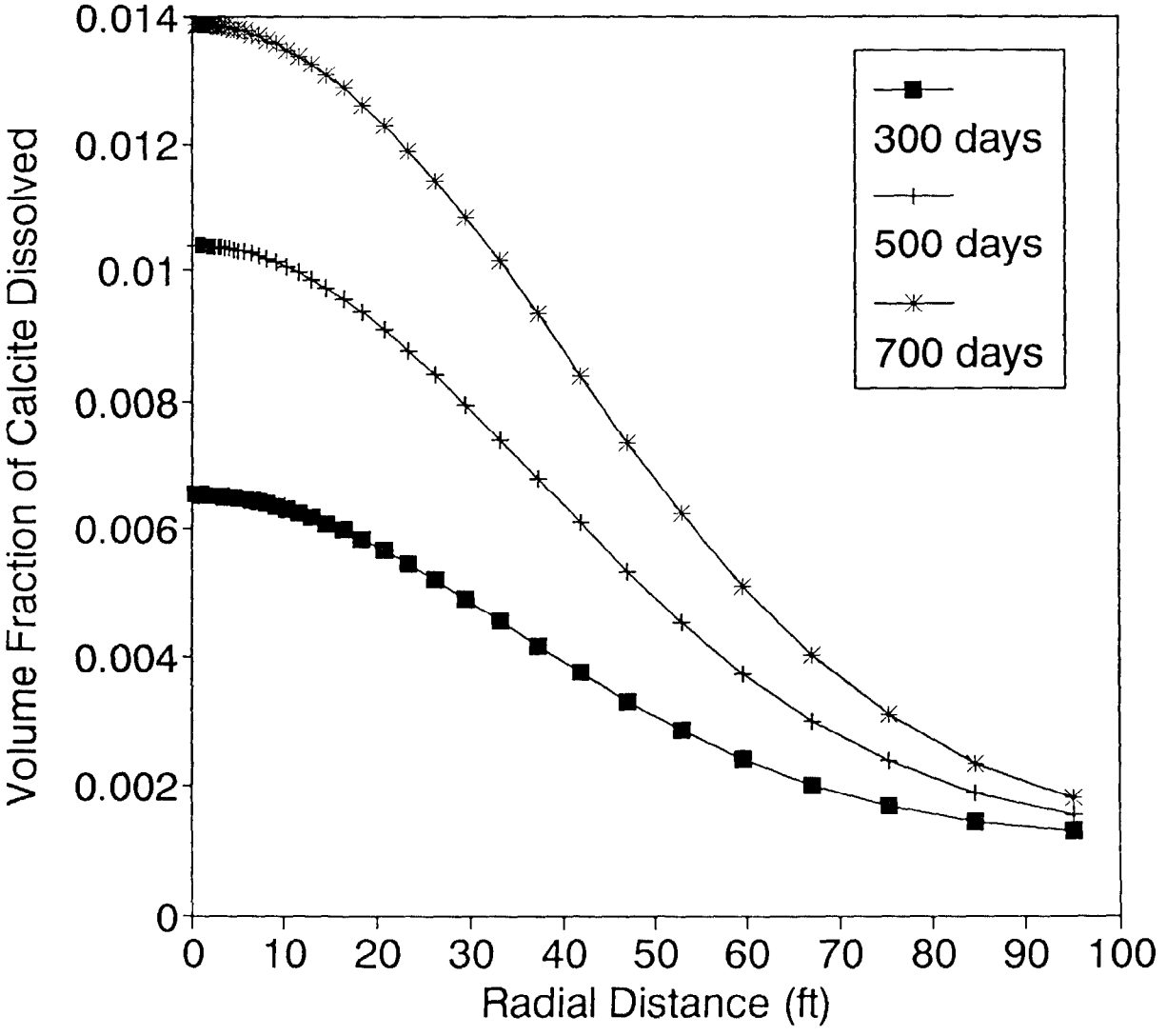

Fig. IV-26 Temporal evolution of the spatial profile of the volume fraction of calcite dissolved during the injection of the diluted waste fluid into the sandstone reservoir.

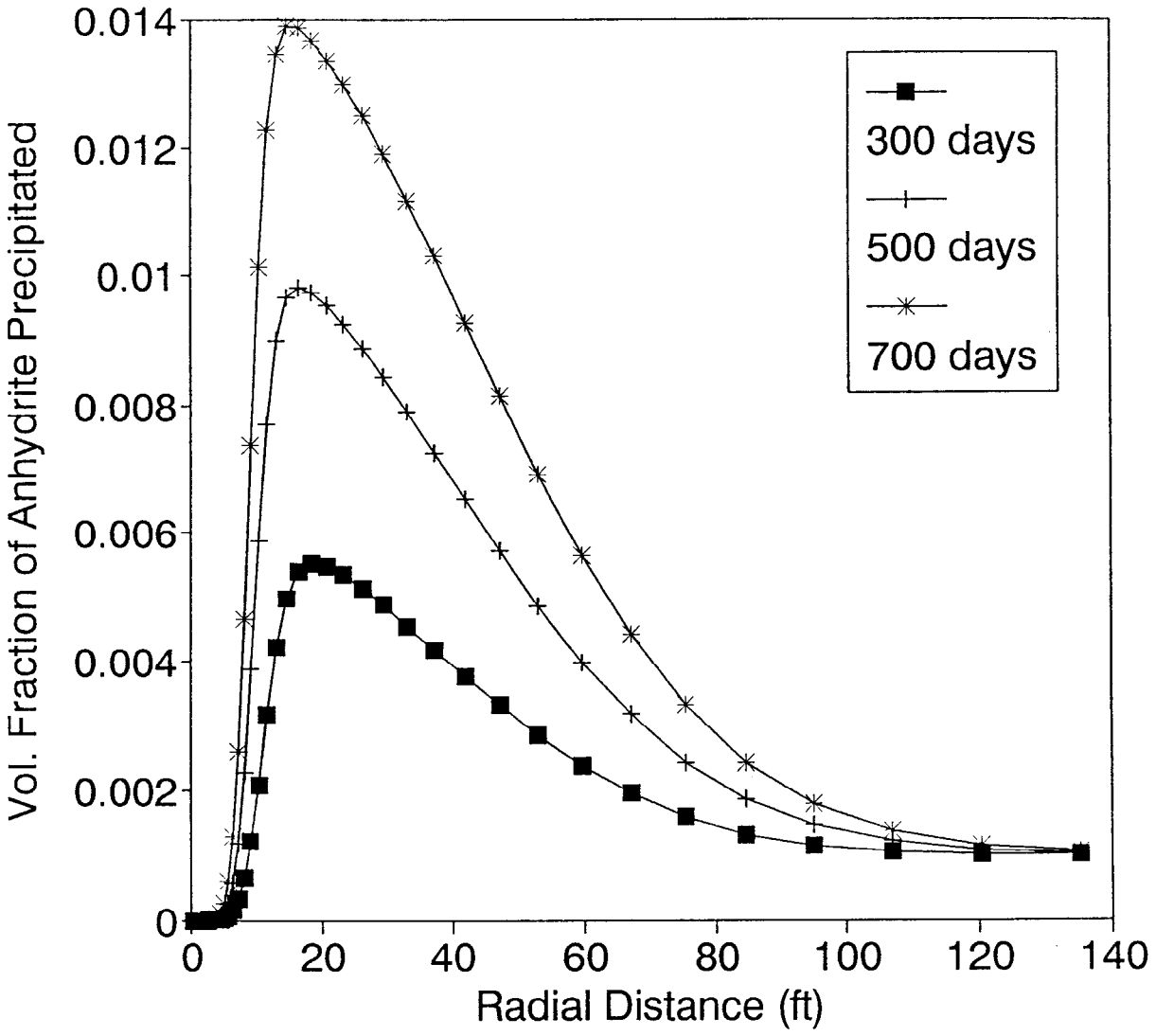

Fig. IV-27 Temporal evolution of the spatial profile of the volume fraction of anhydrite precipitated during the injection of the diluted waste fluid into the sandstone reservoir.

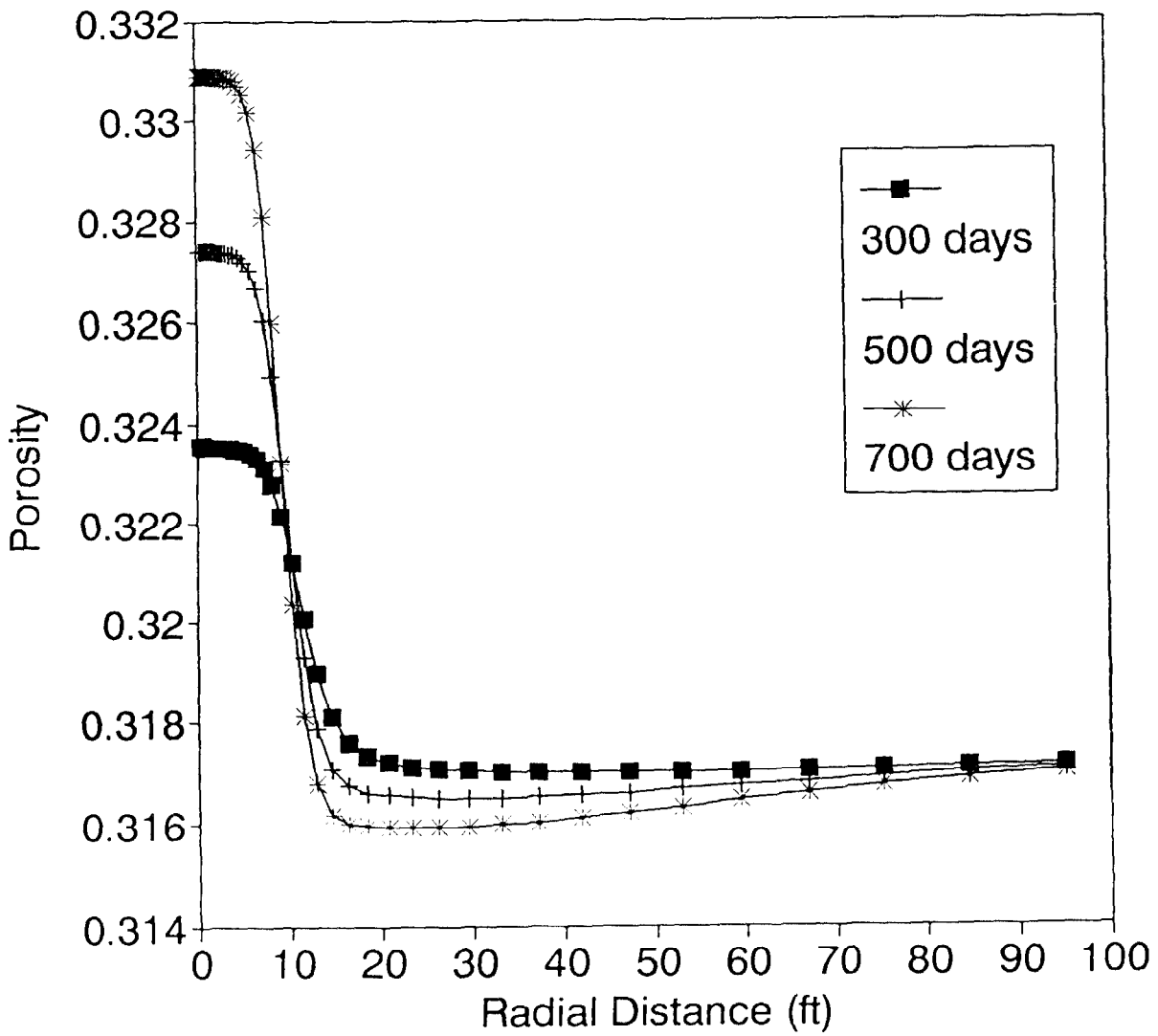

Fig. IV-28 Temporal evolution of the spatial profile of porosity during the injection of the diluted waste fluid into the sandstone reservoir.

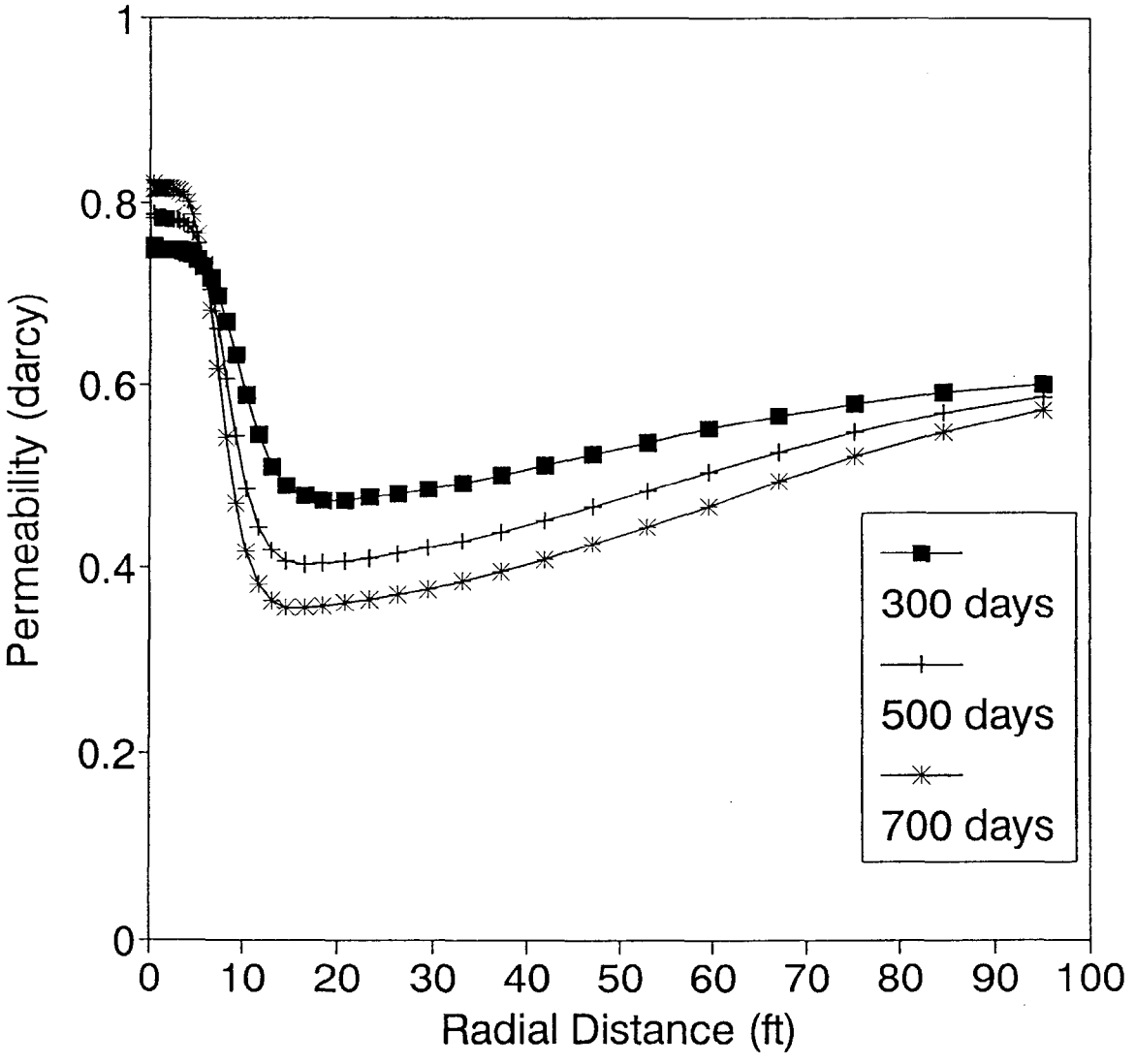

Fig. IV-29 Temporal evolution of the spatial profile of permeability during the injection of the diluted waste fluid into the sandstone reservoir.

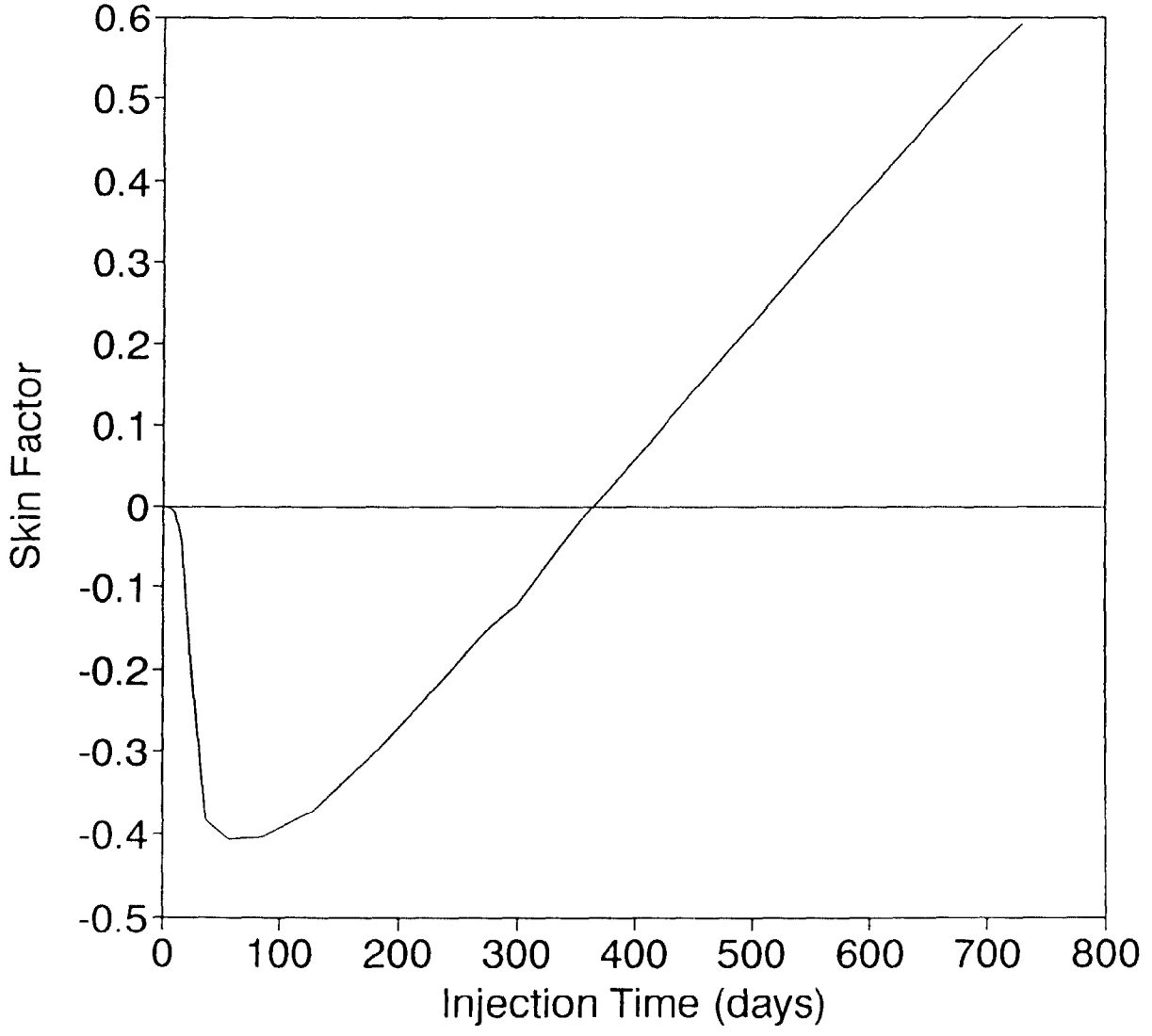

Fig. IV-30 Predicted skin factor due to injection of the diluted waste into the sandstone reservoir is shown as a function of time.

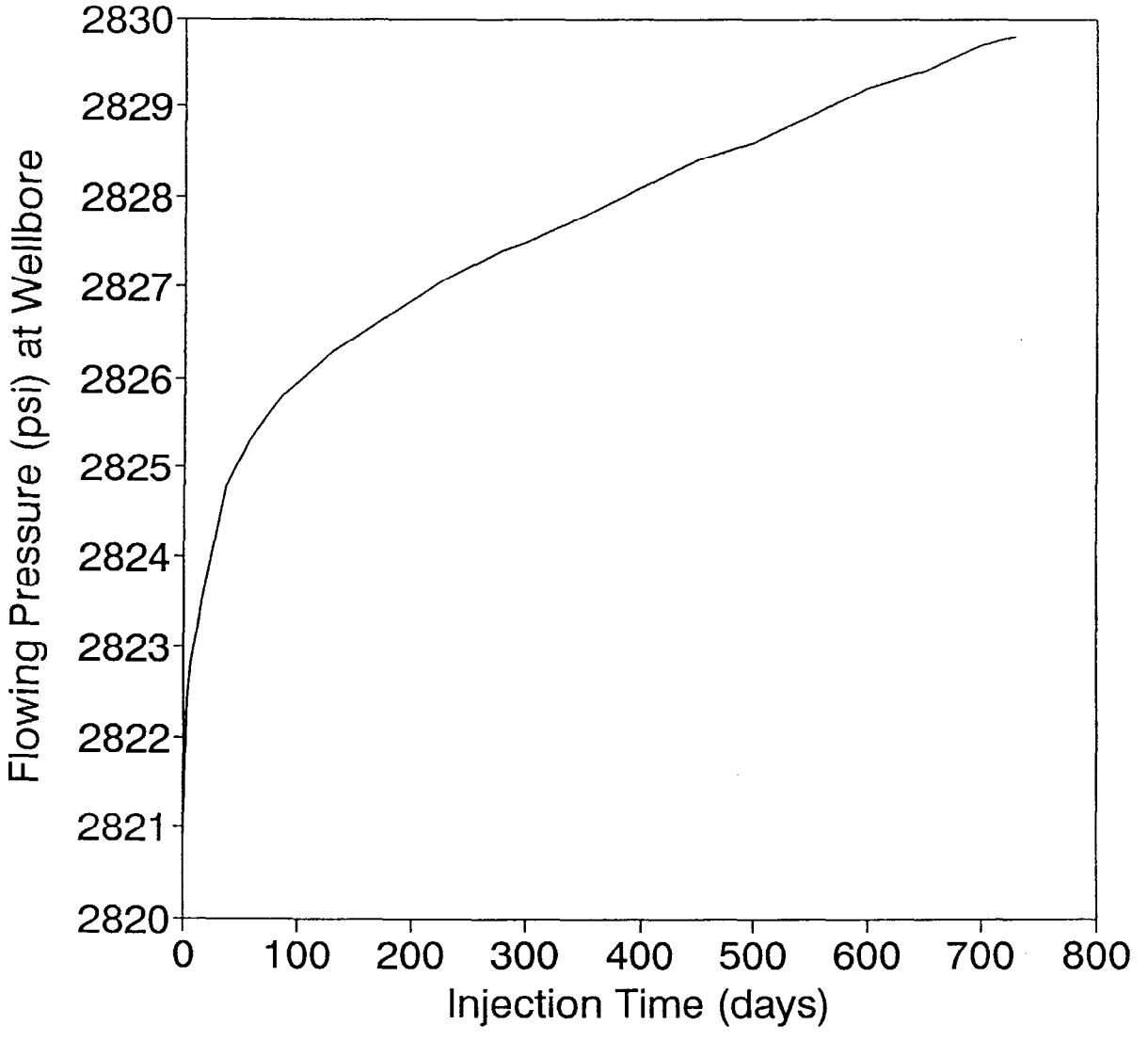

Fig. IV-31 The wellbore pressure predicted as a result of injection of the diluted waste into the sandstone reservoir is shown as a function of time.

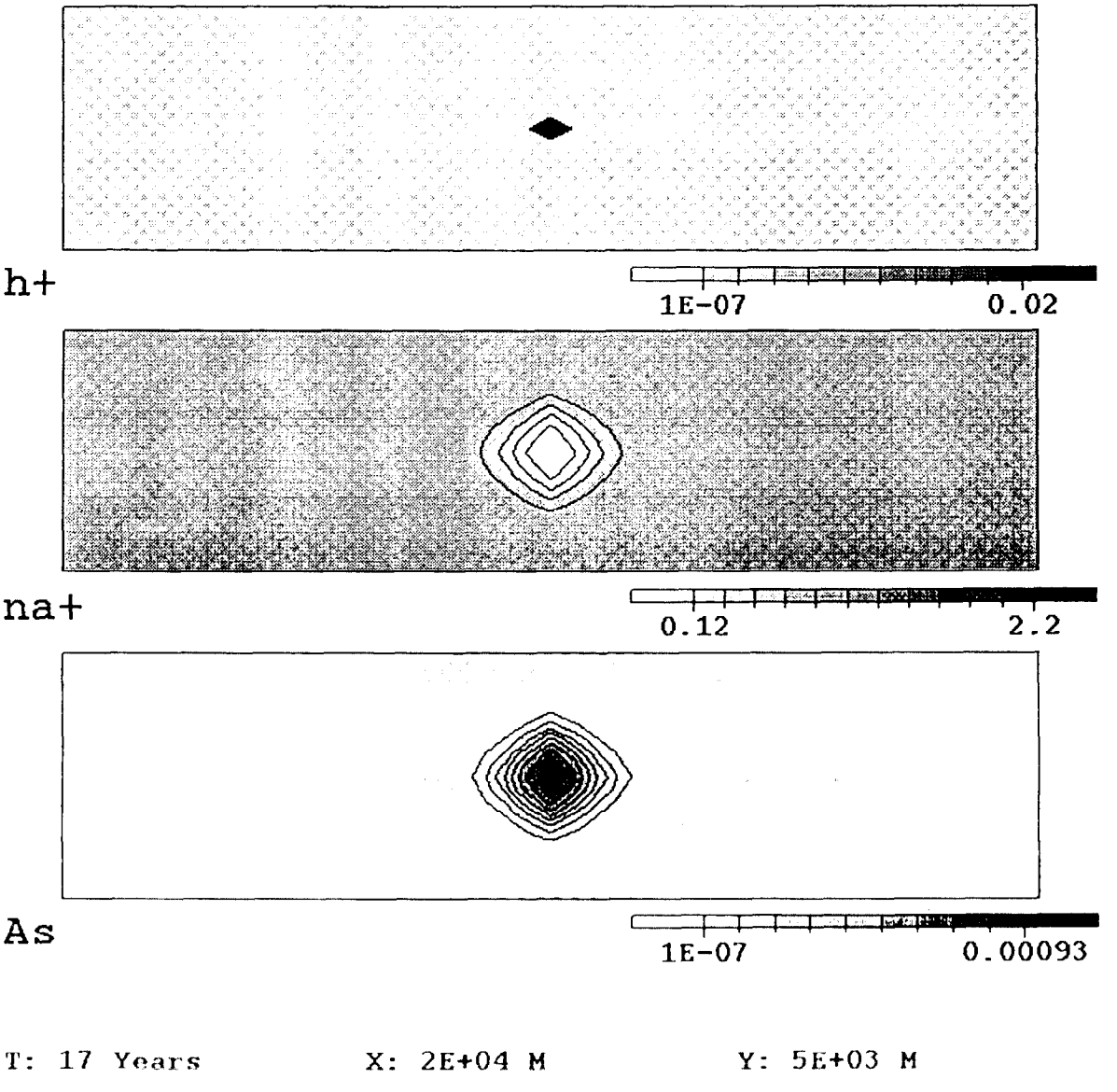

Fig. IV-32 Spatial distribution of acid, sodium and arsenic concentrations in the carbonate reservoir after 17 years of waste injection.

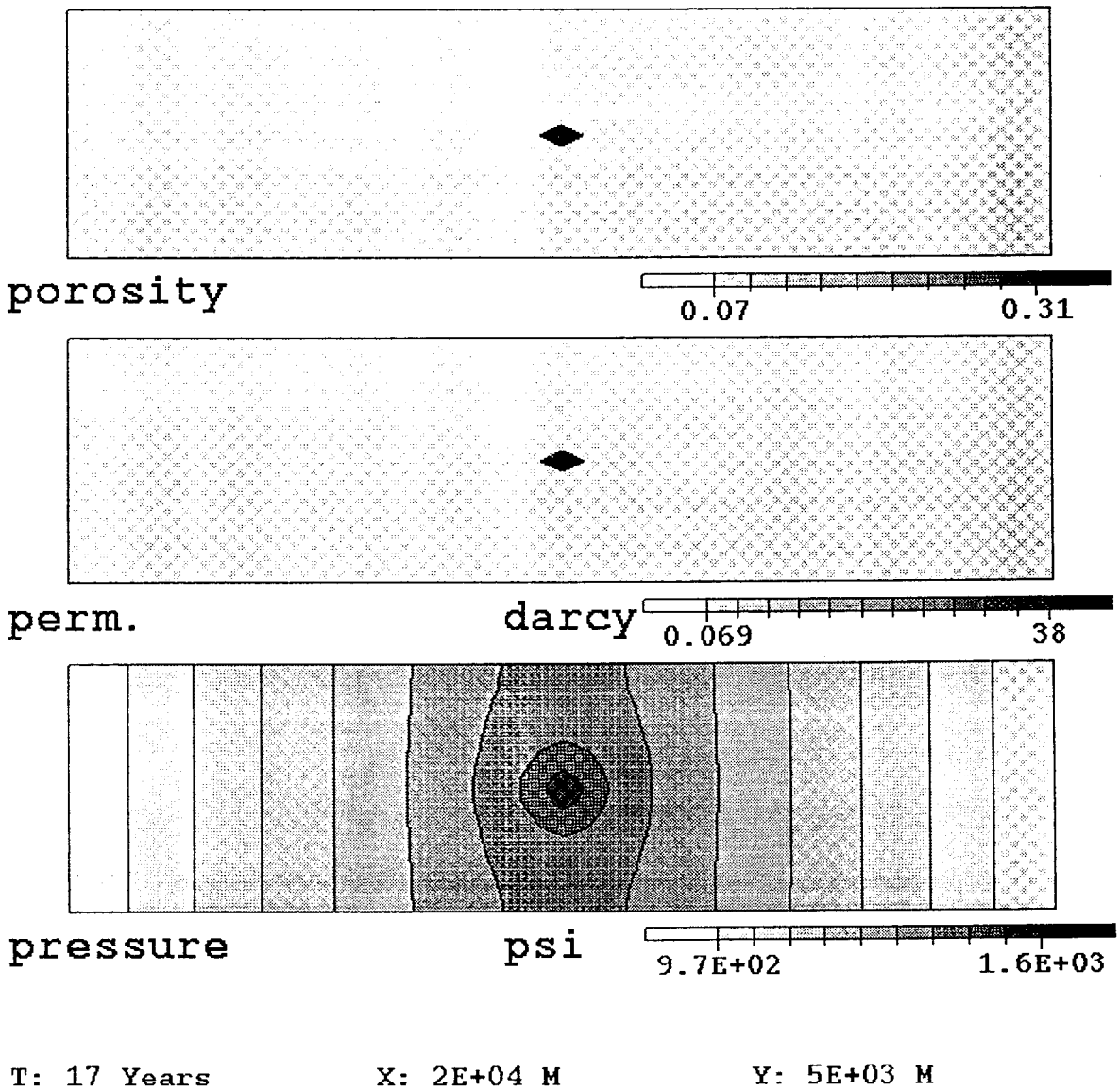

Fig. IV-33 Distribution of porosity, permeability and pressure in the carbonate reservoir after 17 years of waste injection.

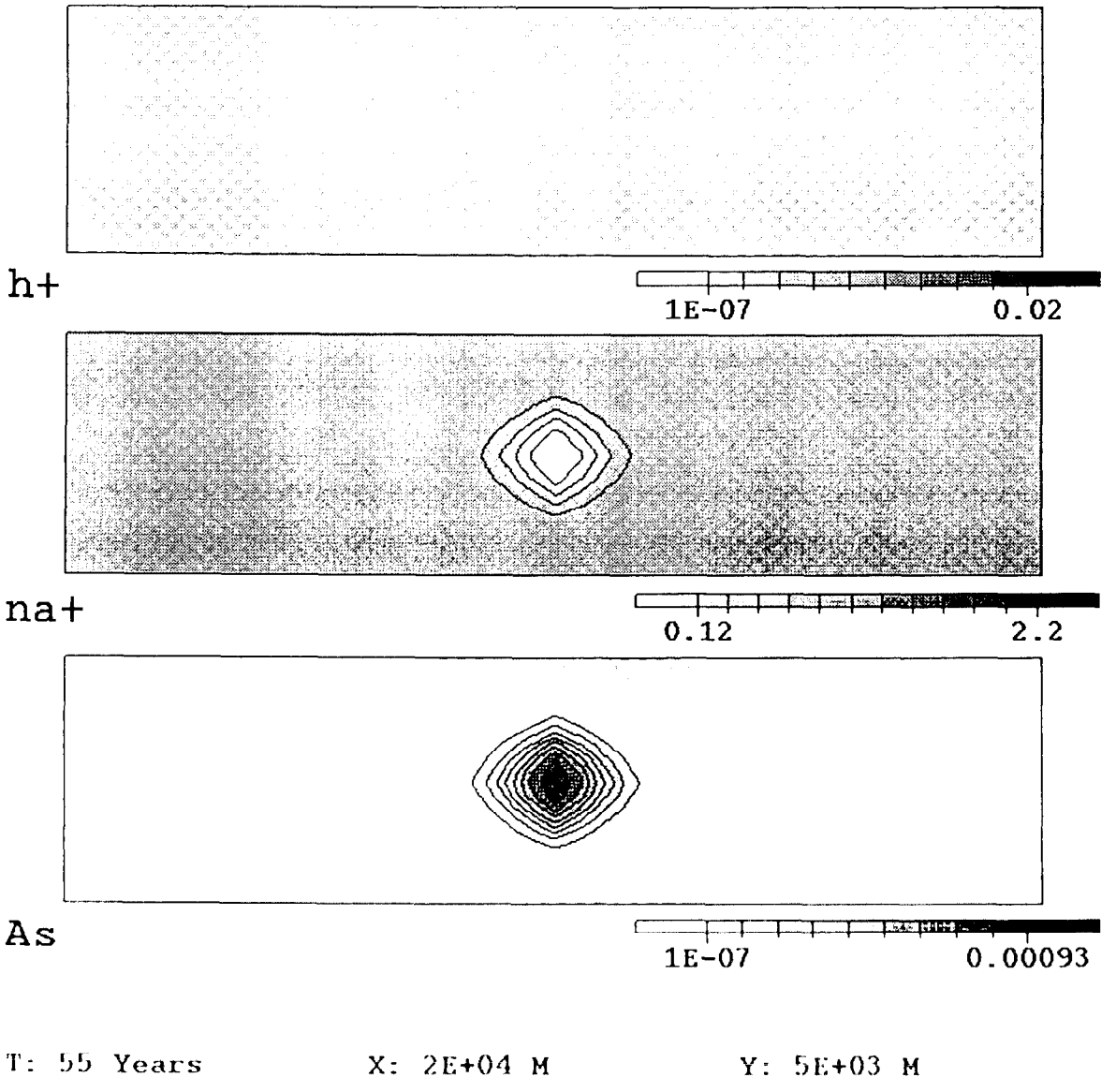

Fig. IV-34 Distribution of acid, sodium and arsenic concentrations at 55 years (38 years after the 17 year injection period) for the same simulation as in Fig. IV-32. Note the effect of acid neutralization by calcite

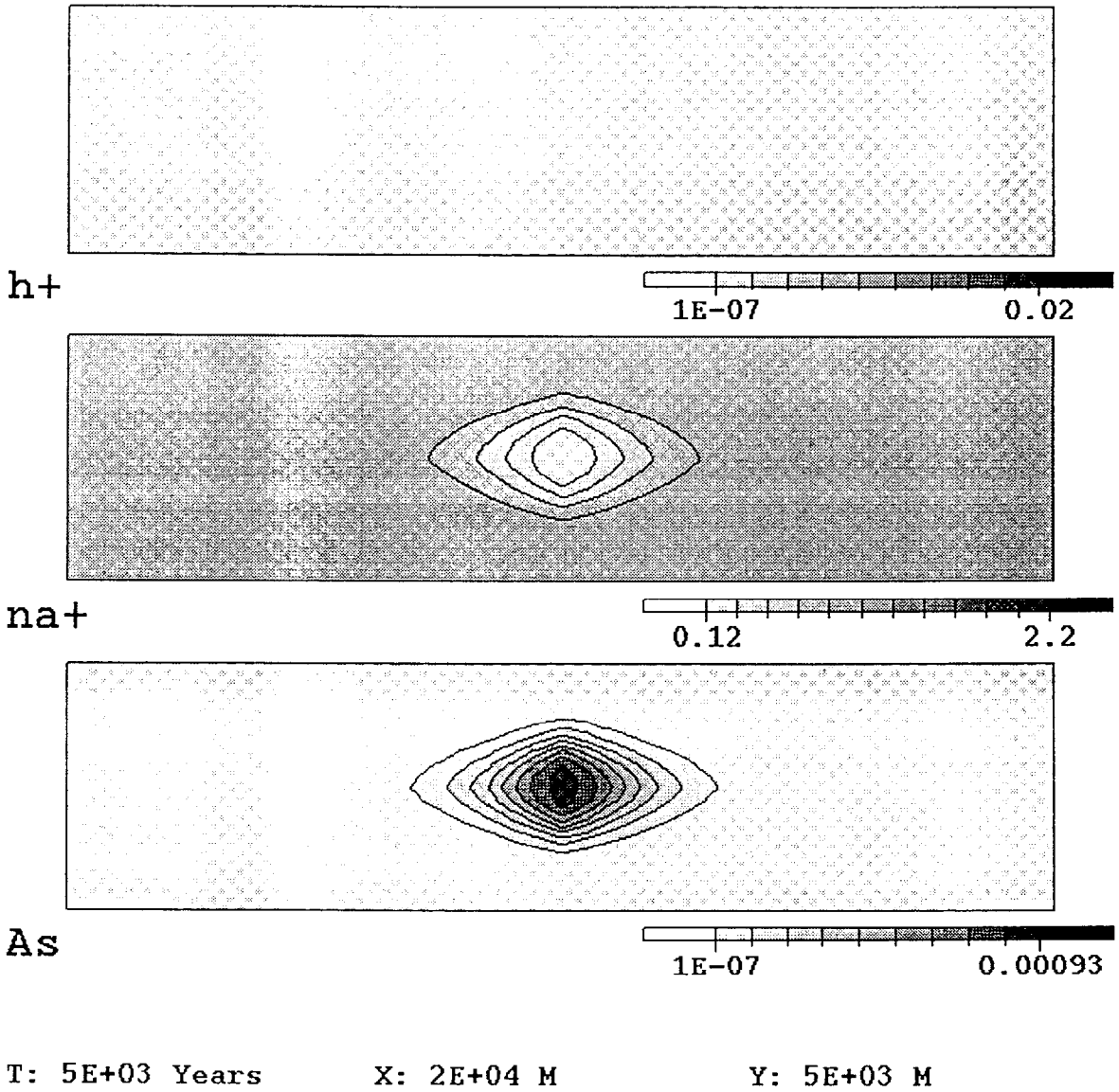

Fig. IV-35 Distribution of acid, sodium and arsenic concentrations in the carbonate reservoir at 5,000 years for the same simulation as in Fig. IV-32. The migration of sodium and arsenic in the reservoir is noted.

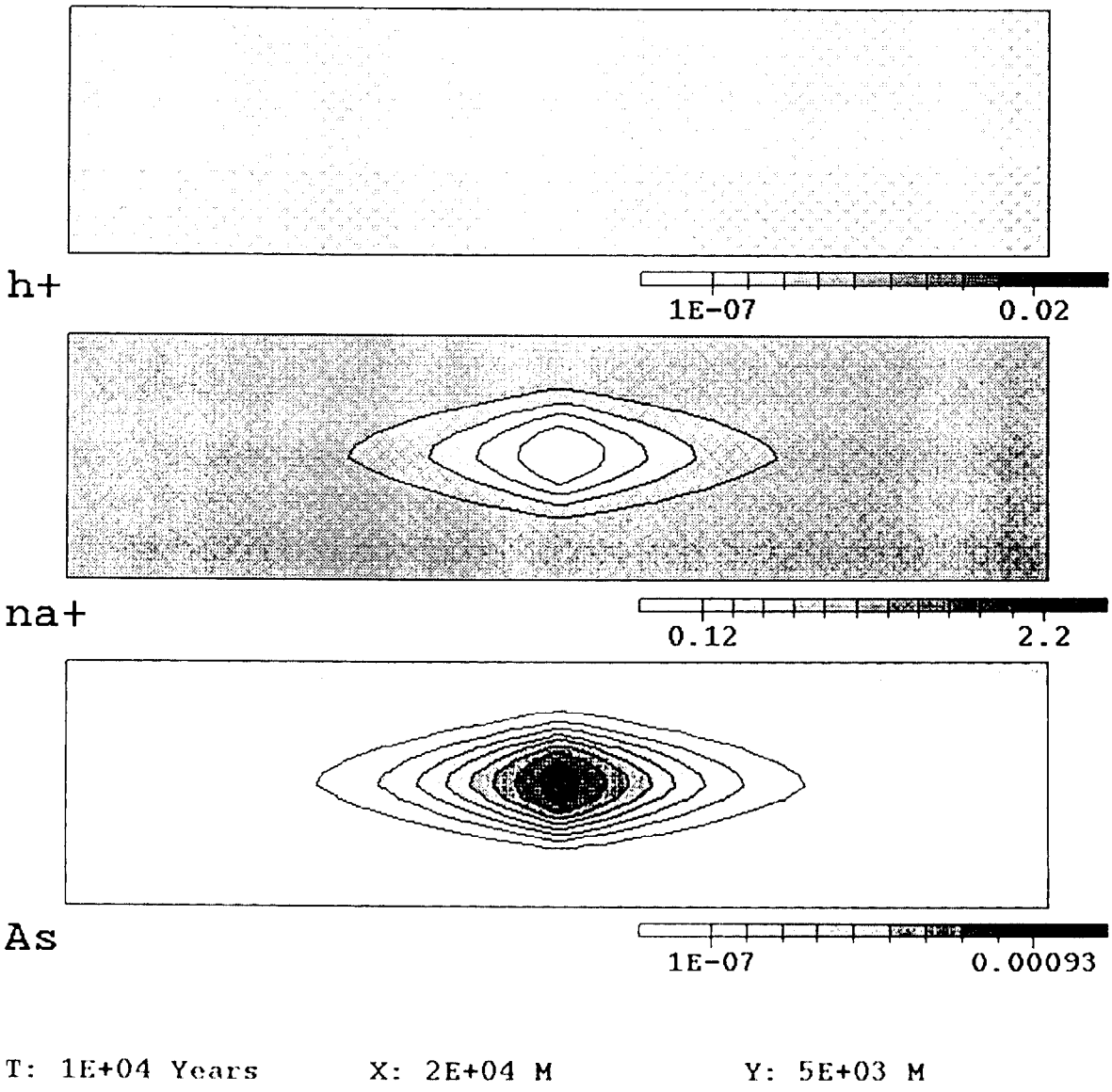

Fig. IV-36 Distribution of acid, sodium and arsenic concentrations in the carbonate reservoir at 10,000 years for the same simulation as in Fig. IV-32. The waste has migrated about 5 kilometers from the well.

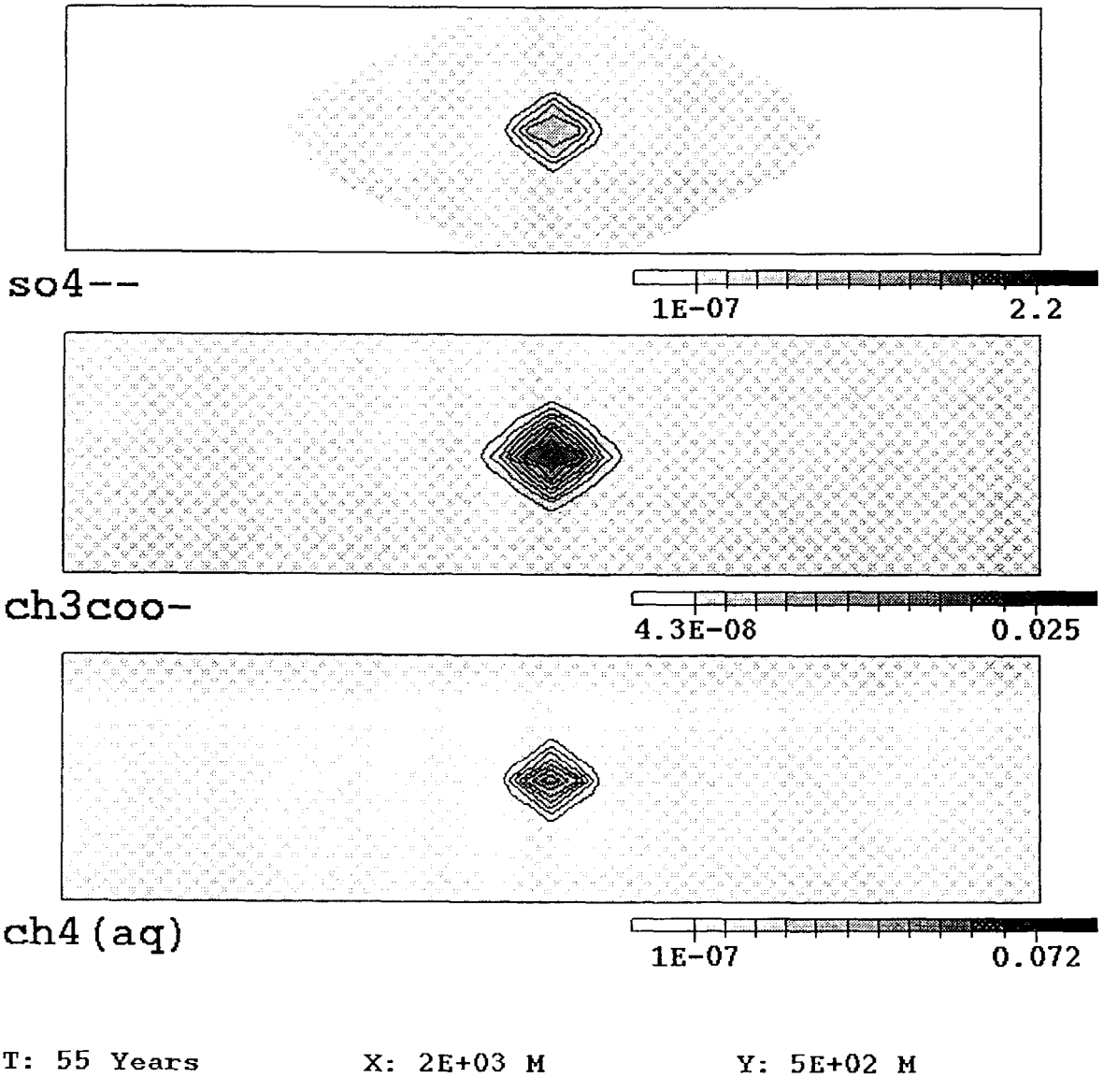

Fig. IV-37 Distribution of SO_4^{--}, $CHCOO^-$, and CH_4 concentrations in the sandstone reservoir at 55 years (53 years after the 2 year injection period). The generation of methane from acetic acid is noted.

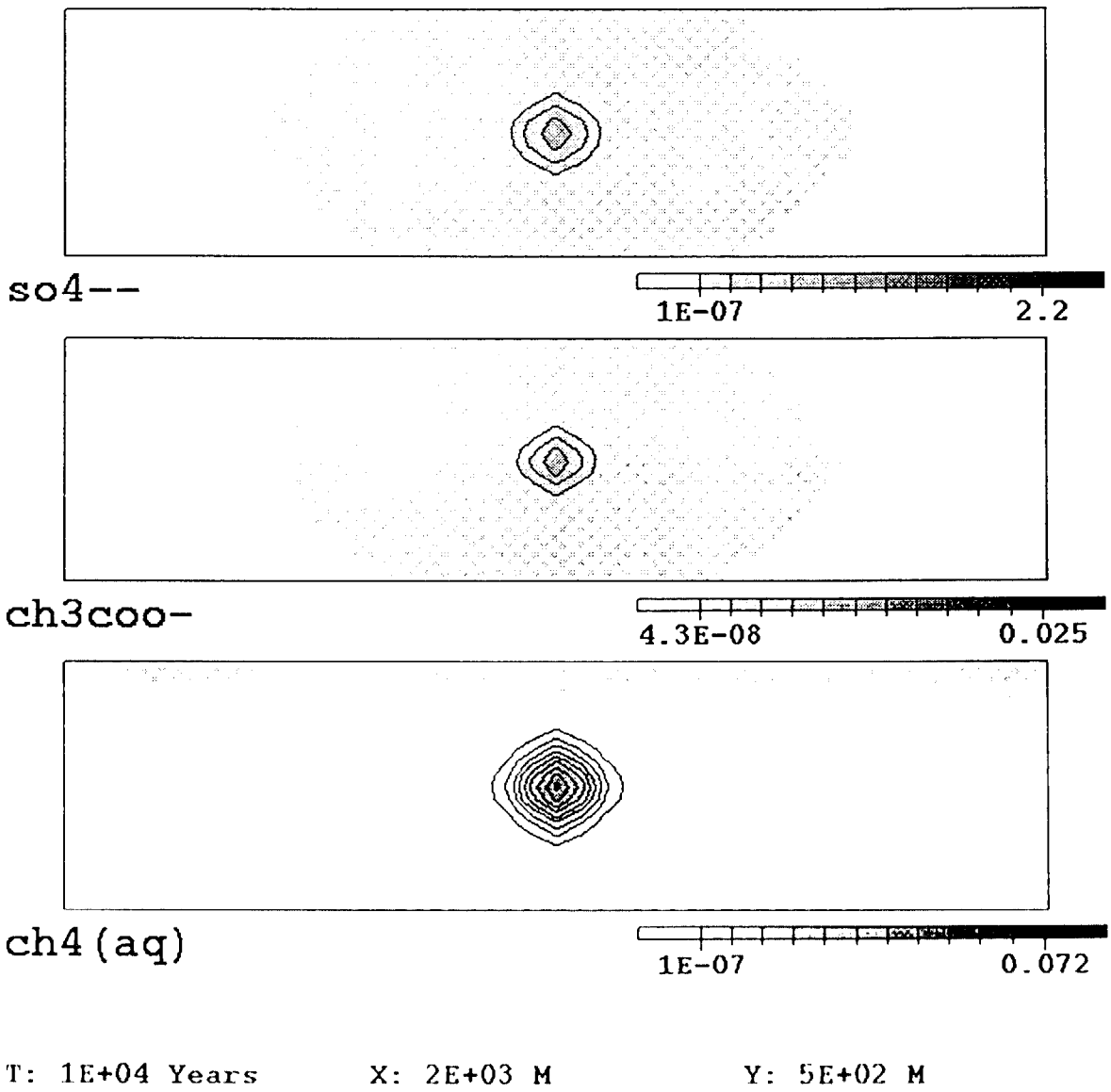

Fig. IV-38 Distribution of SO_4^{--}, $CHCOO^-$, and CH_4 concentrations in the sandstone reservoir at 10,000 years. Note that at this time most acetic acid has been converted to methane.

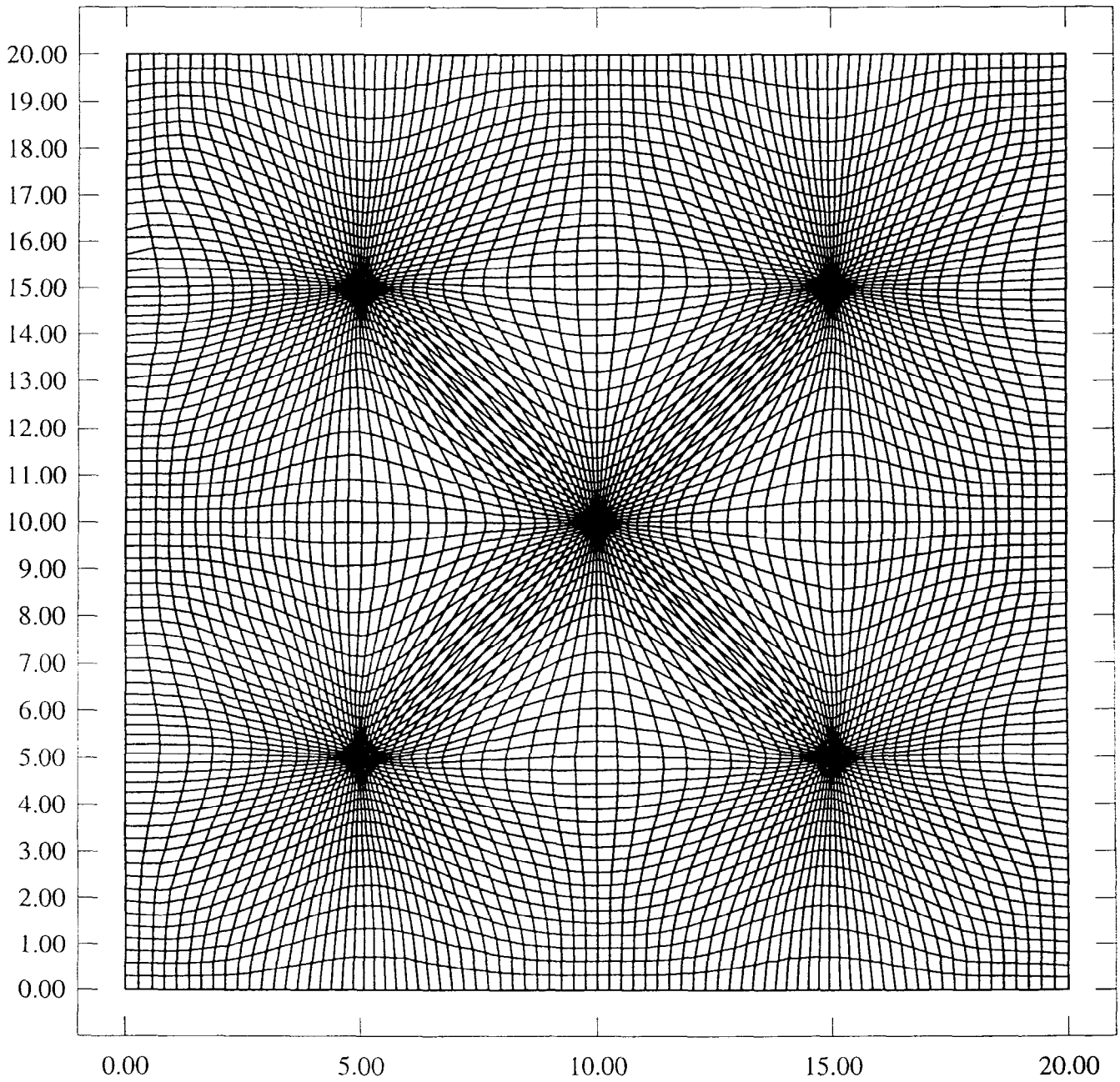

Fig. IV-39 Grid structure adapted for a five-spot injection/production scenario.

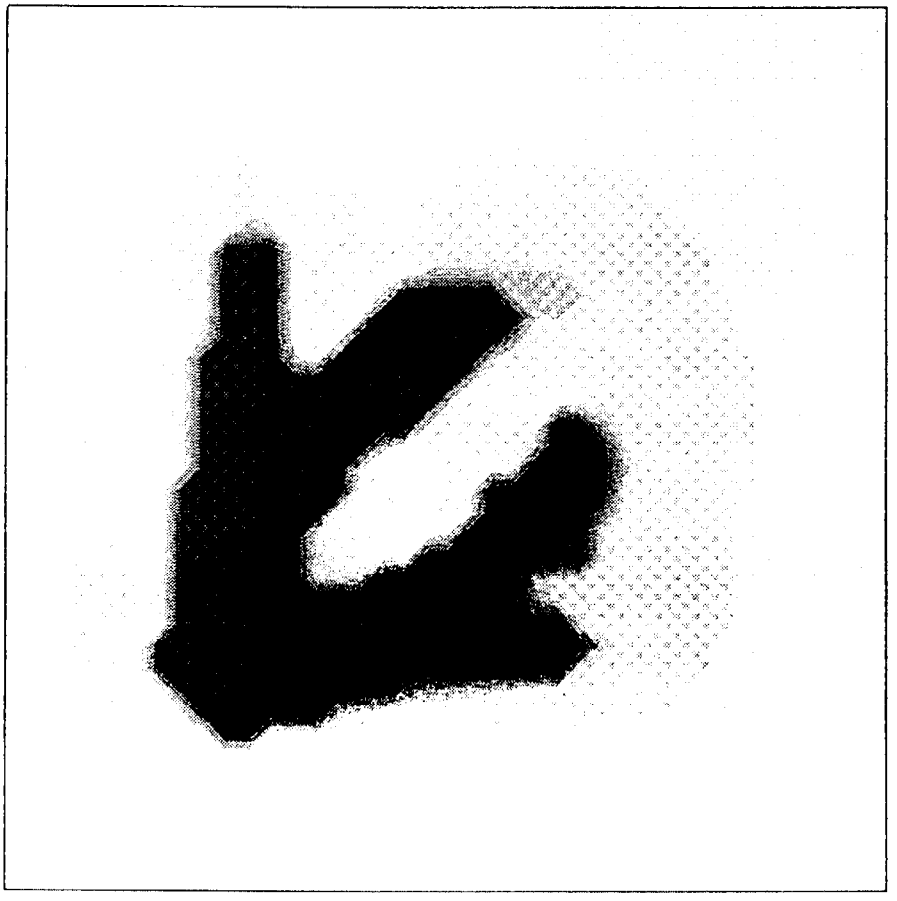

Fig. IV-40 Reservoir scale dissolution finger resulting from the injection of HCl waste (0.1 moles/liter) into a tight calcite cemented sandstone reservoir.

V
Underpressured Compartments

A. Concept

One possibility for hazardous waste disposal, as yet not fully investigated, is the intriguing idea of using naturally underpressured compartments (see Fig. V-1). Such compartments are found in sedimentary basins throughout the world. Examples are cited in the literature (Dickey and Cox, 1977; Powley, 1980, 1990; Bradley, 1975, Bradley and Powley, 1994).

Compartments are of great current interest due to their implications for petroleum and portable water reserves (Powley, 1990; Ortoleva et al., 1994; Ortoleva, 1994a,b; 1996). Compartments are domains of rock of preserved porosity/permeability surrounded by a three dimensionally closed shell of very low permeability (seal) rock. As these features have preserved abnormal pressures on the 10-100 million year time scale, their seal permeability can be nanodarcy or lower. In this way they provide a very attractive possibility for secure waste disposal.

Underpressured compartments have the following desirable repository characteristics:

- the seals that bound the compartments have existed over long periods of geologic time and likely have some capacity to heal themselves, making them stable to tectonic disturbances;
- compartments typically exist below 2.5 kilometers, far from the accessible environment;
- because of the underpressure, even improperly cemented injection wells or unidentified abandoned wells will not provide avenues of fluid escape to overlying normally pressured strata;
- if a seal is breached, loss of waste to the region outside the compartment will be eliminated or minimized due to the underpressuring;
- they may be monitored periodically to assess changes in pressure, fluid content, and other parameters permitting evaluation of predictive models and even modification of them as accumulated data might suggest;
- it may be possible to design the chemistry of the injected waste fluid such that upon interaction with the minerals of the compartment interior their toxicity is reduced. In addition, mineralization may result which incorporates selected species (namely those containing radioactive elements or toxic materials) from the waste fluid;
- waste and reservoir chemistry could be matched so as to improve seal or reservoir characteristics;
- the widespread geographical distribution of underpressured compartments is likely to minimize the need for long distance hazardous waste transportation; and
- many underpressured compartments have already been well characterized by the petroleum industry.

The key to the use of underpressured compartments is to design strategies that sustain their favorable characteristics during and after the waste injection operation period.

Seals and the cements that usually account for their low permeability can be of a variety of mineralogies including clays, silica, carbonates, salts and anhydrite. They often consist of multiple minerals and typically are a few hundred meters thick. The seals often have a sub-meter scale internal structure in the form of a layered distribution of diagenetic cements. They may arise in most common sedimentary rocks, including sandstones, limestones, and shales (Dewer and Ortoleva, 1988; Ortoleva et al., 1995; Al-Shaieb et al., 1989; Tigert and Al-Shaieb, 1990; Shepherd et al., 1994; Ortoleva, 1996). This suggests that one could take advantage of this spectrum of mineral chemistries in selecting ideal compartments for a given class of waste chemistry.

Several properties of seals that have been observed in the Anadarko Basin suggest that mechanics and its coupling to chemistry are important factors in determining the characteristics of seals:

- seals typically show that a source for cements that occlude porosity and destroy permeability is pressure solution;
- seals sometimes display grain comminution apparently induced by grain dissolution and resulting loss of rock compressive strength; and
- lateral seals are often fault-associated (Bradley, 1975; Powley, 1980; Al-Shaieb et al., 1989; Logan, 1989; Ortoleva, 1996).

With this, repository analysis must involve an accounting of mechanical as well as chemical considerations.

B. Examples of Underpressured Compartments

1. The Anadarko Basin

The Anadarko Basin is rich with underpressured compartments in a number of regions. The northern shelf of the Anadarko Basin is one of these regions (Figs. V-2,3).

This shelf contains a thick stratigraphic section of rocks that were uplifted and eroded following the Laramide Orogeny. The northern shelf regionally underpressured compartment complex extends from the Permian to the basement in the Keyes field area (Figs. V-2,3). Within the underpressured complex are several stratigraphic intervals that seem to be potentially suitable for waste disposal. One of the more promising underpressured compartments within this complex is the Morrowan Keyes sandstone reservoir. This compartment is confined laterally and vertically by higher pressured intervals and sealed lithologically by overlying and lateral shale facies. Underlying the Keyes sandstone is another seal that separates the compartment form the Arbuckle horizon. The Keyes compartment is accurately delineated, sufficiently deep, adequately underpressured, and well sealed to make it potentially suitable for waste disposal.

Additional underpressured compartments that may be studied are associated with the Permian and Pennsylvanian carbonate reservoirs of the giant Hugoton field. The underpressured Hugoton gas field in Kansas, Oklahoma, and Texas (Mason, 1968), accurately characterized by wells patterned on a one mile grid, is estimated to span 5.5 million acres. The Permian Wolfcampian formation, which provides the gas production, is composed of limestones, dolostones and shales. It is estimated that each well has a storage capacity of up to $2x10^6$ barrels (see Sect. E below). Thus, the potential capacity for storage is impressive. Further promising underpressured compartments are found in the Pennsylvanian Missourian, Desmoinesian, and Upper Morrowan stratigraphic intervals.

2. Worldwide Underpressuring

Many uplifted, eroded and cooled basins worldwide contain underpressured compartments. A typical U.S. Rocky Mountain underpressured basin profile is shown in Fig. V-4. Underpressuring in the Alberta Basin (Fig. V-5) is believed to be compartment related. Apparently there are many other examples of underpressured compartments worldwide.

C. Estimation of Waste Storage Capacity

The holding capacity Γ of an underpressured compartment is defined here to be the number of moles of injectates that may be imposed such that compartment interior pressure balances with that of the compartment surroundings. The computation of Γ is a complex issue due to a number of factors, including the following:

- the identity and composition of all fluid phases resulting from the injection;
- possible precipitation, dissolution or changes of phases arising from injectate/mineral reactions;
- over- or underpressuring effects arising from injectate-matrix reactions leading to porosity changes; and
- heating/cooling due to heats of induced reactions or differences in temperature between the injectate and the formation.

Thus accurate estimates of holding capacity requires the use of a coupled reaction-transport-mechanical model as described in Chapter II and Section E below.

In simple cases, however, one can make a rough estimate of Γ. Consider the injection of an aqueous waste-bearing solution into a compartment of relatively limited vertical extent (so that intra-compartment gravity effects can be neglected). Let us assume that the equation of state (and in particular the p,T-dependence of volume) of the formation water and the injectates are the same; i.e., $\bar{V}_l(p,T)$ is the volume of the aqueous solution per mole of H_2O (other components assumed to be dilute). Furthermore, let the molar volume of a gas that is assumed to be insoluble in an aqueous solution be denoted $\bar{V}_g(p,T)$.

Let V be the compartment interior volume and ϕ its porosity, and n_l be the number of moles of liquid and similarly for n_g. With this

$$n_l \bar{V}_l(p,T) + n_g \bar{V}_g(p,T) = \phi V \qquad (V.1)$$

In the simplest approach, one may take ϕ, V, and $\overline{V}_\ell$ to be constant and $\overline{V}_g$ to be given by the ideal gas law $\left(\overline{V}_g = \mathcal{R}T/p\right)$. Thus

$$n_\ell \overline{V}_\ell + n_g \frac{\mathcal{R}T}{p} = \phi V. \tag{V.2}$$

Assume that the temperature remains at its original value T_O while the pressure p increases from its original value p_O. Because ϕV remains constant, as does the amount of gas (n_g^o), one has

$$\left(n_\ell - n_\ell^o\right)\overline{V}_\ell = n_g^o \mathcal{R}T\left(\frac{1}{p_o} - \frac{1}{p}\right). \tag{V.3}$$

The holding capacity Γ is the value of $n_\ell - n_\ell^o$ for which p is equal to the pressure p_S of the surrounding formations. Thus

$$\Gamma = \frac{n_g^o \mathcal{R}T}{\overline{V}_\ell}\left(\frac{1}{p_o} - \frac{1}{p_s}\right). \tag{V.4}$$

As the compartment was originally underpressured and if the surroundings are normally pressured then $p_S > p_O$; hence $\Gamma > 0$.

The above result can be recast in more familiar engineering quantities. Let s_g and s_ℓ ($s_g + s_\ell = 1$) be the gas and liquid saturations. Then from the ideal gas law

$$p_o = \frac{n_g^o RT}{\phi V s_g^o} \tag{V.5}$$

while

$$s_\ell^o = \frac{n_\ell^o \overline{V}_\ell}{\phi V}. \tag{V.6}$$

Furthermore, let A be the horizontal compartment area and h its interior height, so that $V = hA$. With this, (XVI.C4) becomes

$$\gamma \equiv \frac{\Gamma}{A} = \frac{\phi h s_g^o}{\overline{V}_\ell}\left(1 - \frac{p_o}{p_s}\right) \tag{V.7}$$

where γ is the holding capacity per mapview compartment area.

Using a similar analysis, Bradley (1985) showed that the Hugoton gas field storage capacity is on the order of 10^4 barrels/acre.

D. Integrated Repository Analysis

A key element of waste repository management in the present context is a predictive model for the evaluation of a given underpressured compartment as a hazardous waste repository. To do so requires the integration of remote, downhole, , petrologic, experimental and modeling studies to arrive at an integrated evaluation strategy. This can be accomplished through the following steps:

- seizmic or other remote characterization of the geometry of the compartment;
- well log, core and field studies of reservoir mineralogy and texture;
- carry out rock mechanics and geochemical experiments on core samples from the site to determine key parameters in the model for materials in their natural and waste-saturated states;
- simulate the time course of the compartment/waste system for various injection scenarios involving the waste of interest; and
- use the modeling results to assess feasibility and suggest specific strategies that will yield the most successful waste implacement.

Criteria for success are to be cast in terms of waste capacity and the longevity of the waste-laden compartment interior and its surrounding seal.

E. Numerical Simulation of Waste Injection

CIRF.A was used in this study to demonstrate waste injection in a compartment. Issues addressed were the comparison of the dynamics of the surrounding seal and its potential breaching for cases of normal and subnormal initial pressures. Results obtained are summarized in the following.

Consider an elliptic-shaped sandstone reservoir surrounded by a calcite-cemented seal. The reservoir consisted of 80% quartz (by volume) and 1% clay (by volume) with the initial porosity and permeability of 0.19 and 0.129 darcy, respectively. The seal consisted of 80% quartz (by volume), 10% clay (by volume) and 9% calcite (by volume) with the initial porosity and permeability of 0.01 and 9.7×10^{-8} darcy, respectively. As no seal is ever perfectly uniform, we further introduce on the right side of the seal a leaky region with a lower clay content. The initial porosity and permeability in this leaky region were 0.05 and 6.0×10^{-6} darcy, respectively. Grain sizes for quartz, clay and calcite are 0.1 millimeter, 50 micrometer and 50 micrometer, respectively. The size of the domain of interest is 3,000 meters by 500 meters with a thickness of 15 meters in the direction normal to the images shown in figures to follow. A total compressibility of 4.0×10^{-5} psi^{-1} was used for the rock and fluid in the system. A waste fluid containing 1.0 moles/liter HCl was injected at 500 barrels/day into a well located in the center of the reservoir for 5 years. No flux boundary conditions at the top and bottom and constant pressure boundary conditions at the left and right were specified. The resulting evolution was then simulated using CIRF.A.

The first example simulated the injection of the acid waste into an initially normally pressured reservoir. At 55 years (50 years after the end of injection), the acid plume, calcite and permeability distributions are seen in Fig. V-6. After 5,000 years, the injected acid waste is gradually attracted to the slightly leaky region of the seal at the right as seen in Fig. V-7. The migration of the waste toward the right resulted from the injection-induced over-pressure in the reservoir. In Fig. V-8, the waste escaping through the leaky region is seen to have dissolved calcite and increase rock porosity and permeability there. The increase in permeability accelerates the waste escape. After 10,000 years, the waste has almost completely escaped out of the reservoir and a region of high porosity and permeability has developed at the originally higher permeability zone on the right. This is illustrated in Fig. V-9.

In contrast, the second example simulated the injection of the acid waste into a reservoir which was similar except that it was initially underpressured. Figs. V-10, 11 and 12 present the spatial distributions of the acid concentration, calcite content and rock permeability at 55 years, 5,000 years and 10,000 years, respectively. The waste fluid did not escape through the leaky zone to the normally pressured exterior as the compartment was originally underpressured; hence injection-induced overpressuring was minimized.

As discussed in Section C, the holding capacity of an underpressured compartment can be roughly determined by the compartment pore volume, pressure increase due to waste injection, and the total compressibility of the rock and fluids in the compartment. The total compressibility we used for the simulations here was higher than the normal one for formation brines and sedimentary rocks. However, the value of the selected total compressibility would be justified if the compartment contained natural gas occupying a few percent of its pore volume. If the total compressibility was reduced by one order of magnitude, the compartment pressure would increase too much for both the normally pressured and underpressured compartments due to the high waste injection rate and limited compartment size used in the current study.

Consider a similar geological setting without an initial leaky region in the seal. Take the reservoir to be normally pressured initially. Instead of placing a well in the center of the reservoir, it was located near the right boundary in the reservoir. In this way the question of the advantage of best well location could be evaluated. The effect of injection of the same amount of waste for a similar time as in the previous examples was then analyzed. Since the well is so close to the seal, the acid starts to dissolve calcite in the seal soon after injection begins. The scenario after 100 years is seen in Fig. V-13. At 150 years of simulation, a dissolution channel starts to form and the waste begins to escape. This is shown in Fig. V-14. Twenty years later (170 years of simulation), the state of the system is as in Fig. V-15. The waste fluid has almost completely escaped out of the reservoir.

In the above simulations the dissolution of calcite from the seal could decrease rock strength. This would occur if the calcite was, due to textual geometry, stress supporting. Thus for appreciable dissolution of calcite-rich rocks the compartment interior could experience matrix grain comminution. The challenge is to predict if the resulting modified, failed rock simply lost permeability (and thereby locked in the waste) or as a result of the induced stress field, fractures extended through the seal and allowed waste to escape. To address this question, one must account for the fact that in an underpressured compartment, fluid pressure is lower and hence effective stress is higher in magnitude. Thus, the matrix already bears a heavier load relative to that for a normally pressured compartment. In the latter the fluid bears a larger share of the overburden and hence guards somewhat against formation collapse.

The analysis of waste injection into a compartment is seen to be subtle. In the above example the acidity was reduced due to calcite dissolution in the seal. However, this could cause formation collapse which could have benefits of locking-in waste but also could cause seal breaching and waste escape from the compartment. Collapse can be a key issue as the reservoirs of interest here are already underpressured. In conclusion, underpressured compartments can be ideal for waste injection when injection strategy is managed properly.

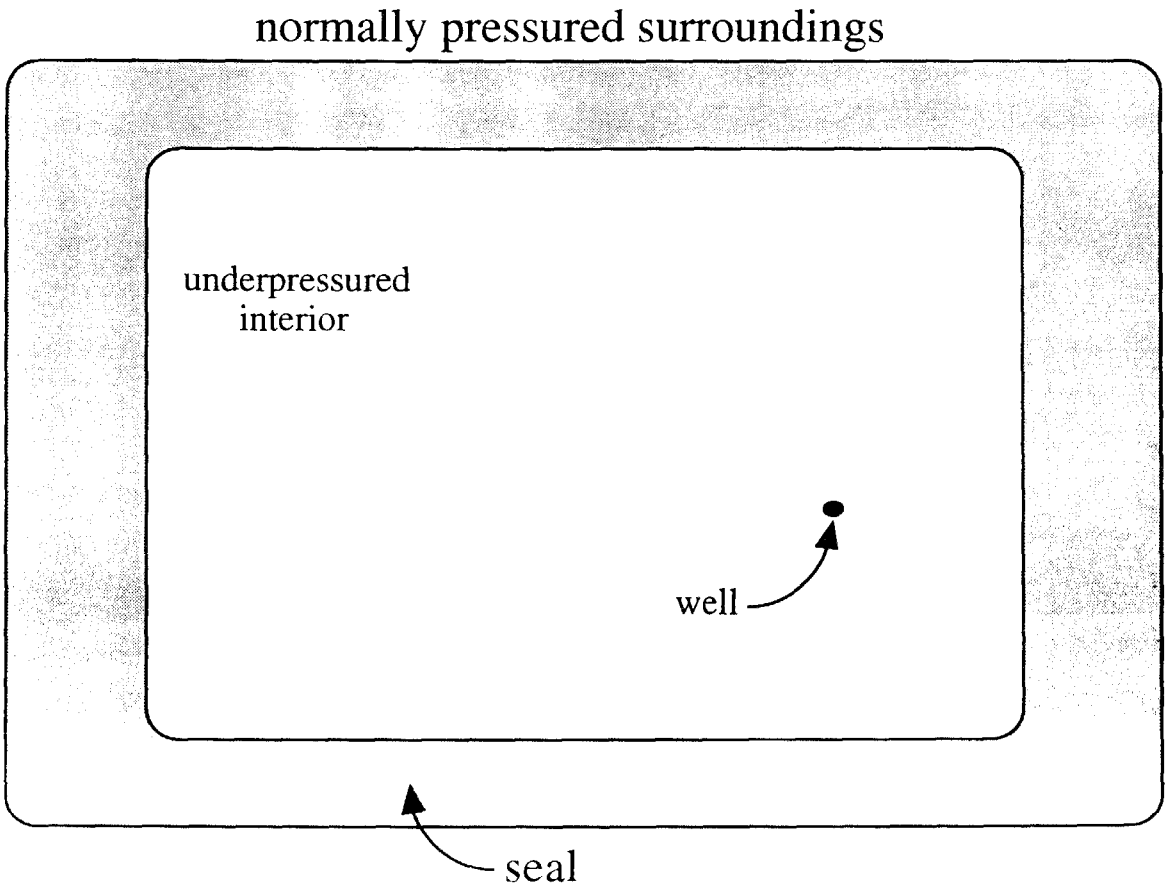

Fig. V-1 Map-view of the configuration for an idealized underpressured compartment.

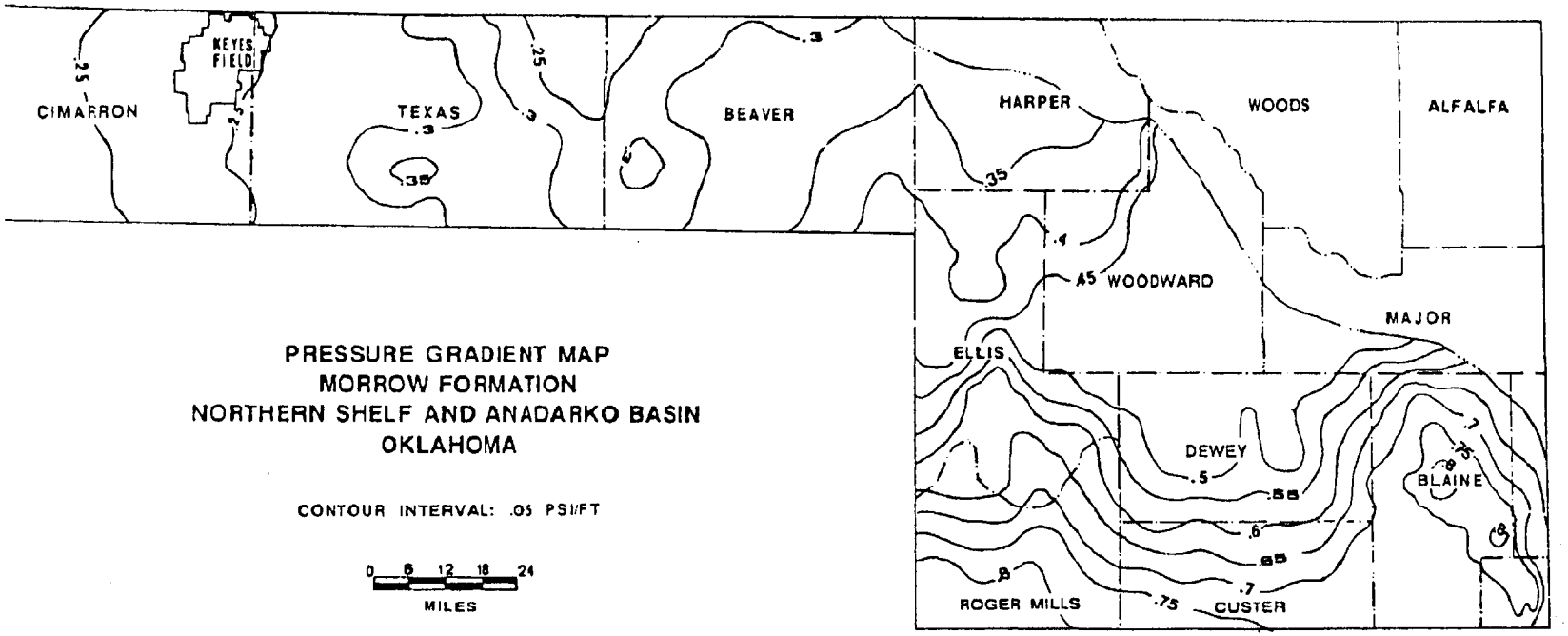

Fig. V-2 Pressure gradient countour map of the Morrow Formation within the Oklahoma part of the northern shelf of the Anadarko basin. Contours reflect change from overpressuring (>0.465 psi./ft) to normal (0.465 psi./ft) to underpressured (<0.465 psi./ft). The Keyes Field is in the area of lowest gradients (>0.25 psi./ft) (Al-Shaieb, 1995, unpublished).

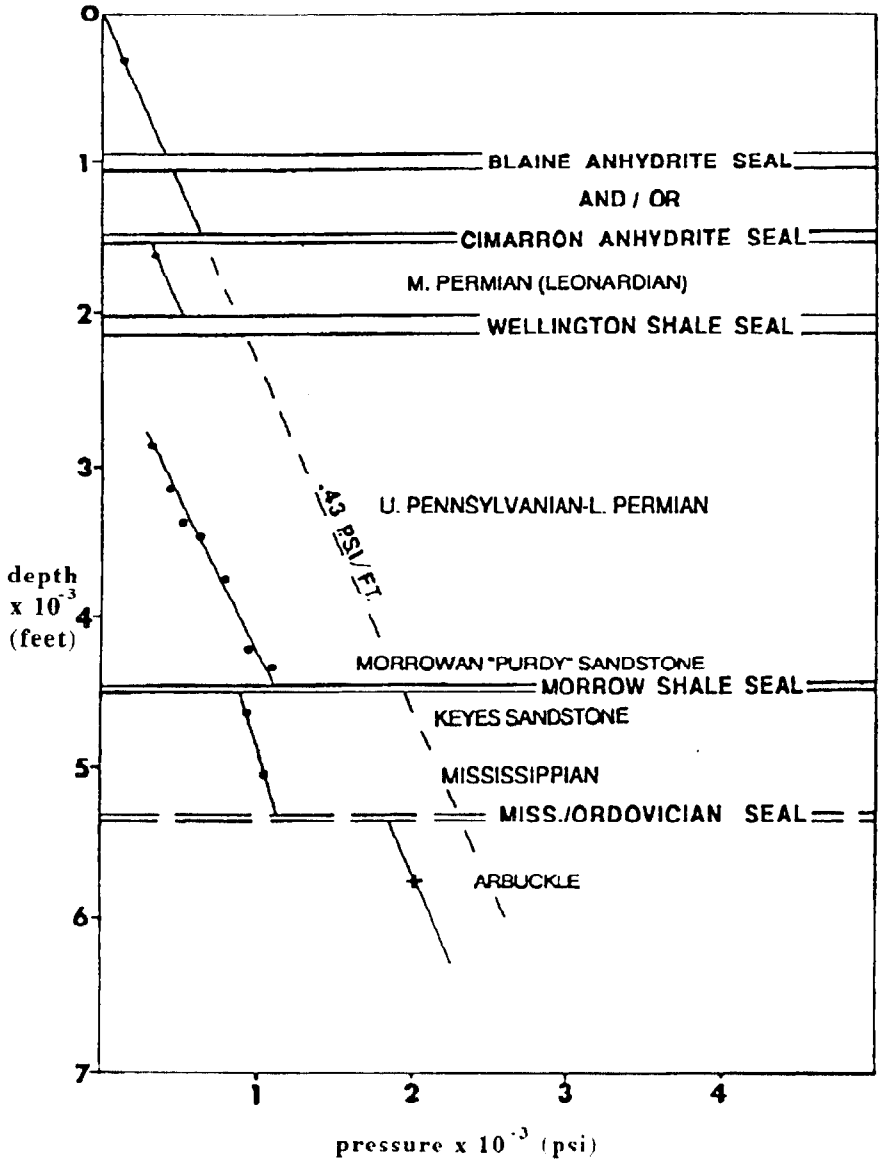

Fig. V-3 Pressure depth profile for the Keyes Field area, Cimarron and Texas Counties, Oklahoma. Profile indicates a large area of underpressuring shown by leftward deviation (lower pressure) from a fresh water gradient of 0.43 psi /ft. The Keyes Sandstone represents an isolated lower pressured compartment within the underpressured area. Pressure data indicates the existence of a number of seals defining distinct underpressured compartments in the Keyes area (Al-Shaieb, 1995, unpublished).

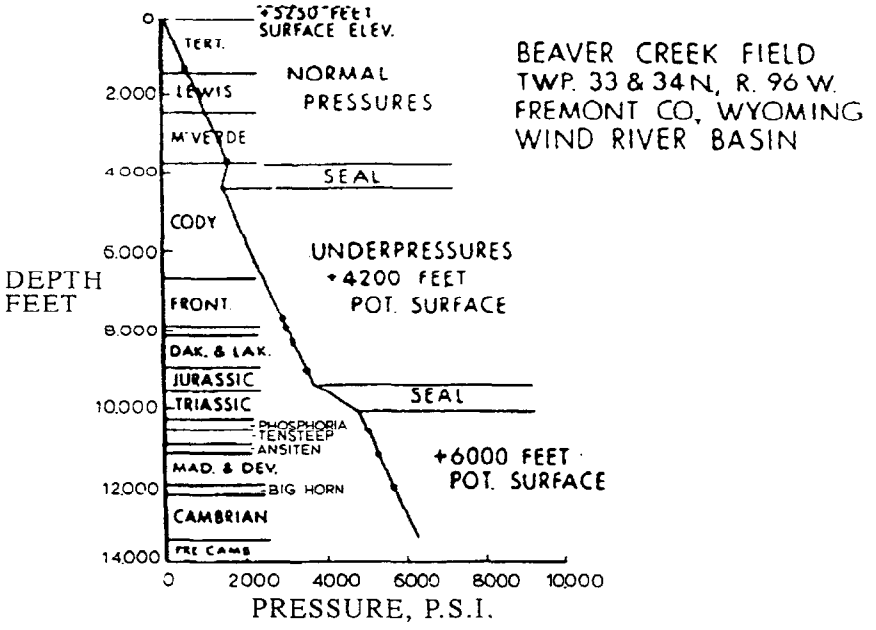

Fig. V-4 Typical pressure/depth profile in a Rocky Mountain basin (from Powley, 1990).

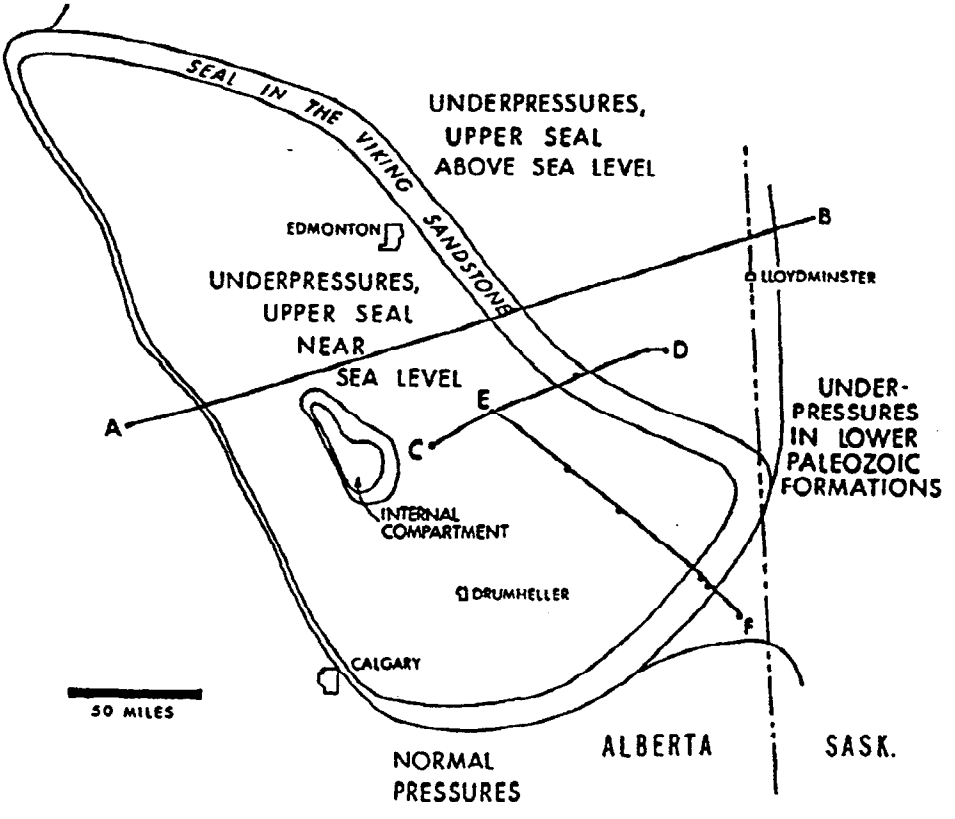

Fig. V-5 Pressure compartments — Alberta Basin (from Bradley and Powley, 1994).

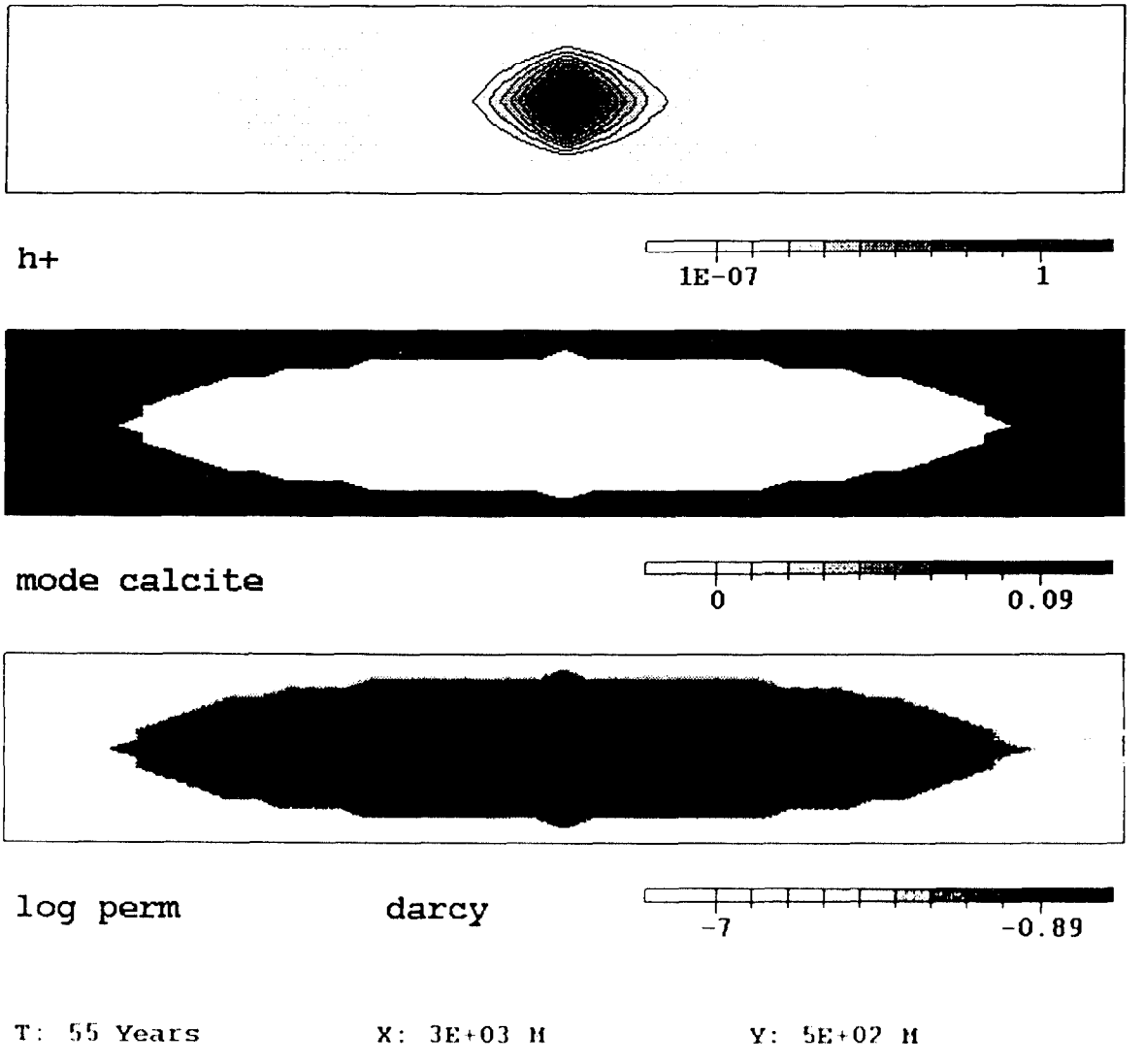

Fig. V-6 Shown here are waste acid plume, calcite content and permeability in a normally pressured compartment at 55 years (50 years after the 5 year injection period).

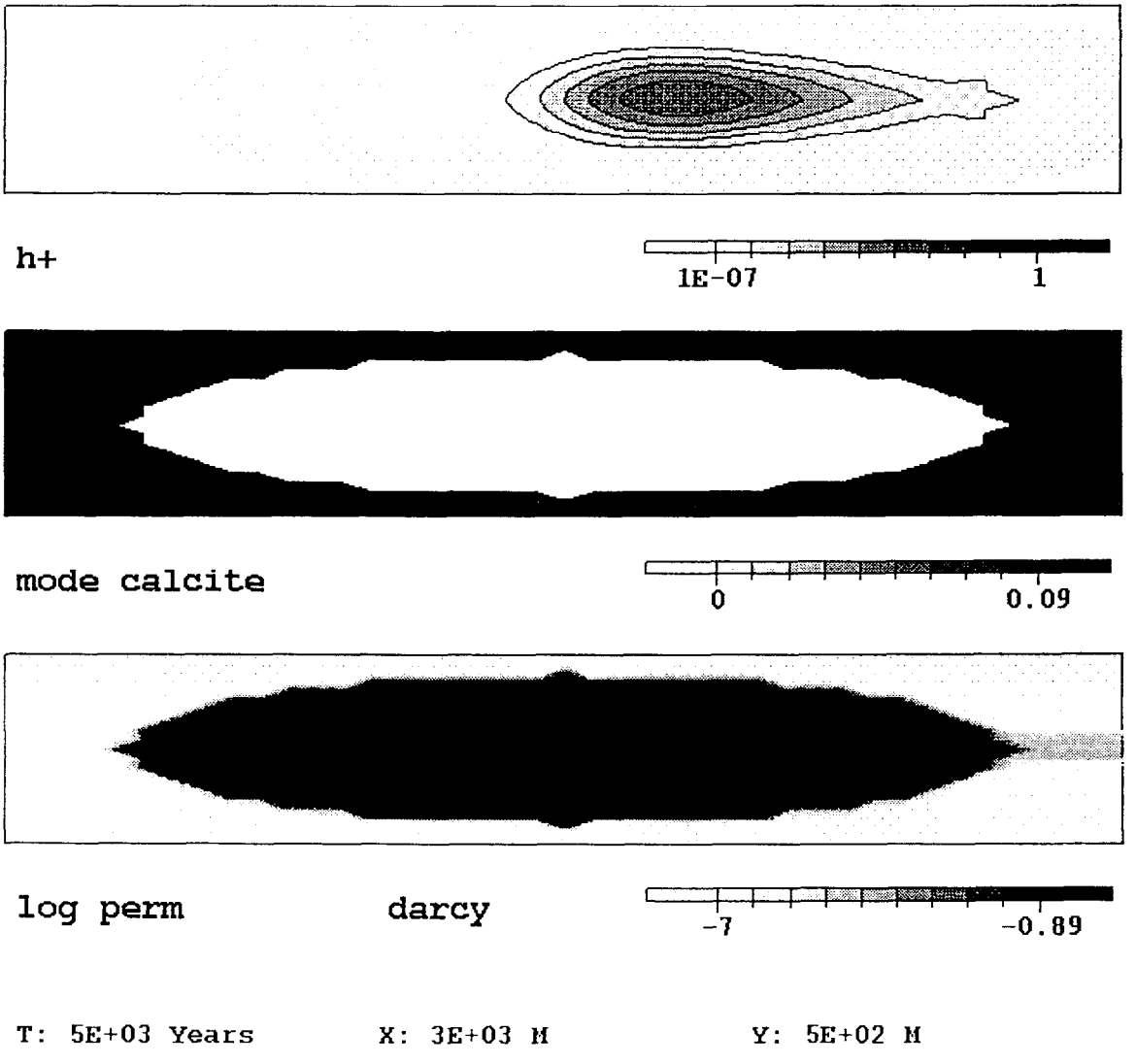

Fig. V-7 Same as in Fig. V-6 except for the simulation results at 5,000 years. Note that the waste moves toward the right.

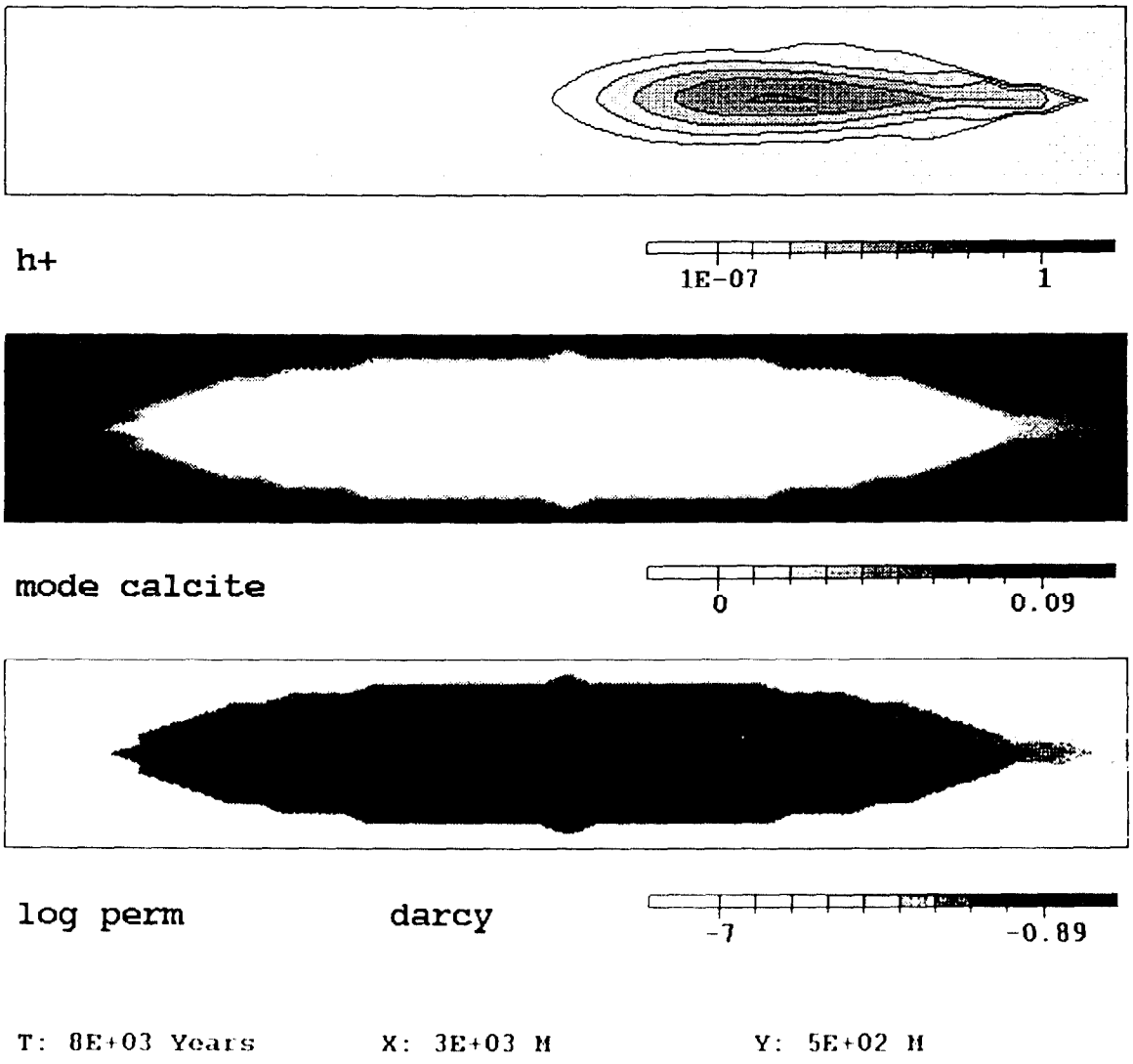

Fig. V-8 Same as in Fig. V-6 except for the simulation results at 8,000 years. At this time the waste is slowly leaking on the right.

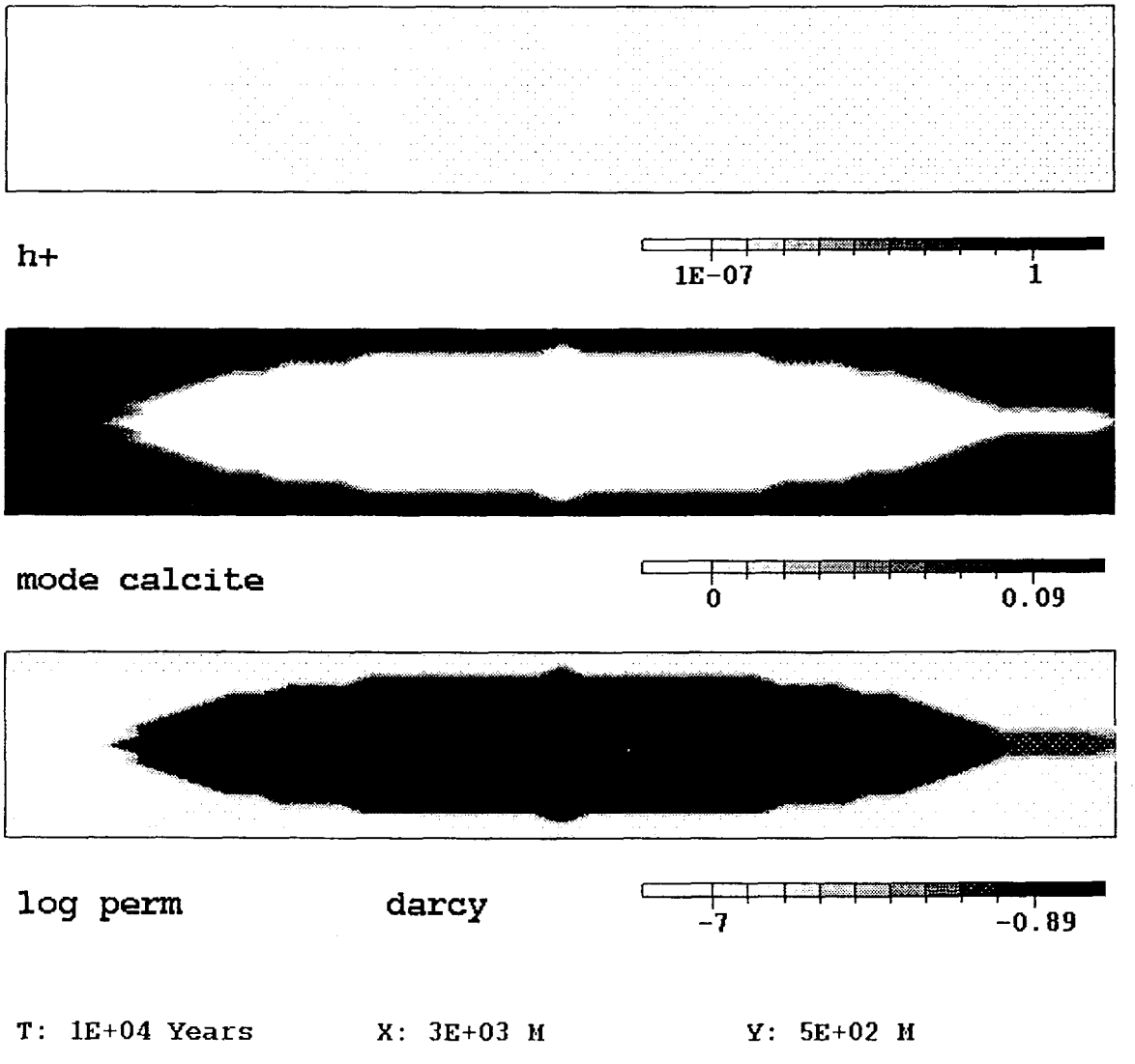

Fig. V-9 Same as in Fig. V-6 except for the simulation results at 10,000 years. At this time the waste has completely escaped due to the destruction of the seal by the acid waste.

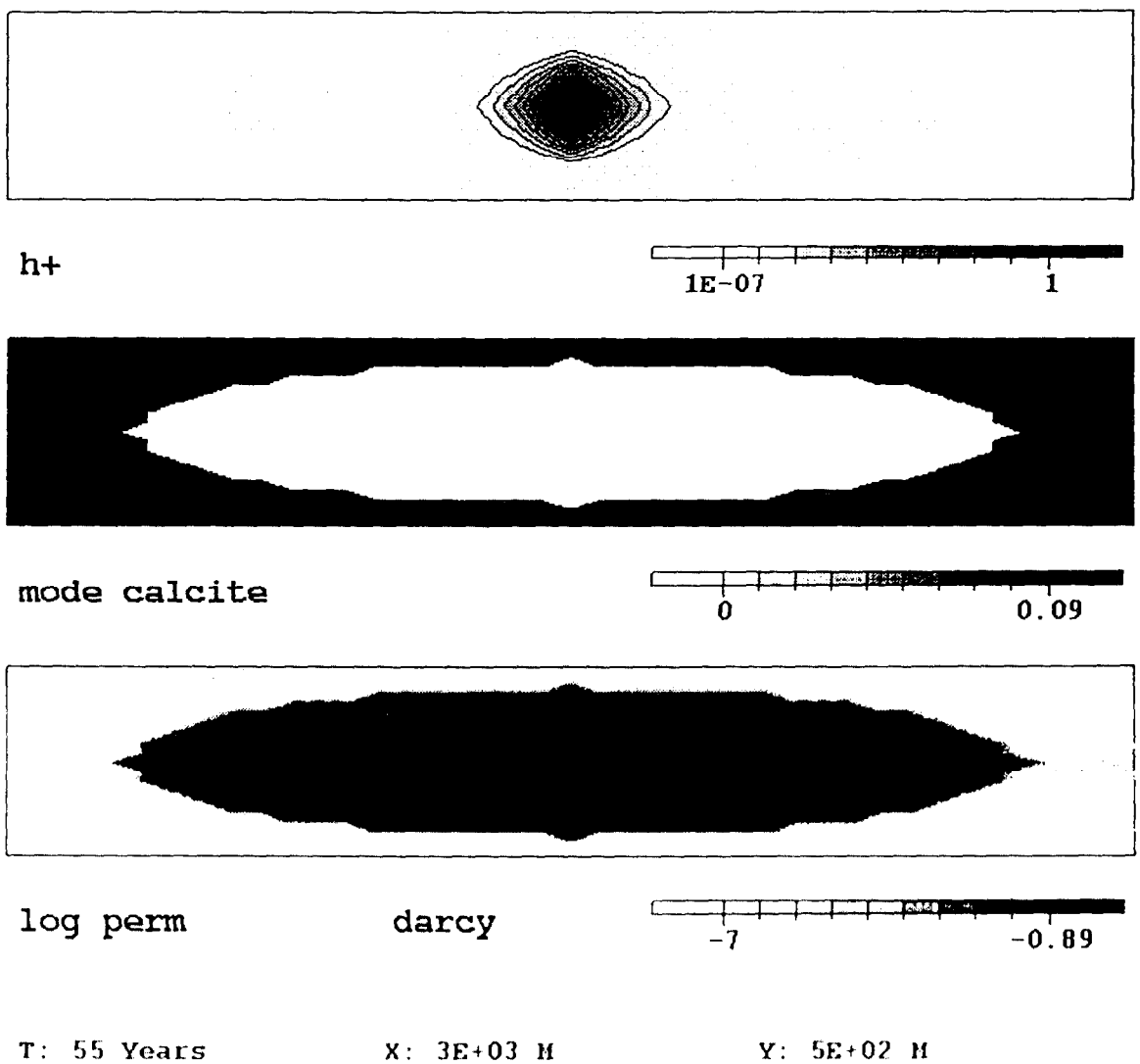

Fig. V-10 Same as in Fig. V-6 except that the initial reservoir pressure is 50% of the hydrostatic pressure for the normally pressured compartment

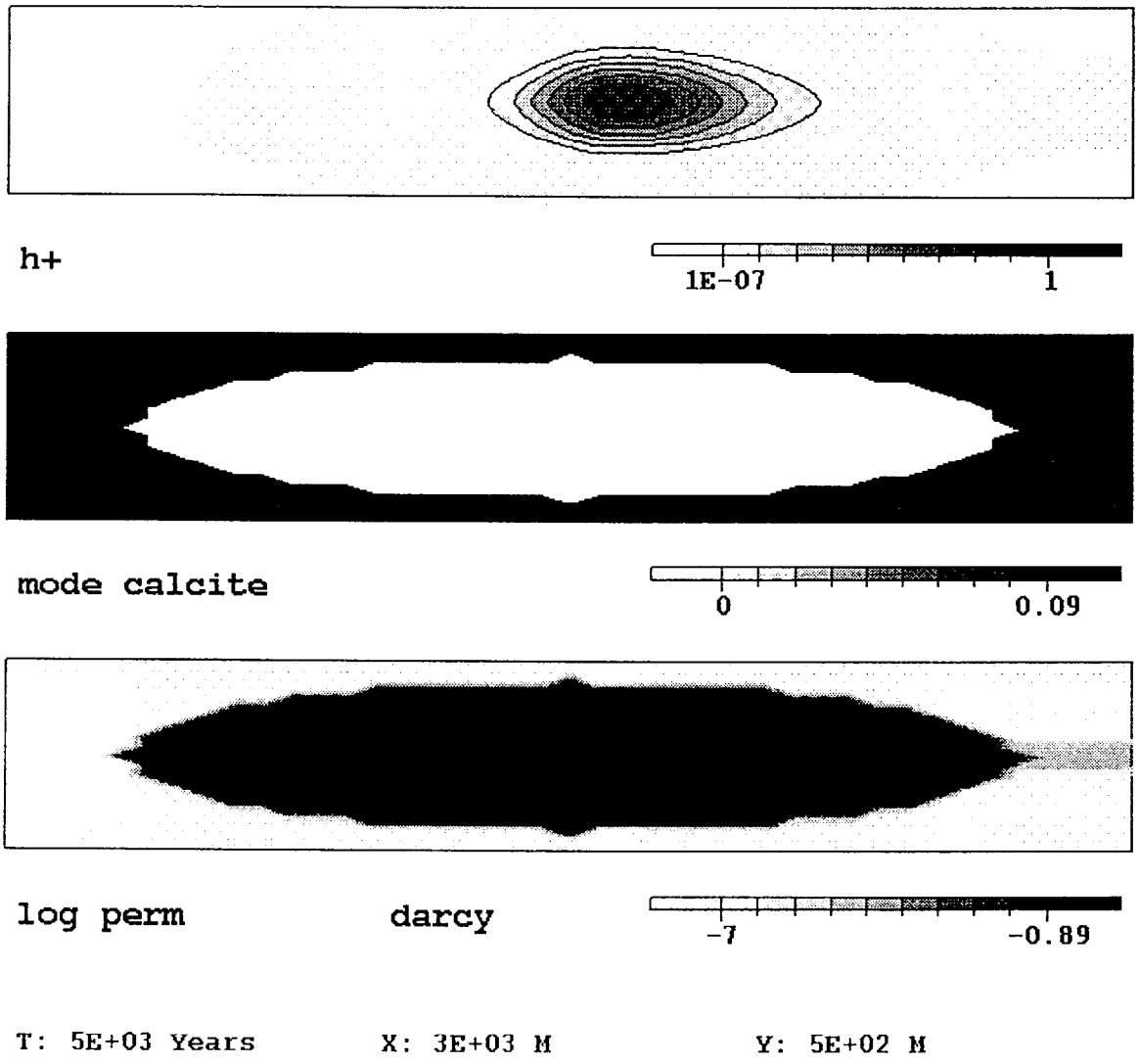

Fig. V-11 Same as in Fig. V-10 except for the simulation results at 5,000 years.

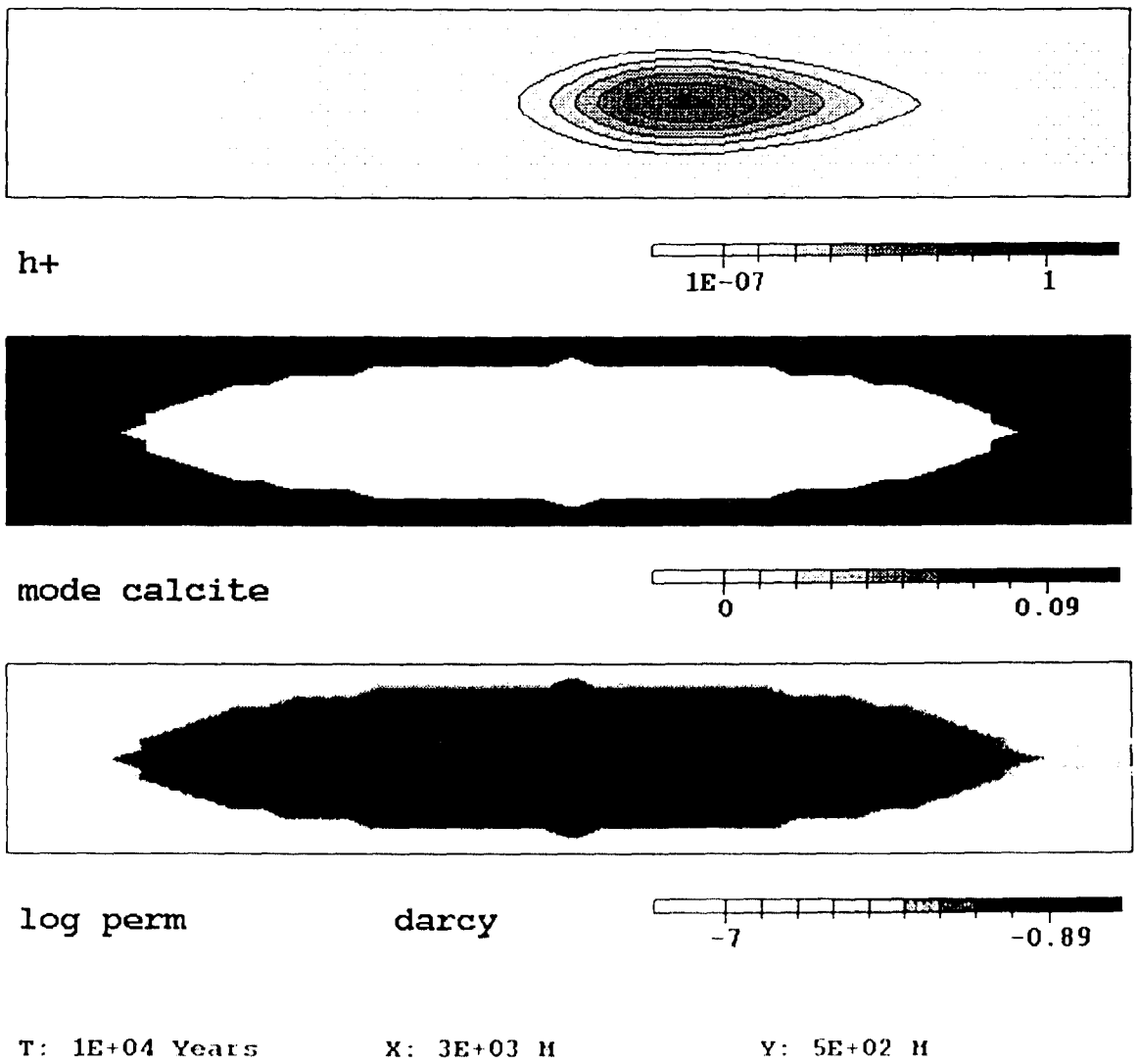

Fig. V-12 Same as in Fig. V-10 except for the simulation results at 10,000 years. Unlike for the normally pressured compartment, the waste is still contained.

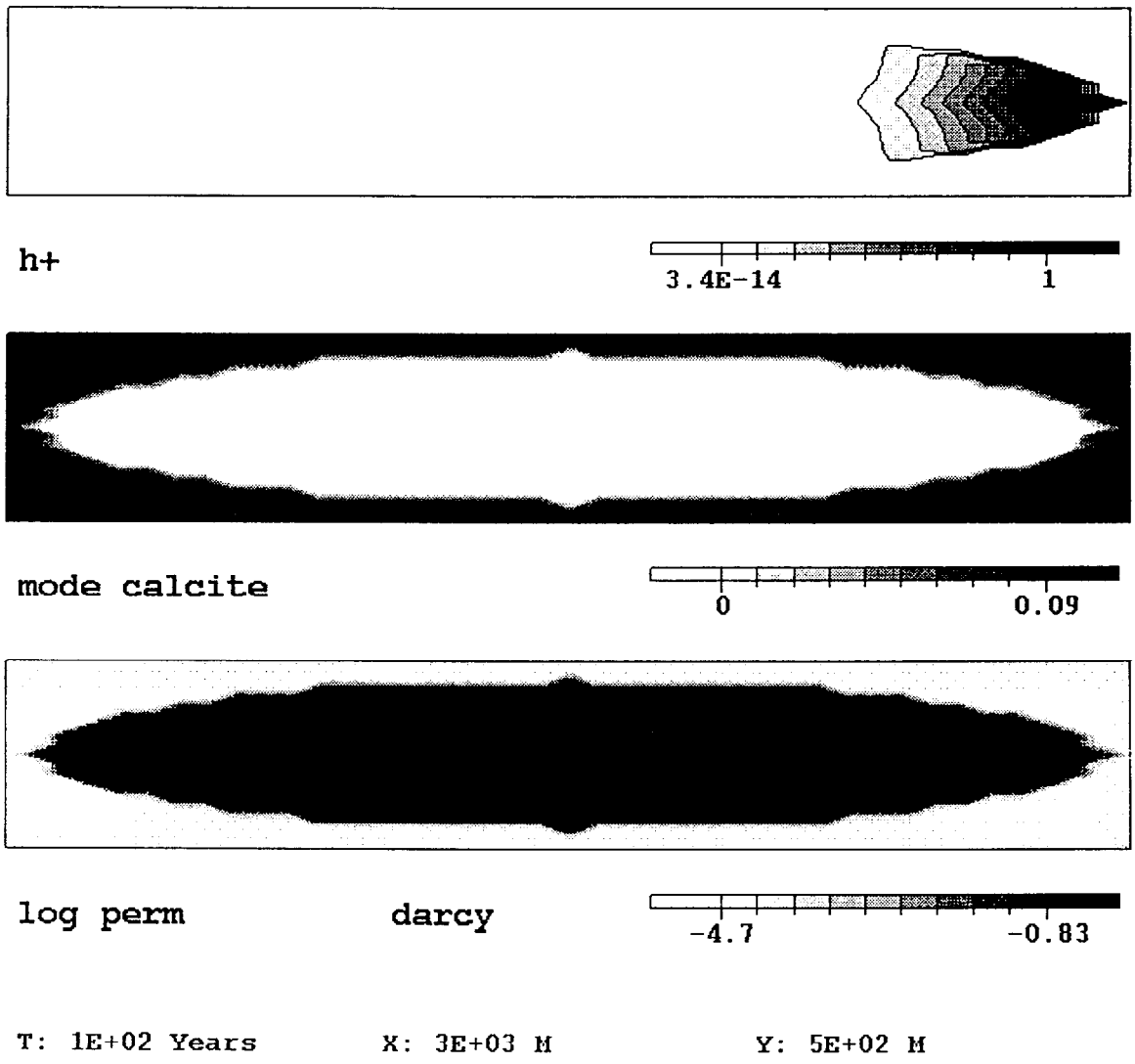

Fig. V-13 Distribution of waste acid, formation calcite and rock permeability after acid waste injection near the calcite-cemented seal in a normally compartment at 100 years (95 years after the 5 year injection period). The location of well too close to the seal has led waste escape.

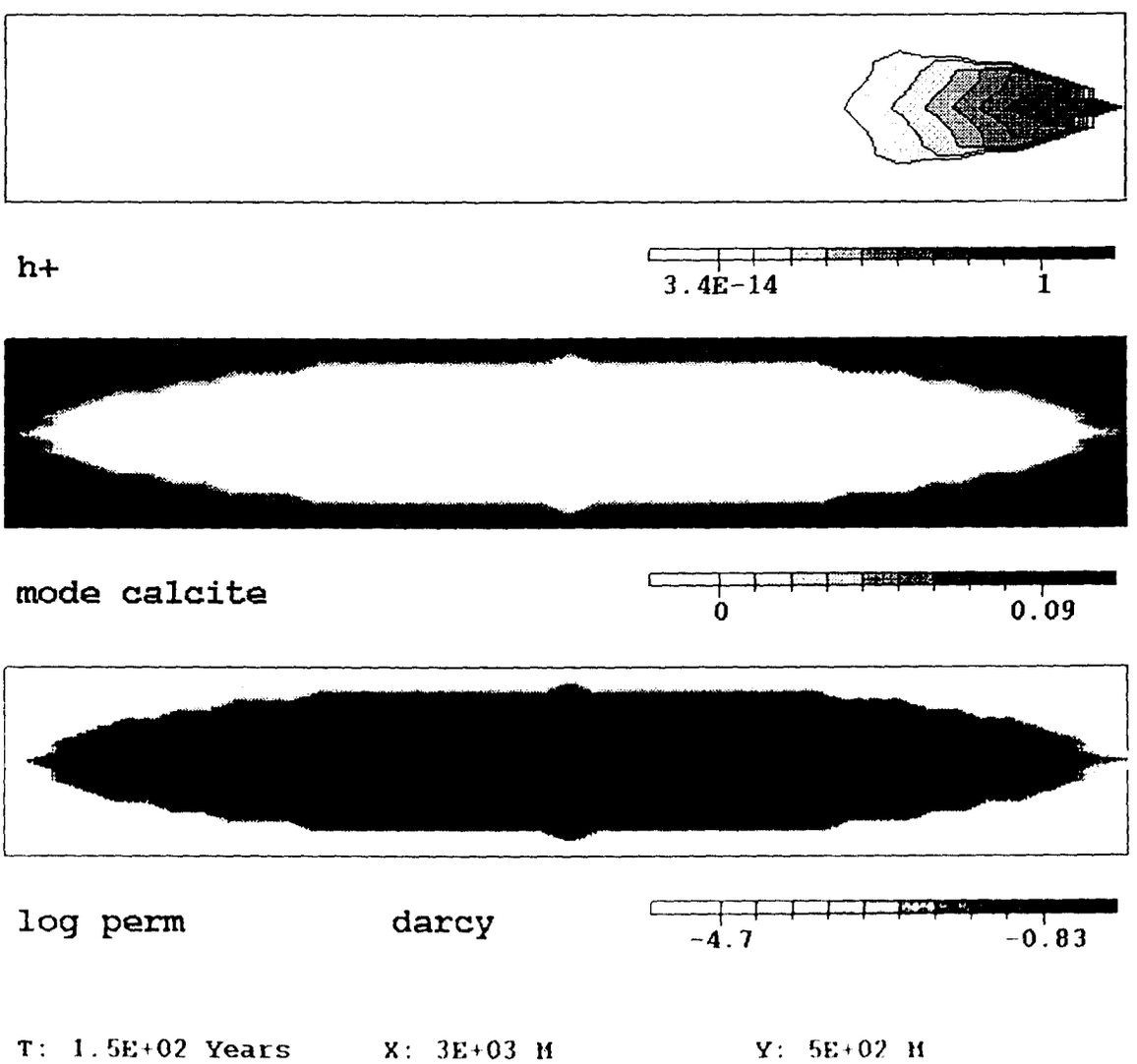

Fig. V-14 Same as in Fig. V-13 except for the simulation results at 150 years.

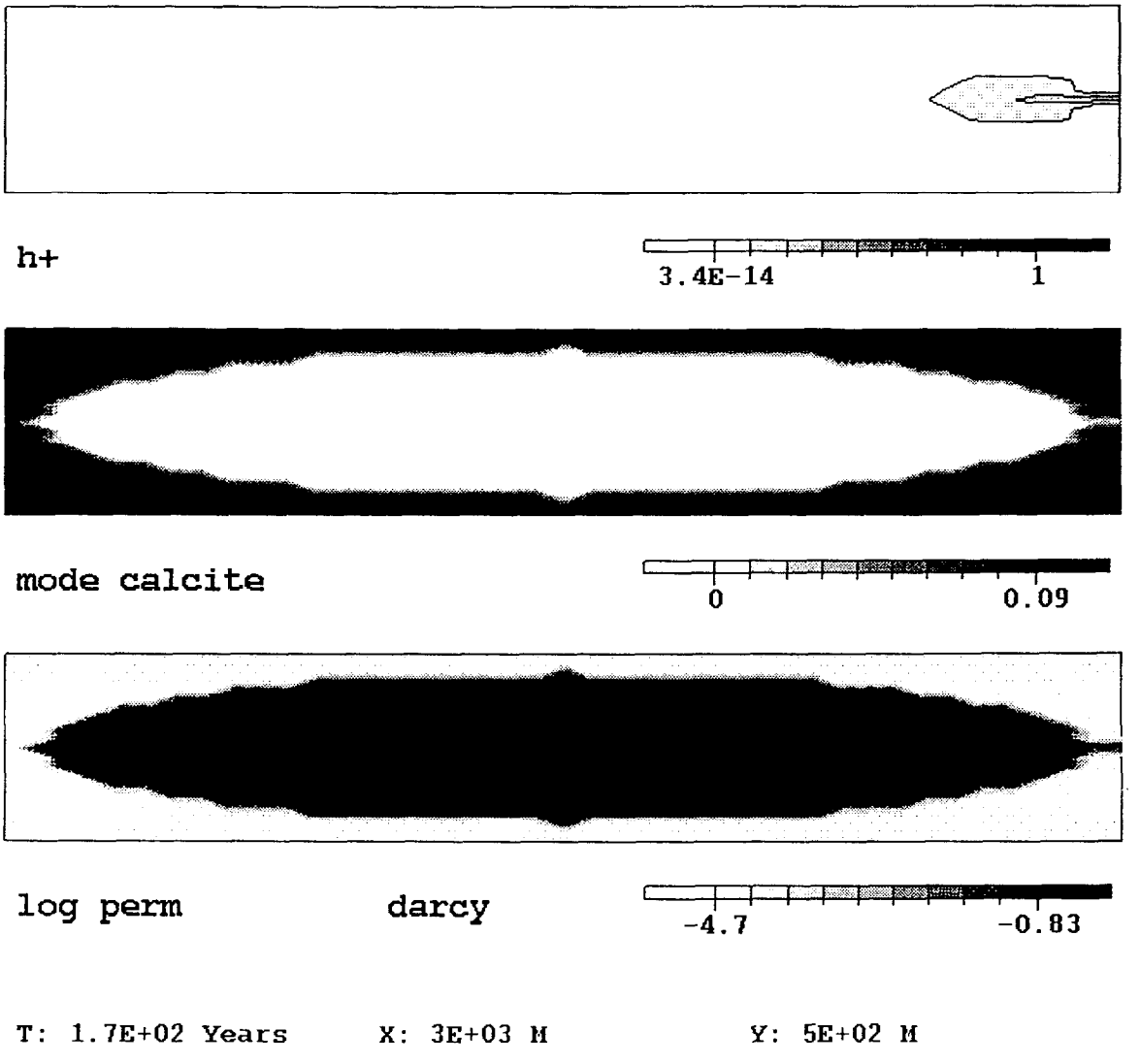

Fig. V-15 Same as in Fig. V-13 except for the simulation results at 170 years. The improper placement of the waste injection well has caused the destruction of the seal and the escape of the waste.

VI
Optimization Technology

A key implication of a reaction-transport analysis of deep reservoir injection is the possibility of determining the optimal emplacement strategy. Clearly this is a complex optimization problem. Key aspects to be considered are as follows:

- Minimize formation damage to insure longevity and good storage capacity and permeability communication between borehole and reservoir.
- Minimize dissolution of seals or confining units bounding the reservoir.
- Avoid excessive matrix dissolution within the reservoir and related formation collapse.
- Minimize reservoir overpressuring to avoid fracturing.
- Maximize loss of waste fluid toxicity through waste fluid-rock or thermal decay fluid phase reactions.
- Avoid gas-producing reactions and possible reaction-induced overpressuring.
- Maintain required injection rates.
- Minimize costs.

Considering the complexity of the fluid and mineral chemistry and the large number of coupled processes it would be very costly to attempt an experimental study to optimize the process subject to this many constraints. In this section, we outline a strategy for using CIRE.A embedded in an optimal control algorithm to determine the best injection scenario.

As an illustrative example, consider the optimization of matrix acidizing to remediate near borehole damage.

Choosing the ideal acidification procedure is a complex balance of a number of competing factors. As a given simulation can be rather CPU-time intensive, it is important to have an efficient search of the parameters characterizing the injection scenario in order to find the best procedure.

Optimal control theory presents itself as an ideal solution to this problem. First, one must delineate the factors to be taken into account:

A. cost of the mud acid and that of the treatment (manpower and equipment);

B. the decrease in recovery resulting from a poorly designed procedure;

C. the increase in cost due to formation damage induced by the procedure; and

D. environmental costs due to regulations or cleanup or disposal of waste fluids.

These factors are then quantified in terms of the set of parameters describing the injection fluid composition, temperature, flow rate and their possible time course. The set of these control parameters is denoted Γ. The parameters describing the spatial distribution of the permeability, porosity and other textural variables is denoted X.

Let F be the total cost of the procedure and take it to be a sum of terms corresponding to the contributions A-D described above

$$F(X,\Gamma) = \mathrm{A}(\Gamma) + \mathrm{B}(X,\Gamma) + \mathrm{C}(X,\Gamma) + \mathrm{D}(X,\Gamma) \tag{VI.1}$$

Note that X describes the state of the reservoir as a result of the Γ-dependent procedure. Once Γ is specified, the reaction-transport processes will uniquely give X. Thus in principle there is a function relating X to Γ. We write this

$$X = X_{\mathcal{R}\Gamma}(\Gamma), \tag{VI.2}$$

the function $X_{\mathcal{R}\Gamma}$ yields the unique value of X for given Γ.

The objective is then to minimize the value of F^*,

$$F^*(\Gamma) = F\left(X_{\mathcal{R}\Gamma}(\Gamma), \Gamma\right) \tag{VI.3}$$

with respect to Γ. This problem can be solved using CIRF.A to provide $X_{RT}(\Gamma)$ as follows.

Let M be an algorithm that minimizes a function F^* with respect to its parameters Γ. M is designed to only require $F^*(\Gamma)$ and not explicit expressions for the derivatives of F^* with respect to Γ. Then M may clearly be coupled to a reaction-transport simulator to yield the optimum value of Γ as suggested in Fig. VI-1.

As a very simple example of a concrete realization of F, consider the following. Let R(t) be the cost rate ($/minute) for the cost of the mud acid and injection procedure. Then

$$A + D = \int_0^{t_f} \mathcal{R}(t;\Gamma). \tag{VI.4}$$

Note that $\mathcal{R}(t;\Gamma)$ clearly depends on the parameters of the treatment scenario. Next, take the benefit B to be expressed here simply in terms of the integrated permeability κ at the final time t_f and for all points in the reservoir $\vec{r}$,

$$\mathrm{B} = -b\int d^3r\kappa\left(\vec{r}, t_f; \Gamma\right). \tag{VI.5}$$

Here b is a parameter used to assess the importance of the permeability enhancement. Finally, we apply a large cost for dissolution-induced formation collapse. Let ϕ be the porosity and ϕ_c its value beyond which there is a strong likelihood of formation collapse. Then consider the formulation

$$C = \int d^3r\gamma\left(\phi/\phi_c\right) \tag{VI.6}$$

where γ is a monotonically increasing function of ϕ/ϕ_c that rapidly increases when its argument exceeds unity and is small otherwise. For example

$$\gamma = e^{(\phi/\phi_c)^\lambda} - 1 \tag{VI.7}$$

for λ>1. If λ is sufficiently large then γ changes rather abruptly as ϕ exceeds ϕ_c; for $\phi \le \phi_c$ γ is essentially 0. For $\phi = \phi_c$, γ=e-1~1.7183. For λ =5 and ϕ =1.2 ϕ_c, then γ =11.041.

At the writing of this report we have not completed coding the optimization routine. We believe, however, that this approach is very promising.

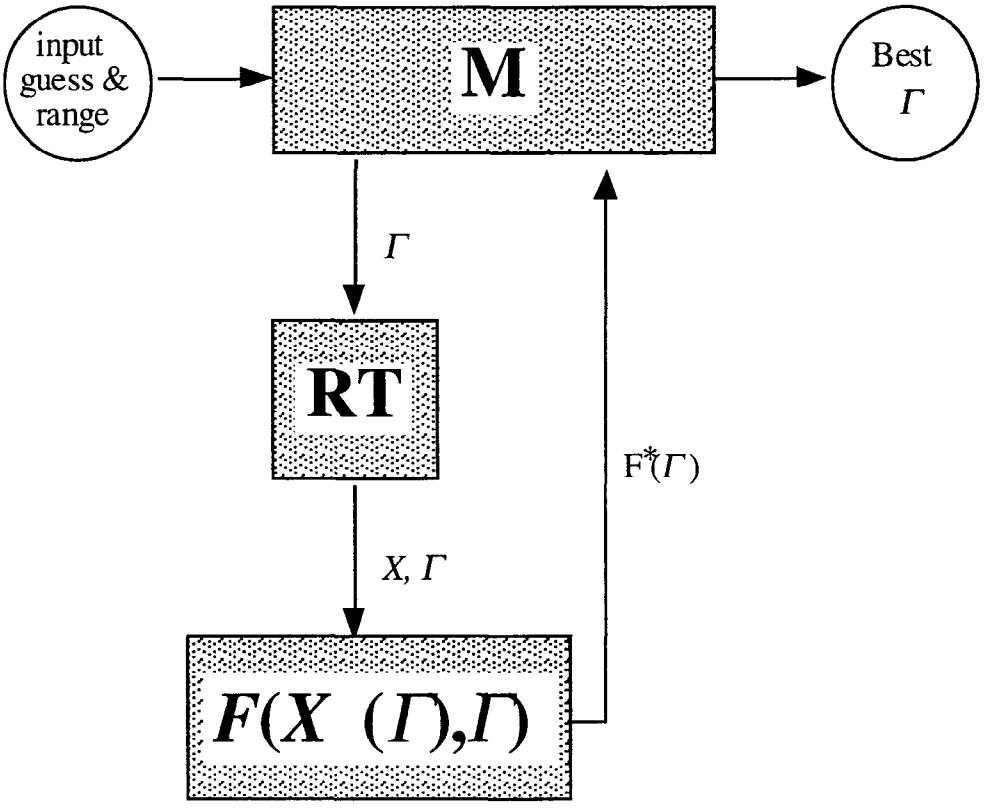

Figure VI-1 Flow chart for the algorithm used to optimize matrix acidification.

VII
Conclusions and Recommendations

A. Conclusions

This study provides valuable insight into the use of reaction-transport modeling for hazardous wastes disposed by deep well injection. Results presented demonstrate in particular that CIRF.A is appropriate for such modeling. Waste injection modeling was shown to be essential in a variety of roles:

- designing procedures for near-borehole damage remediation;
- predicting waste fluid/reservoir mineral reaction-induced breaching of seals separating waste from the accessible environment;
- avoiding or controlling waste fluid/repository mineral-induced formation collapse;
- predicting reservoir storage capability;
- predicting the 10,000 year fate of waste in a repository of given mineralogy, temperature and original (formation) fluid composition and pressure;
- matching a given waste fluid with the ideal (or best) available reservoir mineralogy.

All these functions are central for developing and evaluating No-Migration Petitions, ongoing management and assessment of a repository during the operation and post

operation periods and developing strategies should problems emerge. These types of modeling studies can also be of great value in setting regulatory policy and guidelines.

Examples selected illustrate that a variety of phenomena must be considered that can only be evaluated by a fully coupled reaction-transport model. These phenomena arise out of the coupling of flow and reaction via reaction-induced changes in permeability. This study has demonstrated that CIRF.A is able to reliably model many of these phenomena.

Simulation results using CIRF.A are found to be accurate. Agreement with the commonly used and well-tested code, SWIFT, as well as the analytic solutions for pressure, velocity, and concentration was demonstrated for cases where no reactions take place. The chemical aspects of CIRF.A was verified by theoretical and analytical checks. Verification of CIRF.A was carried out for more complicated cases using laboratory core flood data.

The CIRF.A simulation results indicate that the effects of pressure and temperature on waste fluid/rock interactions can be significant. The results of the simulation of the two field injection cases by CIRF.A are quantitatively consistent with field measured data during the operational period. Use of CIRF.A in predicting the decomposition of organic waste over time and the 10,000 year evolution in geometry and composition of the waste fluid residing in the repository were demonstrated. The escape of waste fluids from a compartment through a seal over a 10,000 year period was also simulated. The latter illustrated the utility of CIRF.A in the context of 10,000 year fate prediction.

This study serves to identify important phenomena occurring during waste injection and to demonstrate the characteristics and capability that a reaction-transport simulator must have in order to be an effective regulatory and repository assessment and management vehicle. In short, the existence of formation damage, reaction front fingering, toxicity evolution, and reaction-induced escape of waste fluid through confining units make the use of a fully coupled reaction-transport code such as CIRF.A a necessary component of No-Migration Petitions.

B . Recommendations

Rec.1 Role for Coupled Reaction-transport Modeling

From our experience in using the reaction-transport code CIRF.A in waste repository analysis, we believe that such a code should be an integral part of any regulatory and No-Migration Petition activity. The critical nature of the No-Migration issue and known problems in formation damage and poor plume containment characterization is essential that there be a reliable reaction-transport model for waste repository analysis.

Rec.2 Necessary Features of a Waste Repository Dynamics Simulator

The important characteristics that such a simulator should have include the following. The symbols are *A* (already in CIRF.A), • (phenomenology known but not in CIRF.A) and *N* (a phenomenology needing development).

A 1 and 2 spatial dimensional options,

A large thermodynamic and kinetic data base,

A flexible capability to add new reactions and other parameters to data base,

A Debye-Hückel ionic strength correction to aqueous species activities,

A Brinkman as well as Darcy single phase flows,

A aqueous and non aqueous liquid multi-phase flow (without interphase exchange reactions),

A gridding adapted to arbitrary domain shape,

A moving adaptive gridding to capture reaction fronts or wormholing/cavitation,

A built-in graphical analysis,

• full 3 spatial dimensional capability,

• full three phase reaction-transport solver with intra-phase and interphase exchange reactions accounting for the effects of relative permeability and capillarity.

- Pitzer ionic strength corrections for very concentrated brines,
- calculation of stress, fracturing and formation collapse,
- user-friendly interface,
- fines migration

N multi-phase Brinkman flow, and

N clay swelling/shrinking in response to changes in ionic strength.

These features will enable the waste injection community to reliably make use of reaction-transport modeling for the optimization, repository analysis, No-Migration Petition, and regulation development studies needed for this crucial technology. To this end, CIRF.A presents itself as an excellent starting point to be extended to a fully three-dimensional, three-phase, reaction-transport simulator. Much of this fundamental model, numerical algorithms and code development to do so has already been completed at the Laboratory for Computational Geodynamics (including all • and *N* items).

Rec.3 Waste Disposal in Underpressured Compartments

From the preliminary results presented Chapter V, we conclude that such a project could be completed in about 2 years. Deep well injection of hazardous wastes into underpressured reservoirs is a promising, environmentally safe means of disposal. Preliminary studies presented in this report demonstrate that compartment underpressuring helps contain waste fluids and increases holding capacity. A thorough analysis of these reservoirs using reaction-transport-mechanical modeling by a team familiar with the geology and physico-chemistry of compartments will be invaluable in assessing this technology and developing guidelines for its safe use.

Rec.4 Optimization Technology

Design of the best injection strategy, near-borehole remediation, and other aspects of waste storage should be done using optimization technique as in Chapter VI of this

report. Well location should also be determined using optimization technology with CIRF.A modeling. This technique should be developed using CIRF.A due to its demonstrated performance in the present application. Such a study should include the development of the appropriate cost function and optimzation algorithm.

Rec.5 CIRF.A Model Parameter Sensitivity Analysis

CIRF.A run in a sensitivity analysis mode should be used to identify those parameters on which repository analysis is most strongly dependent and then carry out chemical and physical experiments to determine these quantities.

CIRF.A Availability

CIRF.A was originally developed by Geo-Chemical Research Associates (GCRA), Bloomington, Indiana. Later its development was continued via a collaboration between GCRA and the Laboratory for Computational Geodynamics (LCG) at Indiana University.

Academic institutions may obtain a user's license for CIRF.A through LCG at a very nominal fee. Industrial licensing of CIRF.A may be obtained through GCRA. Licenses include tutorials which are available over the telephone and by special arrangement at user sites. Starting in 1997 there will also be an annual workshop on the use of CIRF.A and other GCRA/LCG geological modeling tools.

The standard CIRF user's license includes source codes for industrial subscribers while academic licenses are for executable code only. However, a great deal of flexibility is available upon negotiation.

LCG and GCRA also offer other services associated with the CIRF codes:

- site-specific modeling studies;
- developing special versions of CIRF for user proprietary models; and
- collaborative projects wherein LCG or GCRA carry out modeling studies as part of a joint project involving other institutions.

These are some examples of the types of CIRF activities being made available.

Inquiries about CIRF codes can be made to:

Peter Ortoleva, Distinguished Professor of Chemistry and Geological Sciences
Laboratory for Computational Geodynamics
Department of Chemistry
Indiana University
Bloomington IN 47405
Tel: (812) 855-2717
Fax: (812) 855-8300
E-mail: ortoleva@indiana.edu

Publications from This Project

Liu, X., P. Ortoleva and R. Larkin (1995) Use of a reaction-transport model for assessing the geochemical fate of hazardous waste fluids by deep well injection, presented at the AAPG Annual Convention, Houston, Texas.

Ortoleva, P., Y. Chen, X.Liu , A.Ormond and R. Larkin (1996) Simulation of waste injection and migration with the fully coupled hydrologic, mineral, and pore fluid reaction code CIRF.A, in Deep Injection Disposal of Hazardous and Industrial Waste: Scientific and Engineering Aspects, J.A. Apps and C.-F. Tsang, eds., San Diego, CA, Academic Press, 627-636.

Liu, X., A.Ormond, K.Bartko, Y.Li and P. Ortoleva (1996) A geochemical reaction-transport simulator for matrix acidizing analysis and design, to appear in the Journal of Petroleum Science and Engineering.

Liu, X. and P. Ortoleva (1996) A coupled reaction and transport model for assessing the injection, migration and fate of waste fluids, to be presented at the SPE Annual Conference and Exhibition, Denver, CO (Oct. 6-9).

Liu, X. and P. Ortoleva (1996) Analysis of deep well waste injection using a fully coupled reaction-transport simulator, in preparation.

Ortoleva, P. (1996). Basin Compartments, in preparation.

References

Adams, E.E. and L.W. Gelhar (1992) Field study of dispersion in a heterogeneous aquifer, 2, Spatial moments analysis, *Water Resources Research* 28(12), 3293-3307.

Al-Shaieb, Z. V. Tigert, J. Puckette and R. Ely (1989) Genesis of pressure compartments and seals, OKINTEX Group, Progress Report IA for the Gas Research Institute, 15 November 1989.

Arquis, E. (1994) Transferts en milieu poreux et à l'interface: de l'échelle microscopique à l'échelle macroscopique, Mémoire de thèse, Bordeaux University, France, 208 pp.

Bartko, K.M. and D.P. Newhouse (1992) Well stimulation, Internal report, ARCO Oil Exploration and Production Technology, Plano, Texas.

Bear, J (1972) Dynamics of Fluids in Porous Media, New York, American Elsevier Pub. Co.

Bohac, C. E., and S. C. Young (1991) Evaluation of the FASTCHEM model for predicting leachate attenuation at fossil power plants, in Proceedings of the International Symposium on Ground Water in Practice, Bethlehem, G. P. Lennon, ed., 58-63.

Bradley, J.S. (1975) Abnormal formation pressure, *AAPG Bulletin* 59, 957-973.

Bradley, J.S. (1985) U.S. Patent 4,560,503.

Bradley, J.S. and D. Powley (1994) Pressure compartments in sedimentary basins: A review, in Basin Compartments and Seals, P. Ortoleva, ed., *AAPG Memoir* 61, 3-26.

Brinkman, H.C. (1946). A calculation of the viscous forces exerted by a flowing fluid of a dense swarm of particles, *Appl. Sci. Res.*, 27-34.

Chadam, J., D. Hoff, E. Merino, A. Sen and P. Ortoleva (1986) Reactive infiltration instabilities, *J. Appl. Math* 36, 207-221.

Chadam, J., A. Sen and P. Ortoleva (1988) A weakly nonlinear stability analysis of the reactive infiltration interface, *J. Appl. Math.* 48, 1362-1378.

Chadam, J., A. Peirce and P. Ortoleva (1990) Stability of reactive flows in porous media: Coupled porosity and viscosity changes, *J. Appl. Math* 51, 684-692.

Chen, W. and P. Ortoleva (1990) Self-organization in far-from-equilibrium reactive porous media subject to reaction front fingering, in Patterns, Defects and Materials Instabilities, D. Walgraef and N.M Ghoniem, eds, NATO ASI Series, Vol. 183, pp. 203-220.

Chen, W., and P. Ortoleva (1992) Development of complex reaction front morphologies through nonlinear fluid-rock interaction: Modeling, asymptotic and numerical studies, in Modeling and Analysis of Diffusive and Advective Processes in Geosciences, W. E. Fitzgibbon and M. F. Wheeler, eds., Philadelphia, SIAM, 52-70.

Chen, W., A. Ghaith, A. Park and P. Ortoleva (1990) Diagenesis through coupled processes: Modeling approach, self-organization and implications for exploration, in Prediction of Reservoir Quality through Chemical Modeling, I. Meshri and P. Ortoleva, eds., *AAPG Memoir* 49, 103-130.

Dewers, T. and P. Ortoleva (1988) The role of geochemical self-organization in the migration and trapping of hydrocarbons, *Applied Geochemistry* 3, 287-316.

Dickey, P.A. and W.C. Cox (1977) Oil and gas in reservoirs with subnormal pressure, *AAPG Bulletin* 61, 2134-2142.

Donaldson, E.C., N. Ewall and B. Singh (1991) Characteristics of capillary pressure curves, *J. Pet. Sci. and Eng.* 6(3), 249-261.

Earlougher, R.C. (1977) Advances in Well Test Analysis, H.L. Doherty Series Monograph V. 5, SPE of AIME, Dallas, Texas, 264 p.

Felmy, A. R., D. Girvin and E. A. Jenne (1986) MINTEQ - A computer program for calculating aqueous geochemical equilibria, U.S. EPA, Washington, D.C.

Finley, N.C. and M. Reeves (1982) SWIFT Self-Teaching Curriculum, Sandia National Laboratories, Albuquerque, NM., NUREG/CR-1968, SAND81-0410.

Harvie, C.E., N. Moller and J.H. Weare (1984) The prediction of mineral solubilities in natural waters: The Na-K-Mg-Ca-H-Cl-SO_4-OH-HCO_3-CO_3-CO_2-H_2O system to high ionic strengths at 25°C", *Geochim. Cosmochim. Acta* 48, 723-751.

Haskin, H.K., C.H. Moore and P. Ortoleva (1988) Modeling acid stimulation of the Halfway Formation, Canada, using a geochemical computer model, SPE 18133, pp. 283-294.

Hawkins, M.F., Jr. (1956) A note on the skin effect, *Trans. AIME* 207, 355-357.

Helgeson, H.C. (1969) Thermodynamics of hydrothermal systems at elevated temperatures and pressures, *Am. J. Sci.* 267, 729-804.

Helgeson, H.C. and D.H. Kirkham (1974) Theoretical prediction of the thermodynamic behavior of aqueous electrolytes at high pressures and temperatures: II. Debye-Huckel parameters for activity coefficients and relative partial molal properties, *Am. J. Sci.* 274, 1199-1261.

Helgeson, H.C., D.H. Kirkham and G.C. Flowers (1981) Theoretical prediction of the thermodynamic behavior of aqueous electrolytes at high pressures and temperatures: IV. Calculation of activity coefficients, osmotic coefficients, and apparent molal and standard and relative partial molal properties to 600°C and 5kb, *Am. J. Sci.* 281, 1249-1516.

Hoefner, M.L., H.S. Fogler, P. Stenius and J. Sjöblom (1987) Role of acid diffusion in matrix acidizing of carbonates, *J. Petrol. Tech.*, 203-208.

Hung, K.M., A.D. Hill and K. Sepehrnoori (1989) A mechanistic model of wormholes growth in carbonate matrix acidizing and acid fracturing, *J. Petrol. Tech.*, 59-65.

Lake, L.W. (1988). Enhanced Oil Recovery, Eagel Cliffs, NJ, Prentice-Hall.

Larkin, R. G., J. E. Clark and P. W. Papadeas (1994) Comparison of modeled disposal well plumes using average and variable injectate densities, *Ground Water* 32, 35-40.

Leenheer, J.A., R.L. Malcolm and W.R. White (1976). Investigation of the reactivity and fate of certain organic components of an industrial waste after deep-well injection, *Env. Sci. & Tech.* 10(5), 445-451.

Liu, C. W. Chen, and T. N. Narasimhan (1989a) Redox-controlled multiple-sSpecies reactive chemical transport: 1. Model development, *Water Resources Research* 25(5), 869-882.

Liu, C. W., and T. N. Narasimhan (1989b) Redox-controlled multiple-species reactive chemical transport: 2. Verification and application, *Water Resources Research* 25(5), 883-910.

Liu, X., P. Ortoleva and R. Larkin (1995) Use of a reaction-transport model for assessing the geochemical fate of hazardous waste fluids by deep well injection, presented at the AAPG Annual Convention, Houston, Texas.

Liu, X., A. Ormond, K. Bartko, Y. Li and P. Ortoleva (1996) A geochemical reaction-transport simulator for matrix acidizing analysis and design, *J. Pet. Sci. and Eng.*, in press.

Logan, J. (1989) Vertical seals: Their occurrence, formation and importance to pressure chambers, OKINTEX Group, Progress Report IA for the Gas Research Institute, 15 November 1989.

Mason, J.W. (1968) Hugoton Panhandle Field, Kansas, Oklahoma and Texas, in *Natural Gases of North America* 2, AAPG.

McIntosh, D. A. (1991) An overview of EPRI hydro-geochemical code FASTCHEM, in Proceedings of the International Symposium on Ground Water in Practice, G. P. Lennon, ed., Bethlehem, 46-57.

Moeller, N. (1988) The prediction of mineral solubilities in natural waters: A chemical equilibrium model for the Na-Ca-Cl-SO4-H_2O system, to high temperature and concentration, *Geochim. Cosmochim. Acta* 52, 821-832.

Narasimhan, T. N., A. F. White and T. Tokunaga (1986) Groundwater contamination from an inactive uranium mill tailings pile: 2. Application of a dynamic mixing model, *Water Resources Research* 22(13), 1820-1834.

Oelkers, E.H. and H.C. Helgeson (1988) Calculation of the thermodynamic and transport properties of aqueous species at high pressures and temperatures: Aqueous tracer

diffusion coefficients of ions to 1000°C and 5 kb, *Geochim. Cosmochim. Acta* 52, 63-85.

Ortoleva, P. (1996) Basin Compartments, in preparation.

Ortoleva, P., Z. Al-Shaieb and J. Puckette (1995), Genesis and dynamics of basin compartments and seals, *Am. J. Sci.* 295, 345-427.

Ortoleva, P. (1994) Geochemical Self-Organization, New York, Oxford University Press.

Ortoleva, P., E. Merino, J. Chadam and C.H. Moore (1987) Geochemical self-organization I: Reaction-transport feedbacks and modeling approach, *Am. J. Sci.* 287, 979-1007.

Perry, R.H., D.W. Green, and J.O. Maloney, eds. (1984) Perry's Chemical Engineers' Handbook, Sixth Edition, N.Y., McGraw-Hill Book Co.

Pitzer, K.S. (1973a) Thermodynamics of electrolytes. I. Theoretical basis and general equations, J. *Phys. Chem.* 77, 268-277.

Pitzer, K.S. (1973b) Thermodynamics of electrolytes. II. Activity and osmotic coefficients for strong electrolytes with one or both ions univalent, *J. Phys. Chem.* 77, 2300-2307.

Potdevin, J.L., W. Chen, A. Park, Y. Chen and P. Ortoleva (1992) CIRF: A general reaction-transport code: Mineralization fronts due to the infiltration of reactive fluids, in Water-Rock Interaction, Vol. 2, Y.K. Kharaka and A.S. Maest, eds., 1047-1050.

Powley, D. (1980) Normal and abnormal pressure, lecture presented to AAPG Advanced Exploration Schools, 1980-1987.

Powley, D. (1990) Pressures, hydrogeology and large scale seals in petroleum basins, in Self-Organization in Geological Systems: Proceedings of a Workshop held 26-30 June 1988, University of California Santa Barbara, *Earth Science Reviews* 29, P. Ortoleva, B. Hallet, A. McBirney, I. Meshri, R. Reeder and P. Williams, eds., 215-226.

Ramey, H.J., and W.M. Cobb (1977) A general buildup theory for a well in a closed drainage area, *J. Pet. Tech. Trans.*, AIME, 1493-1505.

Reeves, M., D.S. Ward and N.D. Johns (1986) Theory and implementation for SWIFT II, the Sandia Waste-Isolation Flow and Transport Model for Fractured Media, Release 4.84. Sandia National Laboratories, Albuquerque, NM. NUREG/CR-3328, SAND83-1159.

Shepherd, L., P. Drzewiecki, J. Bahr and J.A. Simo (1994) Silica budget for a diagenetic seal, in Basin Compartments and Seals, *AAPG Memoir* 61, P. Ortoleva, ed., 369-384.

Shock, E.L. and H.C. Helgeson (1988) Calculation of the thermodynamic and transport properties of aqueous species at high pressures and temperatures: Correlation algorithms for ionic species and equation of state predictions to 5 kb and 1000°C, *Geochim. Cosmochim. Acta* 52, 2009-2036.

Steefel, C.I., and A.C. Lasaga (1990) Permeability change due to coupled flow reaction, *Am. Chem. Soc.*, 212-225.

Tanger, J.C. IV and H.C. Helgeson (1988) Calculation of the thermodynamic and transport properties of aqueous species at high pressures and temperatures: Revised equations of state for the standard partial molal properties of ions and electrolytes, *Am. J. Sci.* 288, 19-98.

Tigert, V. and Z. Al-Shaieb (1990) Pressure seals: Their diagenetic banding patterns, in Self-Organization in Geological Systems: Proceedings of a Workshop held 26-30 June 1988, University of California Santa Barbara, *Earth Science Reviews* 29, P. Ortoleva, B. Hallet, A. McBirney, I. Meshri, R. Reeder and P. Williams, eds., 227-240.

TNRCC (Texas Natural Resources Conservation Commission) (1993) Reports for Waste Disposal Wells, Central Records, Austin, Texas.

U.S. Environmental Protection Agency (1990) Assessing the Geochemical Fate of Deep-Well-Injected Hazardous Waste: Summaries of Recent Research, EPA/625/6-89/025b.

Wang, Y., Hill, A.D. and R.S. Schechter (1993). The optimum injection rate for matrix acidizing carbonate formation, Proceedings of the SPE 68th Annual Technical Conference, Society of Petroleum Engineers, Richardson, TX, 675-687.

Ward, D.S., M. Reeves, and L.E. Duda (1984) Verification and Field Comparison of the Sandia Waste-Isolation Flow and Transport Model (SWIFT). Sandia National Laboratories, Albuquerque, NM. NUREG/CR-3316, SAND83-1154.

Williams, B.B., J.L. Gidley and R.S. Schechter (1979) Acidizing Fundamentals, Richardson, TX, Society of Petroleum Engineers, 124 pp.

Wolery, T.J., (1983) EQ3NR, a computer program for geochemical aqueous speciation-solubility calculations: the theoretical manual, user's guide, and related documentation, Lawrence Livermore National Laboratory, Livermore, California.

Wolery, T.J. (1992) EQ3/6 A Software Package for Geochemical Modeling of Aqueous Systems: Package Overview and Installation Guide (Version 7.0). Lawrence Livermore National Laboratory.

Wolery, T.J. and S.A. Daveler (1992) EQ6, A Computer Program for Reaction Path Modeling of Aqueous Geochemical Systems: Theoretical Manual, User's Guide, and Related Documentation (Version 7.0). Lawrence Livermore National Laboratory.